ISSN 1860-0387

DISSERTATION 7 | 2019

DISSERTATION 7 | 2019
Helmholtz Zentrum für Umweltforschung – UFZ
Department Technische Umweltchemie

Maria Vogel

Anwendung von Eisen-Aktivkohle-Systemen zur Grundwassersanierung

Helmholtz Zentrum für
Umweltforschung – UFZ
Permoserstraße 15
04318 Leipzig
www.ufz.de

NICHT ZUM VERKAUF BESTIMMT.

Maria Vogel | Anwendung von Eisen-Aktivkohle-Systemen zur Grundwassersanierung

7 | 2019

HELMHOLTZ
ZENTRUM FÜR
UMWELTFORSCHUNG
UFZ

Anwendung von Eisen-Aktivkohle-Systemen zur Grundwassersanierung

Von der Fakultät für Chemie und Mineralogie

der Universität Leipzig

genehmigte

Dissertation

zur Erlangung des akademischen Grades

doctor rerum naturalium

(Dr. rer. Nat.)

vorgelegt

von Diplom-Lebensmittelchemikerin Maria Vogel

geboren am 11.04.1987 in Karl-Marx-Stadt

Gutachter: Prof. Dr. Frank-Dieter Kopinke

Univ.-Doz. Mag. Dr. Thomas Reichenauer

Tag der Verleihung: 17.07.2019

Die vorliegende Dissertation wurde im Zeitraum von November 2012 bis September 2017 am Helmholtz-Zentrum für Umweltforschung - UFZ unter der Leitung von **Frau Dr. Katrin Mackenzie** und **Herrn Prof. Dr. Frank-Dieter Kopinke** (Department Technische Umweltchemie) sowie **Frau Dr. Ivonne Nijenhuis** (Department Isotopenbiogeochemie) angefertigt.

Bibliographische Beschreibung

Maria Vogel

Anwendung von Eisen-Aktivkohle-Systemen zur Grundwassersanierung

Universität Leipzig, Dissertation

140 Seiten, 35 Abbildungen, 7 Tabellen

Kurzreferat

Im Mittelpunkt der vorliegenden Dissertation stehen die Untersuchung und Weiterentwicklung von Eisen-Aktivkohle-Systemen für die *In-situ*-Grundwassersanierung, wobei ein besonderer Schwerpunkt auf das Kompositmaterial Carbo-Iron® gelegt wird. Nachdem die prinzipielle Eignung des *In-situ*-Reagenzes bereits in früheren Studien gezeigt wurde, kann in dieser Arbeit eine deutliche Optimierung der Partikel hinsichtlich ihrer Korrosionsbeständigkeit, der Dechlorierungseffizienz sowie ihrer Lebensdauer durch die Anwendung reduzierter Schwefelspezies erzielt werden. Der positive Einfluss von Carbo-Iron auf den mikrobiologischen Schadstoffabbau wird am Beispiel einer Feldstudie gezeigt. Auf Grundlage der dabei gewonnenen Erkenntnisse werden verschiedene Möglichkeiten des Zusammenspiels von Eisen-Aktivkohle-Kompositen und biotischen Vorgängen diskutiert.

Ein weiterer Schwerpunkt der vorliegenden Arbeit stellt die Untersuchung des Einflusses von Aktivkohle auf die Selektivität und Kinetik der mikroeisenbasierten Reduktion chlorierter Ethene dar. Eine deutliche Beschleunigung der eisenbasierten Dechlorierung kann vor allem in Gegenwart von Aktivkohlesorten mit redoxaktiven funktionellen Gruppen beobachtet werden. Die Ergebnisse zeigen, dass Aktivkohle bei der Dechlorierung nicht nur als Sorptionsmittel agiert, sondern aktiv an der chemischen Reaktion teilnehmen bzw. diese sogar beschleunigen kann.

Die in der vorliegenden Dissertation gewonnenen Erkenntnisse liefern ingesamt einen substanziellen Beitrag zur effizienten Gestaltung von Eisen-Aktivkohle-Systemen, wodurch ihre Anwendungsmöglichkeiten in der Grundwassersanierung ausgebaut werden.

Bibliographic description

Maria Vogel

Application of Iron-Activated Carbon-Systems for Groundwater Remediation

University Leipzig, Doctoral Thesis

140 Pages, 35 Figures, 7 Tables

Abstract

The present thesis is focused on the investigation and development of iron-activated carbon-systems for *in-situ* groundwater remediation with a main emphasis on the composite material Carbo-Iron®. After the basic suitability of the *in-situ* reagent has been shown in previous studies, a significant optimization of the particles with regard to corrosion resistance, dechlorination efficiency and life time is achieved in this work through the application of reduced sulfur species. The positive influence of Carbo-Iron on microbial contaminant degradation is shown in a field study. On the basis of the observations, possible interactions between the composite material and biotic processes are discussed. Another focus of the dissertation is the investigation of the influence of activated carbon on the selectivity and kinetics of the iron-based reduction of chlorinated ethenes. The results show that activated carbon types with redox-active oxygen-containing surface groups are particularly effective in accelerating iron-based dechlorination. The findings of the dissertation help to create highly efficient iron-activated carbon-systems, which are promising for practical application.

Inhaltsverzeichnis

1. Einleitung 9

2. Theoretischer Teil 12

2.1. Chlorierte Ethene als Grundwasserkontaminanten 12

2.2. Metallisches Eisen als Reduktionsmittel zur Grundwassersanierung 13

2.2.1. Reduktion chlorierter Ethene an Eisenpartikeln 14

2.2.2. Anaerobe Korrosion von Eisen als unerwünschte Nebenreaktion 16

2.2.3. Einfluss von Schwefelspezies auf die Reaktivität von Eisenpartikeln 17

2.3. Eisen-Kohlenstoff-Systeme als neuartige *In-situ*-Reduktionsmittel 20

2.3.1. Partikeleigenschaften und Reaktionsverhalten von Carbo-Iron 22

2.4. Mikrobiologischer Abbau chlorierter Ethene in Grundwasser 25

2.4.1. Grundlagen der mikrobiologischen Dechlorierung 25

2.4.2. Einfluss von Eisenpartikeln auf den biotischen Abbau chlorierter Ethene 27

3. Praktischer Teil - Ergebnisse und Diskussion 30

3.1. Acceleration of microiron-based dechlorination in water in contact with fibrous activated carbon 33

3.2. Sulfidation of ZVI/AC composite leads to highly corrosion-resistant nanoremediation particles with extended life time 60

3.3. Combined chemical and microbiological degradation of PCE during the application of Carbo-Iron at a contaminated field site 93

4. Zusammenfassung 126

5. Literaturverzeichnis 132

1. Einleitung

Mangelnde Schutzvorkehrungen und sorgloser Umgang mit umweltgefährdenden Stoffen führen immer wieder zu einer Belastung der wertvollen Ressource Grundwasser. Allein in Deutschland existieren nach aktuellen Angaben des Umweltbundesamtes (2017) über 260 000 altlastverdächtige Flächen, von denen potenziell eine Gefahr für den Menschen und das angrenzende Ökosystem ausgeht [1]. Ein beträchtlicher Anteil der Grundwasserbelastungen wird durch die chlorierten Kohlenwasserstoffe Perchlorethen (PCE) und Trichlorethen (TCE) verursacht [2–4], welche in weiten Teilen der Industrie Anwendung gefunden haben. Im Grundwasserleiter ist ein biologischer Abbau dieser Schadstoffe unter gewissen Voraussetzungen möglich, erfolgt jedoch relativ langsam und ist häufig mit einer Akkumulation der Intermediate *cis*-Dichlorethen und des kanzerogenen Vinylchlorids verbunden [5].

Vielerorts ist daher eine Sanierung des kontaminierten Aquifers erforderlich, wobei die *In-situ*-Reduktion der Schadstoffe mit metallischen Eisenpartikeln in Form von permeablen reaktiven Barrieren eine vielversprechende Möglichkeit darstellt [6]. Das Metall eignet sich dank seiner Reduktionskraft sowie seiner Umweltverträglichkeit. Vor allem nanoskalige Eisenpartikel mit ihrer großen spezifischen Oberfläche und der damit einhergehenden hohen Reaktivität standen in den letzten 15 Jahren im Mittelpunkt der Forschung [6]. Trotz der prinzipiellen Eignung der Nanoeisenpartikel für die *In-situ*-Grundwassersanierung bestehen Limitationen, welche die Anwendung der Technologie in der Praxis beschränken: Zu den kritischen Faktoren gehören unter anderem die schwache Sorptionsaffinität der chlorierten Ethene zur Metalloberfläche sowie die geringe Mobilität der Partikel im Aquifer [7,8].

Eine Möglichkeit, das Potenzial des Nanoeisens besser auszunutzen, besteht in der Kombination von metallischem Eisen mit kohlenstoffbasierten, sorptionsaktiven Trägermaterialien. In der vorliegenden Dissertation wird im Speziellen Carbo-Iron, ein Kompositmaterial aus kolloidaler Aktivkohle und darin eingebetteten Nanoeisenstrukturen [9–12], näher thematisiert. Hierbei kann durch die lokale Anreicherung der hydrophoben Schadstoffe in unmittelbarer Nähe der Eisenzentren sowie die sorptionsbedingte erhöhte Aufenthaltszeit der Substanzen in der *in situ* gebildeten reaktiven Zone vor allem bei niedrigen Schadstoffkonzentrationen, wie im Bereich der Fahne, eine vorteilhafte Nutzung des Eisens erreicht werden. Zudem weist das Komposit-

material im Vergleich zu reinem Eisen eine geringere Dichte und eine günstigere Oberflächenbeschaffenheit auf, wodurch es im Grundwasserleiter wesentlich besser transportiert werden kann [10].

In ihrer chemischen Reaktivität gegenüber Schadstoffen weisen Eisen-Aktivkohle-Systeme wie Carbo-Iron und reine Eisenpartikel ein ähnliches Verhalten auf, jedoch kann davon ausgegangen werden, dass sich die ablaufenden Reaktionswege aufgrund der Sorptionskomponente unterscheiden. Während im Fall von reinem Eisen sowohl Adsorption und Reaktion der Kontaminanten an der Metalloberfläche erfolgen, finden diese Vorgänge beim Einsatz von Eisen-Aktivkohle-Systemen, zumindest teilweise, räumlich getrennt voneinander statt. Die Bildung der reaktiven Spezies geschieht an der Eisenoberfläche, die Adsorption der Schadstoffe hingegen an der Aktivkohle [13,14]. Diese räumliche Trennung wirft verschiedene Fragen auf: Wie gelangen reaktive Spezies vom Reduktionsmittel zu den Kontaminanten? Ist Aktivkohle in der Lage, die Kinetik und Selektivität der Reaktion zu verändern und welche Rolle spielen dabei die Oberflächeneigenschaften der Aktivkohle? In der vorliegenden Dissertation werden diese Fragestellungen beispielhaft für den Abbau von PCE und TCE in einem Modellsystem mit mikroskaligen Eisenpartikeln und verschiedenen Arten textiler Aktivkohle untersucht. Die dabei gewonnenen Erkenntnisse sollen dazu beitragen, das Reaktionsverhalten von Eisen-Aktivkohle-Systemen besser zu verstehen, sodass ein möglichst effizienter Schadstoffabbau erzielt werden kann.

Als Reduktionsmittel für chlorierte Ethene hat sich das Eisen-Aktivkohle-Kompositmaterial Carbo-Iron seit seiner ersten wissenschaftlichen Darstellung im Jahr 2008 sowohl im Labormaßstab als auch bereits in einem Feldversuch als geeignet erwiesen [9–12]. Um das Kompositmaterial jedoch möglichst wirkungsvoll in der Praxis einsetzen zu können, ist es erforderlich, sein Verhalten im komplexen System Grundwasser besser zu verstehen und Partikeleigenschaften weiter zu optimieren. So beschränkt sich beispielsweise die hohe Reaktivität der enthaltenen Nanoeisenpartikel nicht nur auf die abzubauenden Schadstoffe, sondern führt auch zu unerwünschten Nebenreaktionen, wie etwa mit Wasser. Für reines Nanoeisen ist bekannt, dass durch die sogenannte anaerobe Korrosion häufig mehr Reduktions-äquivalente des Eisens verbraucht werden als durch den eigentlichen Schadstoffabbau, was zu einer Limitierung der Partikellebensdauer auf einige Stunden bis hin zu wenigen Wochen

führt [15–18]. Carbo-Iron ist zwar vergleichsweise korrosionsstabil, jedoch besteht auch für dieses Material der Bedarf einer Optimierung. Für die Entwicklung eines korrosionsbeständigen, hocheffizienten und langlebigen Kompositmaterials soll die Modifizierung mit reduzierten Schwefelspezies angewendet werden, die, wie in kürzlich erschienenen Studien gezeigt werden konnte, das Reaktionsverhalten von reinen Nanoeisenpartikeln verbessern, indem der Schadstoffabbau tendenziell beschleunigt und die Korrosion leicht gesenkt werden kann [19,20].

Die hohe Reaktivität nanoeisenbasierter Reagenzien spielt jedoch nicht nur für die Partikeleffizienz eine Rolle, sondern führt auch zu Veränderungen der Aquiferbedingungen, wodurch der am Standort ablaufende biologische Schadstoffabbau möglicherweise beeinflusst werden kann [21,22]. Um unerwünschte Effekte auszuschließen und bestenfalls beide Prozesse synergistisch miteinander zu koppeln, ist es notwendig, die Interaktion von chemischen und biologischen Abbauvorgängen näher zu untersuchen. Am Beispiel eines Feldstandortes charakterisiert diese Arbeit daher mit chemisch-analytischen und molekularbiologischen Methoden den mikrobiologischen Schadstoffabbau nach der Injektion von Carbo-Iron und diskutiert potenzielle Möglichkeiten des Zusammenspiels.

Insgesamt soll diese Dissertation durch ein verbessertes Verständnis des mechanistischen Zusammenspiels von Eisen und Aktivkohle, der Optimierung der Partikeleigenschaften von Carbo-Iron sowie durch die gesamtheitliche Betrachtung des chemischen und biologischen Schadstoffabbaus dazu beitragen, Eisen-Aktivkohle-Systeme effizienter zu gestalten und ihre Anwendungsmöglichkeiten in der *In-situ*-Grundwassersanierung zu erweitern.

2. Theoretischer Teil

2.1. Chlorierte Ethene als Grundwasserkontaminanten

Die leichtflüchtigen chlorierten Kohlenwasserstoffe (CKW) Perchlorethen (PCE) und Trichlorethen (TCE) zählen in den Industrieländern zu den bedeutendsten Grundwasserkontaminanten anthropogenen Ursprungs [2–4]. Aufgrund ihrer chemischen Eigenschaften, wie der hohen Lipophilie und Flüchtigkeit sowie ihrer Nichtbrennbarkeit, werden sie seit den 1920er Jahren unter anderem als Lösungsmittel in der chemischen Reinigung und Textilverarbeitung, als Entfettungsmittel in der Metallindustrie sowie für die Synthese organischer Verbindungen eingesetzt [2,3].

Infolge unsachgemäßer Lagerung, Verwendung und Entsorgung konnten vor allem bis in die 1970er und 1980er Jahre große Mengen der Substanzen in die Umwelt gelangen. So wurden beispielsweise in Deutschland im Jahr 1984 circa 70 000 t PCE verbraucht, wovon etwa 60 000 t in die Umwelt gelangten, davon etwa 90 % in die Luft, 9 % in Boden und 1 % in Wasser [23]. Häufig gelangen chlorierte Ethene punktuell in den Grundwasserleiter, wo sie charakteristische Kontaminationsprofile erzeugen. So bilden sie aufgrund ihrer hohen Dichte (ρ_{TCE} = 1,46 g cm^{-3} und ρ_{PCE} = 1,63 g cm^{-3} bei 25 °C), der niedrigen kinematischen Viskosität und der geringen Oberflächenspannung eine Schwerphase aus, die mehrere Grundwasserstockwerke kontaminieren kann [24,25]. Ausgehend von dieser Schadstoffquelle können PCE und TCE infolge ihrer geringen, aber substantiellen Wasserlöslichkeit (c_{TCE} = 1,1 g l^{-1} und c_{PCE} = 0,15 g l^{-1} bei 25 °C) und der schwachen Retardierung an natürlichen Sedimentoberflächen Kontaminationsfahnen von bis zu 10 km Länge bilden [24,26]. Aufgrund der gesundheitsschädlichen Eigenschaften der chlorierten Ethene stellen Kontaminationen des Aquifer ein Risiko für den Menschen und seine Umwelt dar [2,3].

Im Grundwasserleiter findet ein natürlicher Schadstoffabbau statt, vor allem durch mikrobiologische Dechlorierung, jedoch verläuft dieser häufig sehr langsam und hängt stark von den geochemischen Verhältnissen des Standortes ab. Aufgrund der hohen Persistenz und Toxizität ist daher häufig eine Sanierung des kontaminierten Aquifers erforderlich. Dabei kommen neben sogenannten Pump and Treat-Verfahren immer häufiger *In-situ*-Sanierungsverfahren mit metallischem Eisen bzw. eisenbasierten Materialien zum Einsatz [25].

2.2. Metallisches Eisen als Reduktionsmittel zur Grundwassersanierung

Anfang der 1990er Jahre konnte gezeigt werden, dass sich metallisches Eisen für den *In-situ*-Abbau chlorierter Ethene in Grundwasserleitern eignet [27]. Aufgrund seiner günstigen reduktiven Eigenschaften ($E^0_{Fe/Fe2+}$ = -440 mV), aber auch aus wirtschaftlichen Gründen ist das umweltverträgliche Eisen heute eines der am häufigsten eingesetzten Reduktionsmittel in der *In-situ*-Sanierung. Die praktische Umsetzung kann z.B. in Form von reaktiven permeablen Barrieren erfolgen, wobei granuläre Metallpartikel durch eine Baumaßnahme in Form einer reaktiven Wand in den Boden eingebracht werden, die vom kontaminierten Grundwasser durchflossen wird (siehe Abbildung 1a).

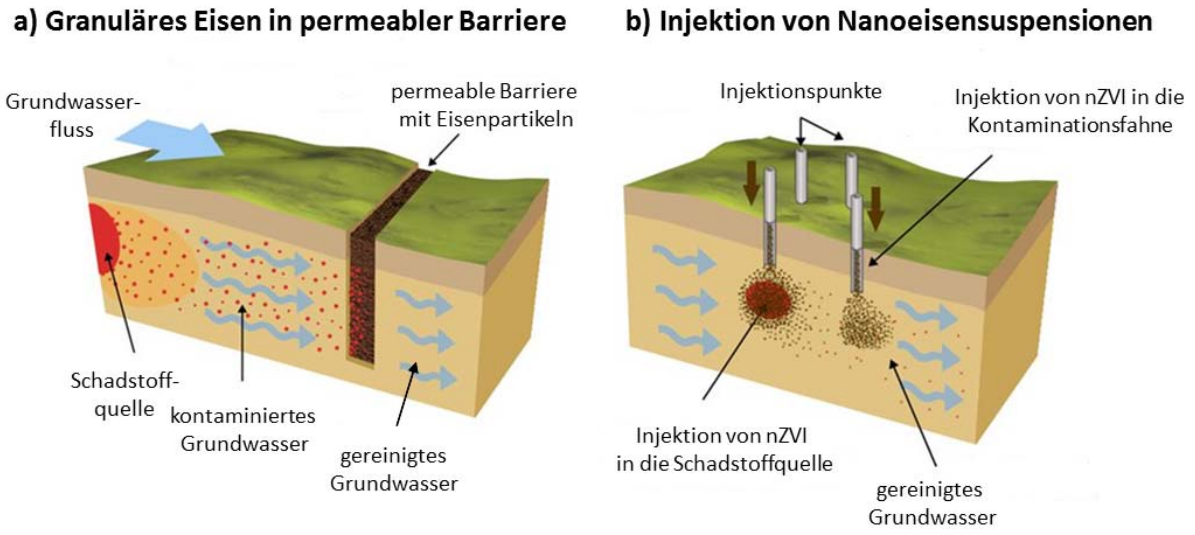

Abbildung 1 - Schematische Darstellung der *In-situ*-Sanierung mit a) granulärem Eisen in einer permeablen Barriere und b) durch Injektion von nanopartikulärem Eisen (nZVI) (abgeändert nach Crane [28]).

Da der Abbau der Schadstoffe an der Eisenoberfläche stattfindet, sind die Reaktionsraten abhängig von den angewandten Eisenoberflächenkonzentrationen. Mit granulären Partikeln, die eine verhältnismäßig kleine spezifische Oberfläche aufweisen (circa 0,04 bis 4 $m^2\ g^{-1}$) ist folglich die Reinigungsleistung stark limitiert [15,29,30]. Heutzutage ist daher der Einsatz von nanoskaligen elementaren Eisenpartikeln (nZVI) dominierend. Im Vergleich zu granulärem Eisen weisen diese eine um 10–100-fach höhere spezifische Oberfläche auf (10–50 $m^2\ g^{-1}$), wodurch bei gleicher eingesetzter Eisenmenge wesentlich höhere Geschwindigkeits-

konstanten erreicht werden [29]. Neben der hohen Reaktivität bieten Eisennanopartikel weiterhin den Vorteil, dass sie als kolloidale Suspensionen in die kontaminierte Zone injiziert werden können, wodurch auch Kontaminationen in tieferen oder bebauten Bereichen erreichbar werden (siehe Abbildung 1b) [28].

2.2.1. Reduktion chlorierter Ethene an Eisenpartikeln

An der Grenzfläche Wasser/Eisenoberfläche werden PCE und TCE bei einem stöchiometrischen Eisenüberschuss überwiegend zu chlorfreien C_2-Kohlenwasserstoffen reduziert (Produktanteil > 80 %), während partiell chlorierte Ethene, wie Dichlorethene oder Vinylchlorid lediglich in sehr geringen Mengen gebildet werden [17,31,32]. Die Tatsache, dass beim Schadstoffabbau kaum unerwünschte chlorierte Nebenprodukte entstehen, kann darauf zurückgeführt werden, dass die Dechlorierung von PCE und TCE vor allem über den Mechanismus der beta-Eliminierung und nur in geringem Ausmaß über eine direkte Hydrogenolyse verläuft (siehe Abbildung 2).

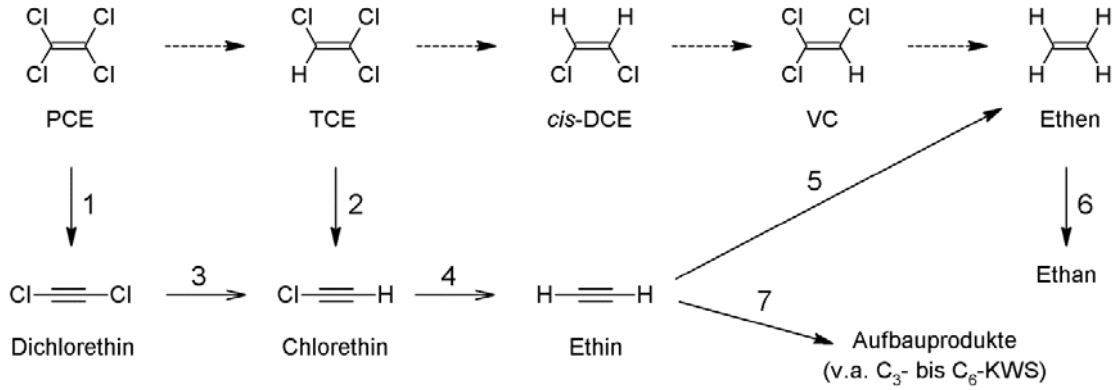

Abbildung 2 - Hauptreaktionswege der reduktiven Dechlorierung von PCE bzw. TCE mit Eisen unter anoxischen Bedingungen: Beta-Eliminierung (1, 2) mit anschließender Hydrogenolyse (3, 4) und Hydrierung (5, 6) sowie radikalischer Addition (7).

Bei der beta-Eliminierung werden zwei Chloratome unter der Bildung einer weiteren C-C-Bindung abgespalten (Schritte 1 und 2) [32]. Die dabei gebildeten, kurzlebigen Intermediate Dichlorethin bzw. Chlorethin reagieren anschließend via Hydrogenolyse zu Ethin (Schritte 3 und 4), welches weiter zu Ethen und Ethan hydriert werden kann (Schritte 5 und 6). Durch die Rekombination von intermediär gebildeten Radikalen oder deren Addition an ungesättigte

Intermediate werden außerdem chlorfreie Aufbauprodukte, vor allem C_3- bis C_6-Kohlenwasserstoffe gebildet (Schritt 7).

Die Produktselektivität der Dechlorierungsreaktion wird unter anderem von der Struktur bzw. den Oberflächeneigenschaften der Eisenpartikel beeinflusst [17]. Während bei thermisch hergestellten kristallinen Eisenpartikeln vor allem Ethen als Hauptprodukt der Dechlorierung gebildet wird, können bei amorphem Nanoeisen, welches mittels Natriumborhydrid synthetisiert wird ($nZVI_{NaBH4}$), stärker hydrierte Produkte, wie Ethan sowie ein höherer Produktanteil von C_3- bis C_6-Kohlenwasserstoffen detektiert werden. Die Unterschiede werden zum Teil auf die katalytische Wirkung des eingebrachten Bors in der Eisenstruktur zurückgeführt [17].

Bei der reduktiven Dechlorierung sind als reaktive Spezies sowohl Elektronen als auch reaktive Wasserstoffspezies beteiligt, die in Abhängigkeit von den Reaktionsbedingungen dominieren [33]. Elektrochemische Untersuchungen von Wang und Farrell zeigen, dass die Reduktion von TCE bei niedrigen pH-Werten vor allem über atomaren Wasserstoff erfolgt, während bei neutralen pH-Werten beide reaktive Spezies beteiligt sind. Im Gegensatz dazu verläuft die Reduktion von PCE sowohl unter sauren als auch neutralen Bedingungen vorwiegend über den direkten Elektronentransfer [33].

Kinetik der CKW-Dechlorierung

Wird Eisen im Vergleich zum Schadstoff im deutlichen stöchiometrischen Überschuss eingesetzt, sodass die Eisenkonzentration während der Reaktion nahezu konstant bleibt, so kann für die Dechlorierungsreaktion eine Kinetik pseudo-erster Ordnung bezüglich der Konzentration des eingesetzten chlorierten Kohlenwasserstoffs beobachtet werden (Gleichung 1 und Gleichung 2).

$$R\text{-}Cl + Fe^0 + H_2O \xrightarrow{k_{beob}} Fe^{2+} + R\text{-}H + OH^- + Cl^- \qquad \text{Gleichung 1}$$

$$\frac{dc_{CKW}}{dt} = -k_{beob} \cdot c_{CKW} \qquad \text{Gleichung 2}$$

k_{beob} messbare Geschwindigkeitskonstante pseudo-erster Ordnung [h^{-1}]

c_{CKW} Konzentration des gelösten chlorierten Kohlenwasserstoffs [g l^{-1}]

Um verschiedene Eisenpartikel bezüglich ihrer Reaktionskinetik vergleichen zu können, wird unter Berücksichtigung der Eisenkonzentration eine Reaktionskonstante zweiter Ordnung gebildet. Üblicherweise wird eine Normierung der beobachteten Geschwindigkeitskonstante erster Ordnung k_{beob} auf die spezifische Eisenoberflächenkonzentration σ_{Fe} angewendet, sodass von der Oberflächenkonzentration unabhängige, oberflächenspezifische Geschwindigkeitskonstanten erhalten werden (Gleichung 3) [34].

$$k_{SA} = \frac{k_{beob}}{S_{m,Fe} \cdot c_{Fe}} = \frac{k_{beob}}{\sigma_{Fe}}$$ Gleichung 3

k_{SA}	oberflächenspezifische Geschwindigkeitskonstante [l h^{-1} m^{-2}]
$S_{m,Fe}$	spezifische massebezogene Eisenoberfläche [m^2 g_{Fe}^{-1}]
c_{Fe}	Konzentration des Eisens [g l^{-1}]
σ_{Fe}	Oberflächenkonzentration von Eisen in Suspension [m^2 l^{-1}]

Oberflächennormierte Geschwindigkeitskonstanten für den Abbau von PCE und TCE mit sowohl Mikro- als auch Nanoeisen liegen im Bereich von $1 \cdot 10^{-3}$ bis $1 \cdot 10^{-4}$ l h^{-1} m^{-2} [35]. Für sehr reines oder oberflächenpassiviertes Eisen wurden auch deutlich niedrigere Geschwindigkeitskonstanten von bis zu $1 \cdot 10^{-6}$ l h^{-1} m^{-2} gefunden [15,36].

2.2.2. Anaerobe Korrosion von Eisen als unerwünschte Nebenreaktion

Die hohe Reaktivität von Eisen ist nicht nur auf bestimmte Zielschadstoffe gerichtet, sondern führt auch zu Reaktionen des Metalls mit verschiedensten Grundwasserbestandteilen, vor allem mit Wasser selbst. Die Reaktion von Eisen mit Wasser unter den im Aquifer typischen anoxischen Bedingungen wird als anaerobe Korrosion bezeichnet und führt zur Bildung von molekularem Wasserstoff (Gleichung 4).

$$Fe^0 + 2\ H_2O \longrightarrow Fe^{2+} + H_2 + 2\ OH^-$$ Gleichung 4

Einerseits wird durch die anaerobe Korrosion das reduktive Potenzial des Reduktionsmittels nicht vollständig ausgenutzt, was vor allem in Anbetracht der kostenintensiven Synthese von Nanoeisenpartikeln nicht hinnehmbar ist. Andererseits kann es durch die unerwünschte Gasbildung und Präzipitationen in der reaktiven Barriere zu Clogging-Effekten kommen, wobei Fließwege behindert werden und der Sanierungserfolg beeinträchtigt wird [37].

Als Reaktion an der Grenzfläche Wasser/Eisenoberfläche hängt die anaerobe Korrosion sowohl von den Partikeleigenschaften als auch von der Zusammensetzung des umgebenden wässrigen Mediums ab. Nanoeisenpartikel, welche durch die Reduktion mit Natriumborhydrid hergestellt wurden, sind aufgrund ihrer amorphen Struktur wesentlich korrosionsanfälliger als thermisch hergestellte, kristalline Partikel [17,38]. Ubiquitäre Grundwasserbestandteile, wie Hydrogen-carbonate/Carbonate, natürliche organische Materie, aber auch ein niedriger pH-Wert der wässrigen Phase können den Eisenverbrauch durch anaerobe Korrosion beschleunigen. Daneben beeinflusst die Schadstoffkonzentration das Korrosionsverhalten der Eisenpartikel. Mit sinkender TCE-Konzentration nimmt der Anteil der anaeroben Korrosion im Verhältnis zum Gesamteisenverbrauch zu [39].

Die unerwünschte anaerobe Korrosion stellt keine vernachlässigbare Nebenreaktion dar, wie unter anderem Studien von Fan et al. oder Schöftner et al. zeigen [16,40]. Über 95 % der Reduktionsäquivalente des eingesetzten Nanoeisens werden durch die Reaktion mit Wasser verbraucht. Außerdem wird durch die parasitäre Reaktion die Lebensdauer der Nanopartikel auf wenige Stunden bis hin zu wenigen Wochen beschränkt und somit die Effizienz der Sanierung maßgeblich beeinträchtigt [15–18,38,41].

2.2.3. Einfluss von Schwefelspezies auf die Reaktivität von Eisenpartikeln

In den letzten zehn Jahren gab es vielfältige Bestrebungen, Nanoeisenpartikel hinsichtlich ihrer Reaktivität gegenüber Schadstoffen zu optimieren. Die in der Literatur beschriebenen Methoden basieren meist auf dem Zusatz von katalytisch aktiven Edelmetallen (Palladium, Platin, Silber), der Veränderung der Oberflächeneigenschaften mit Hilfe von Polymeren (Carboxymethylcellulose, Polyacrylsäure) oder dem Aufbringen oxidischer oder kohlenstoff-haltiger Schichten [6,42]. Entscheidend für einen Sanierungserfolg ist jedoch nicht nur die hohe Reaktivität der Eisenpartikel, sondern auch die Selektivität zugunsten des Schadstoffabbaus

gegenüber unerwünschten Nebenreaktionen, wie der anaeroben Korrosion. Vor allem in Anbetracht der oftmals kostenintensiven Synthese der Nanoeisenpartikel ist die Erzeugung eines korrosionsstabilen und dechlorierungseffizienten Reagenzes erstrebenswert.

Eine sehr vielversprechende Möglichkeit, Eisenpartikel hinsichtlich ihrer Reaktivität gegenüber Schadstoffen und Wasser zu optimieren, besteht in der Modifikation der Eisenpartikel mit schwefelhaltigen Verbindungen. Bereits frühe Studien weisen darauf hin, dass der eisenbasierte Abbau chlorierter Ethene durch die Zugabe von Natriumsulfid deutlich beschleunigt werden kann [43,44]. Auch die geringe Korrosionsneigung und die damit einhergehende lange Lebensdauer von „reactive nanoscale iron particles“ (RNIP, Toda Kogyo Corp.) im wässrigen, anoxischen Medium kann möglicherweise auf die herstellungsbedingte Anwesenheit von Schwefel in der Partikelstruktur (> 1000 ppm) zurückgeführt werden [45,46].

Die gezielte Modifikation von Eisenpartikeln durch verschiedene Schwefelspezies ist jedoch erst in den letzten Jahren in den Fokus der Forschung geraten [19,20]. Bei der sogenannten „Sulfidierung“ werden Schwefelverbindungen meist in ihrer reduzierten Form, zum Beispiel als Sulfid, Dithionit oder Thiosulfat, während der wässrigen Synthese der Nanoeisenpartikel oder direkt vor dem Schadstoffabbau zum Reaktionsmedium zugesetzt [19,20]. Unter Verbrauch von metallischem Eisen kommt es an der Oberfläche zur Bildung von amorphem bzw. nanokristallinem Mackinawit (FeS), Di- und Polysulfiden, wie zum Beispiel Pyrit (FeS_2) oder Greigite (Fe_3S_4) [47–49]. Der Effekt der Sulfidierung auf die Reaktivität von Eisen hängt dabei weniger von der Art der eingesetzten reduzierten Schwefelspezies und der Sulfidierungstechnik als von der Konzentration des Additivs ab. Als Maß für die Schwefeldosierung wird in der Literatur das molare Verhältnis von Schwefel zu Eisen (S/Fe) angegeben, welches jedoch nur bedingt aussagekräftig ist, da Unterschiede in Partikelgröße und -oberfläche zwischen verschiedenen Nanoeisenpartikeln nicht berücksichtigt werden. Häufig werden in den Studien jedoch keine Partikelgrößen angeben, sodass der S/Fe-Quotient als einzige Charakterisierungsgröße herangezogen werden kann.

Tendenziell kann für die Reduktion von TCE bei einem niedrigen Sulfidierungsgrad der Eisenpartikel von S/Fe = 0,02–0,25 eine 10 bis 60-fach erhöhte Dechlorierungsrate im Vergleich zu unbehandeltem Eisen beobachtet werden [44,47–49]. Als Ursache für den beschleunigten Abbau von TCE wird vor allem die Anwesenheit von FeS an der Eisenoberfläche gesehen.

Eisen(II)-Spezies besitzen eine deutlich höhere Leitfähigkeit als oberflächengebundene Eisen(III)-Oxide mit Halbleitereigenschaften [50,51], sodass der Elektronentransport vom Eisenkern zum Schadstoff begünstigt wird. Die Anwesenheit von Schwefelspezies macht die Eisenoberfläche zudem hydrophober, was einerseits die Physisorption organischer Schadstoffe erhöht und andererseits die Sorption von Wassermolekülen hemmt [52].

Neben der Beschleunigung der Dechlorierungsreaktion konnte in verschiedenen Studien die Absenkung der anaeroben Korrosion der Nanoeisenpartikel um maximal den Faktor drei beobachtet werden [47–49]. Eine Ausnahme stellt die Studie von Fan et al. dar, in der die Anwendung hoher Dosen von Sulfid oder Dithionit (S/Fe > 0,33) zu einer starken Absenkung der Korrosion und einer gleichbleibenden Dechlorierungsaktivität führte [40]. Hierbei wurde jedoch ein sehr korrosionsanfälliges Eisen verwendet (Halbwertszeit der unbehandelten Eisenpartikel $t_{1/2}$ = 0,4 d) und das Korrosionsverhalten lediglich über einen Zeitraum von zwei Tagen verfolgt, sodass die Daten nur begrenzt aussagekräftig sind. Als Ursache für die Senkung der anaeroben Korrosion wird neben der erhöhten Hydrophobie der Oberfläche die Unterdrückung der Rekombination von aktiven Wasserstoffspezies zu molekularem Wasserstoff gesehen [47,53].

Eine Sulfidierung von Eisenpartikeln unter anoxischen Bedingungen kann jedoch auch zu unerwünschten Effekten führen. So zeigt die elektrochemische Studie von Turcio-Ortega et al. eine erhöhte Korrosionsanfälligkeit der Eisenpartikel in Gegenwart von Natriumsulfid im Vergleich zu unbehandeltem nanoskaligen Eisen [54]. In einer Studie von Hansson et al. wird die Sulfidierung von mikroskaligem Eisen beschrieben, die zunächst die erwünschte Passivierung des Eisens bewirkt, aber nach einigen Tagen zu einer Erhöhung der Korrosionsaktivität führt [55]. Dieser Vorgang wird auf die Ablösung der Eisensulfidschicht und der damit verbundenen Freilegung der ungeschützten und korrosionsanfälligen Eisenoberfläche zurückgeführt. Auch in der Praxis ist die beschleunigte Korrosion eisenbasierter Materialien in Gegenwart von Sulfid bekannt. Im Rahmen der „chemisch mikrobiell beeinflusste Korrosion“ werden Eisenstrukturen durch bakteriell gebildetes Sulfid angegriffen und führen zu Lochfraßkorrosion [56].

Fan et al. führen die unterschiedlichen Auswirkungen von reduzierten Schwefelspezies auf das Korrosionsverhalten auf die Art der an der Oberfläche gebildete FeS-Schicht zurück. Sie nehmen an, dass bei der Zugabe von Sulfid zu einer Nanoeisensuspension in einem initialen Schritt

zunächst HS^--Ionen an der Eisenoberfläche adsorbieren, welche die OH^--Ionen an der Eisenoberfläche ersetzen und anschließend eine dünne primäre Schicht FeS formen. Durch die erhöhte lokale Acidität wird die Korrosion von Eisen erhöht, wodurch Fe(II) gebildet wird, welches weiter mit HS^- reagieren kann und weiteres FeS bildet. Sekundär gebildetes FeS ist nach Fan et al. dagegen in der Lage, eine schützende Hülle zu bilden und die anaerobe Korrosion zu unterdrücken [19].

Während verschiedene Studien die Sulfidierung reiner Eisenpartikel näher thematisieren [19,20], sind die Auswirkungen von Schwefelspezies auf das Reaktionsverhalten von Eisen-Aktivkohle-Systemen, wie Carbo-Iron, noch nicht näher untersucht.

2.3. Eisen-Kohlenstoff-Systeme als neuartige *In-situ*-Reduktionsmittel

Reine Eisenpartikel weisen neben ihrer hohen Reaktivität mit Wasser einen weiteren wesentlichen Nachteil für die *In-situ*-Sanierung auf: die geringe Sorptionsaffinität von organischen Schadstoffen zur Metalloberfläche [7,57,58]. So ist zum Beispiel bei niedrigen Schadstoffkonzentrationen, wie sie etwa im Bereich der Schadstofffahne im Grundwasser üblich sind (wenige mg l^{-1}), der Abbau durch eine geringe Eisenoberflächenkonzentration beeinträchtigt. Die geringe Sorptionsaffinität führt außerdem zu einer geringen Aufenthaltsdauer der Schadstoffe in der reaktiven Zone, sodass der zur Verfügung stehende Zeitraum für einen chemischen Abbau verhältnismäßig kurz ist. Eine Möglichkeit, das Potenzial der Eisenpartikel effektiver zu nutzen, besteht in der Kombination des Reduktionsmittels mit kohlenstoffbasierten, sorptionsaktiven Materialien, wie Bio- oder Aktivkohle [10,59–67]. In Kompositpartikeln dient die Kohlenstoffkomponente dabei häufig als Trägermaterial für nano- und mikroskalige Eisencluster, aber auch eine Ummantelung der Eisenpartikel mit Kohlenstoff ist prinzipiell möglich. Im Mittelpunkt der vorliegenden Dissertation steht das Eisen-Aktivkohle-Komposit Carbo-Iron, welches eine Kombination aus kolloidaler Aktivkohle und eingebetteten Nanoeisenstrukturen darstellt und in Kapitel 2.3.1 näher vorgestellt wird.

In ihrer chemischen Reaktivität gegenüber Schadstoffen weisen Eisen-Aktivkohle-Komposite, wie Carbo-Iron und reine Metallpartikel, ein ähnliches Verhalten auf. So ist beispielsweise das Verbundmaterial in der Lage, chlorierte Ethene zu chlorfreien C_2-Kohlenwasserstoffen zu reduzieren, wobei lediglich eine minimale Bildung partiell chlorierter Intermediate zu

beobachten ist [10]. Ein Abbau chlorierter Ethene im wässrigen Milieu ist sogar mit Eisen-Kohlenstoff-Systemen möglich, wenn beide Komponenten nicht in permanentem Kontakt stehen, sondern lediglich miteinander kollidieren [13,14]. Das Produktspektrum ähnelt dabei dem der eisenbasierten Dechlorierung [13,14]. Die Tatsache, dass Eisen und Eisen-Kohlenstoff-Systeme eine vergleichbare chemische Reaktivität aufweisen, ist bemerkenswert, da davon ausgegangen werden kann, dass sich die bei der Dechlorierung ablaufenden Reaktionswege aufgrund der Sorptionskomponente unterscheiden. Während im Fall von reinem Eisen sowohl Adsorption und Reaktion der Kontaminanten an der Metalloberfläche erfolgen, findet bei Eisen-Aktivkohle-Systemen die Bildung reaktiver Spezies an der Eisenoberfläche und damit räumlich entfernt von den an der Aktivkohle adsorbierten Schadstoffen statt [13,14]. Dabei stellt sich die Frage, wie reaktive Spezies von ihrem Bildungsort zum Schadstoff gelangen und welche Rolle dabei das Trägermaterial spielt.

Generell sind kohlenstoffbasierte Materialien in der Lage, aktiv an chemischen Reaktionen teilzunehmen bzw. diese sogar zu beschleunigen. Dies gilt beispielsweise für die Hydrolyse von 1,1,2,2-Tetrachlorethan [68,69] oder die Reduktion von Nitroaromaten in Gegenwart von Sulfid [70–73]. Eine entscheidende Rolle spielen dabei die Struktur- bzw. Oberflächeneigenschaften der Kohlenstoffkomponente. So ist bekannt, dass Fehlstellen in der graphitischen Struktur, ungesättigte Valenzen der Randatome oder die Anwesenheit von Heteroatomen bzw. funktionellen Gruppen den Ablauf chemischer Reaktionen beeinflussen [74]. Inwiefern Aktivkohle die Selektivität und Kinetik der eisenbasierten Dechlorierung von PCE und TCE beeinflusst und welche Rolle dabei sauerstoffhaltige funktionelle Gruppen an der Kohlenstoffoberfläche spielen, stellt einen Schwerpunkt der vorliegenden Dissertation dar. Ein Überblick über wichtige sauerstoffhaltige funktionelle Gruppen an der Oberfläche kohlenstoffbasierter Materialien wird in Abbildung 3 gegeben. Für die Beeinflussung chemischer Reaktionen durch sauerstoffhaltige Oberflächengruppen sind vor allem redoxaktive Gruppen, wie z.B. Chinon/Hydrochinon-Gruppen relevant. Diese sind in der Lage, als Redoxmediatoren einen Elektronentransfer zwischen Kohlenstoff und Reduktionsmittel bzw. Kohlenstoff und Schadstoff zu vermitteln [73,75,76].

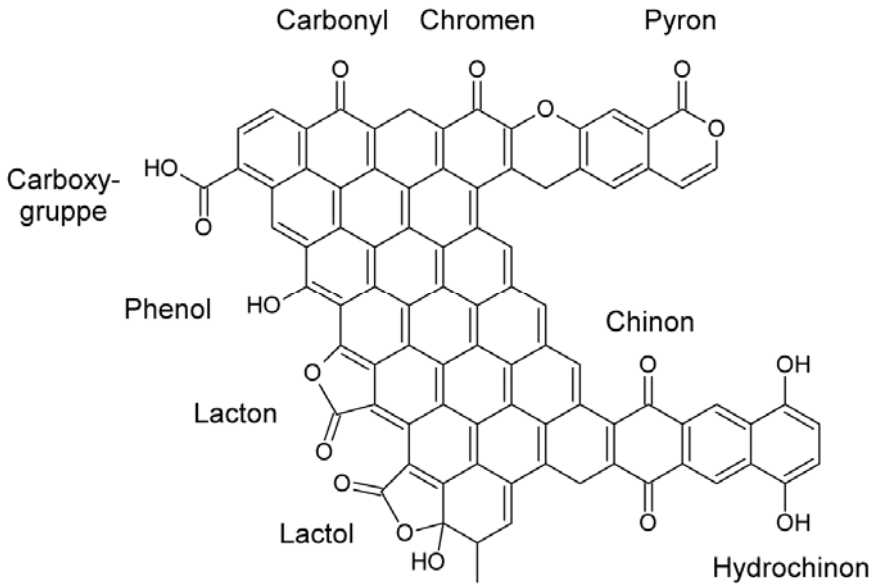

Abbildung 3 - Sauerstoffhaltige funktionelle Gruppen an der Aktivkohleoberfläche.

Neben der Übertragung reaktiver Spezies zwischen Aktivkohle und Oxidations- bzw. Reduktionsmittel, ist für den Ablauf einer chemischen Reaktion auch der Transport der Spezies innerhalb bzw. auf dem Sorbens entscheidend. Elektronen, als eine Form reaktiver Spezies, können innerhalb elektrisch leitfähiger Modifikationen des Kohlenstoffs, wie Aktivkohle oder Graphit, im Leitungsband transportiert werden. Im Gegensatz dazu findet in Gegenwart eines nichtleitenden Sorptionsmittels und Eisenpartikeln kein Schadstoffabbau statt [14]. Neben dem Transport von Elektronen könnte möglicherweise auch der Transfer von reaktiven Wasserstoffspezies vom Eisen zum Schadstoff über die Kohlenstoffkomponente erfolgen, wie Tang et al. und Kopinke et al. vorschlagen. Während der Transport von Wasserstoffspezies an Graphit im wässrigen Medium gezeigt werden konnte [77], fehlt bislang ein klarer Nachweis für den Wasserstoff-Spillover an Aktivkohle in wässriger Phase [13,14,77].

2.3.1. Partikeleigenschaften und Reaktionsverhalten von Carbo-Iron

Carbo-Iron stellt ein neuartiges Reagenz für die *In-situ*-Grundwassersanierung dar und besteht aus kolloidaler Aktivkohle, in deren Porenstruktur Nanoeisenstrukturen eingebettet sind (siehe Abbildung 4). Das Material wurde bereits intensiv unter Labor- und Feldbedingungen untersucht und hat sich für den Abbau chlorierter Ethene im Aquifer als geeignet herausgestellt [9–12].

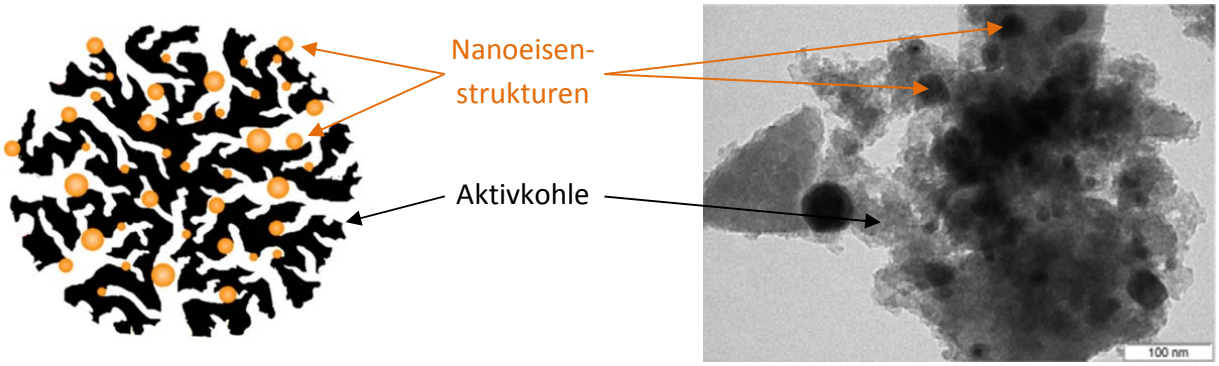

Abbildung 4 - Links: die schematische Darstellung von Carbo-Iron. Rechts: eine TEM-Aufnahme des Kompositmaterials aus Mackenzie et al. [11].

Hergestellt werden die Partikel, indem Aktivkohlekolloide mit gut wasserlöslichen Eisensalzen, wie $Fe(NO_3)_3 \cdot 9\ H_2O$ oder $FeCl_3$ imprägniert und anschließend thermisch reduziert werden [9]. Einerseits ist die Reduktion durch molekularen Wasserstoff bei Temperaturen um 500 °C möglich, andererseits kann metallisches Nanoeisen durch das *in situ* gebildete Kohlenmonoxid bei Temperaturen ab 700 °C gebildet werden. Die physikalischen und chemischen Eigenschaften der synthetisierten Partikel sind in Tabelle 1 zusammengefasst. In Abhängigkeit von den Herstellungsbedingungen kann es zu geringfügigen Variationen kommen.

Tabelle 1 - Physikalische und chemische Eigenschaften von Carbo-Iron [9,11].

Parameter	**Wert**
BET-Oberfläche (N_2-Sorption bei 77 K) [$m^2\ g^{-1}$]	600–800
Partikelgröße [µm]	d_{50} = 0,8–1,3
Materialdichte [$g\ cm^{-3}$]	≈ 2,9
Dichte wassergefüllter Partikel [$g\ cm^{-3}$]	≈ 2
Fe^0-Gehalt [Ma.-%]	15–25
Kohlenstoffgehalt [Ma.%]	50–60
Gesamtporenvolumen [$cm^3\ g^{-1}$]	0,6
Mittlerer Porendurchmesser [nm]	4
Zeta-Potenzial [mV]*	-55 ± 5

* bei pH = 7,5; $c_{Carbo\text{-}Iron}$ = 1 g l^{-1}; c_{CMC} = 0,2 g l^{-1}; c_{KNO3} = 10 mM

Das Kompositmaterial eignet sich sowohl für die Quellen- als auch für die Fahnensanierung und bietet im Vergleich zu Nanoeisen wesentliche Vorteile. So kann die Aktivkohle aufgrund ihrer Sorptionsaktivität Schadstoffe in der räumlichen Nähe zu den reaktiven Eisenzentren anreichern und somit den Reinigungsprozess unterstützen. Außerdem begünstigen die geringe Dichte sowie die negative Oberflächenladung den Transport der Partikel im Aquifer, während die erhöhte Hydrophobizität des Materials eine bessere Benetzung mit einer organischen Schadstoffphase erlaubt.

Carbo-Iron weist eine ähnliche chemische Reaktivität wie ungeträgertes Nanoeisen auf und ist unter anderem in der Lage, chlorierte Ethene vor allem zu chlorfreien C_2-Kohlenwasserstoffen, wie Ethen und Ethan zu reduzieren, während die Bildung partiell chlorierter Intermediate vernachlässigbar ist [10].

Kinetik der CKW-Dechlorierung

Wie bei reinem Nanoeisen folgt auch im Eisen-Aktivkohle-System der Schadstoffabbau einer Kinetik pseudo-erster Ordnung bezüglich der CKW-Konzentration, sofern Eisen in einem deutlichen stöchiometrischen Überschuss eingesetzt wird und die Metallkonzentration während der Dechlorierung nahezu konstant bleibt. Im Unterschied zur Reaktionskinetik an reinem Nanoeisen ist mit Carbo-Iron die Dechlorierungsgeschwindigkeit über einen weiten Bereich der eingesetzten Carbo-Iron-Konzentration konstant und damit unabhängig von der Eisenkonzentration in Suspension. Sofern der überwiegende Teil des CKW am Carbo-Iron adsorbiert ist ($c_{CKW,ads} >> c_{CKW,gelöst}$) und ausreichend Eisen für die reduktive Dechlorierung zu Verfügung steht, wird $k_{beob} = k' \cdot x_{Fe}$ nicht durch die Eisenkonzentration in Suspension, sondern durch den Eisengehalt des Kompositmaterials bestimmt (mit $c_{CKW,ads} \approx \frac{c_{CKW,ges}}{c_{Carbo\text{-}Iron}}$ und $x_{Fe} = \frac{c_{Fe}}{c_{Carbo\text{-}Iron}}$) (siehe Gleichung 5 bis Gleichung 7). Vor allem bei niedrigen Schadstoffkonzentrationen kann durch die sorptive Anreicherung der hydrophoben Kontaminanten eine sehr effiziente Ausnutzung der Reduktionsäquivalente des Eisens erfolgen [10].

$$\frac{dc_{CKW}}{dt} = -k' \cdot c_{Fe} \cdot c_{CKW,ads} \qquad \text{Gleichung 5}$$

$$\frac{dc_{CKW}}{dt} = -k' \cdot x_{Fe} \cdot c_{CKW,ges} \qquad \text{Gleichung 6}$$

$$\ln \left(\frac{c_{CKW,0}}{c_{CKW,t}}\right)_{total} = k_{beob} \cdot t \qquad \text{Gleichung 7}$$

k'	Geschwindigkeitskonstante zweiter Ordnung [l g^{-1} h^{-1}]
c_{Fe}	Konzentration des nullwertigen Eisens in Suspension [g l^{-1}]
$c_{CKW,ads}$	lokale Konzentration des adsorbierten CKW [g_{CKW} $g_{Carbo\text{-}Iron}^{-1}$]
$c_{CKW,ges}$	Konzentration des CKW in Suspension [g l^{-1}]
k_{beob}	messbare Geschwindigkeitskonstante pseudo-erster Ordnung [h^{-1}]
x_{Fe}	Massenanteil von nullwertigem Eisen in Carbo-Iron [g_{Fe} $g_{Carbo\text{-}Iron}^{-1}$]
t	Reaktionszeit [h^{-1}]

Die Form des Geschwindigkeitsgesetzes für die Dechlorierung mit Carbo-Iron (Gleichung 6) erscheint zunächst ungewöhnlich, weil die Konzentration des Reagenz in der wässrigen Suspension nicht explizit eingeht. Man kann diesen experimentell verifizierten Befund mit folgender Vorstellung veranschaulichen: Für die Reaktionsgeschwindigkeit im Carbo-Iron-Partikel ist nicht die Gesamtkonzentration des CKW in Suspension, sondern seine lokale Konzentration ($c_{CKW,ads}$) relevant. Erhöht man nun die Carbo-Iron-Konzentration in Suspension, erhöht man zwar die Anzahl der Carbo-Iron-Partikel, aber man verringert im gleichen Maß die lokale CKW-Konzentration durch „Verdünnung“. Beide Effekte kompensieren sich in ihrer Wirkung auf die Gesamtreaktionsgeschwindigkeit.

2.4. Mikrobiologischer Abbau chlorierter Ethene in Grundwasser

2.4.1. Grundlagen der mikrobiologischen Dechlorierung

Bis Anfang der 1980er Jahre wurde angenommen, dass Chlorethene nicht biologisch abbaubar sind. Diese Annahme schien bis dahin gerechtfertigt, da diese Substanzen nicht natürlich in der Biosphäre vorkommen [78]. Heute ist hinreichend bewiesen, dass der biologische Abbau von

PCE und TCE in kontaminierten Aquiferen möglich ist, jedoch sind die Verbindungen im Vergleich zu halogenfreien Kohlenwasserstoffen relativ schwer und nur unter besonderen Milieubedingungen abbaubar [5]. Der bakterielle Abbau verläuft in kontaminierten Aquiferen vor allem über die anaerob-reduktive Dechlorierung, wobei schrittweise ein Chloratom durch ein Wasserstoffatom ersetzt wird (Abbildung 5). Dichlorethene treten als Intermediate bzw. Endprodukte vor allem als *cis*-Isomer auf, während die Bildung von *trans*-DCE und 1,1-DCE lediglich in Ausnahmefällen beobachtet wird [79].

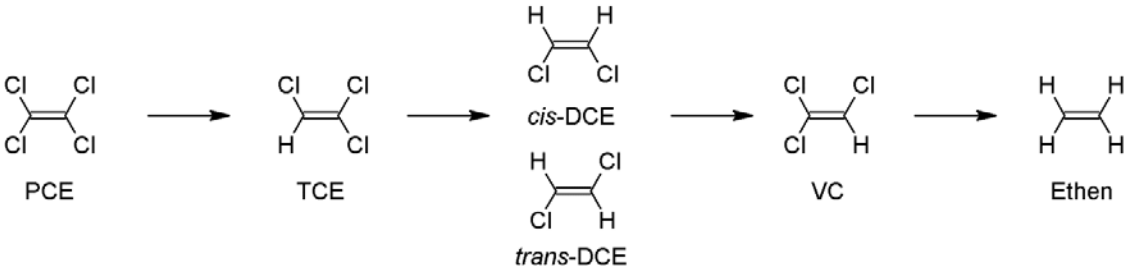

Abbildung 5 - Mikrobiologische Dechlorierung von PCE unter anoxischen Bedingungen über partiell chlorierte Intermediate bis zum Ethen als Endprodukt.

Der Prozess kann zwar prinzipiell cometabolisch verlaufen, erfolgt aber überwiegend durch Organohalidrespiration, eine spezielle Form der anaeroben Atmung. Die dabei beteiligten organohalid-respirierenden Bakterien (OHRB) sind in der Lage, Elektronen von einem Elektronendonator wie molekularem Wasserstoff auf die chlorierten organischen Verbindungen zu übertragen. Dabei ist die reduktive Dehalogenierung an die Energiekonservierung über Elektronentransportphosphorylierung gekoppelt [80,81]. Verschiedenste Mikroorganismen, wie z.B. *Geobacter*, *Desulfitobacterium* oder *Sulfospirillum* können PCE oder TCE zu *cis*-DCE dechlorieren, während zur weiteren Dechlorierung des *cis*-DCE über Vinylchlorid zu Ethen lediglich einzelne Vertreter der Gattung *Dehalococcoides* befähigt sind. Die nach bisherigem Wissensstand einzige Spezies, die PCE vollständig zu Ethen abbauen kann, ist *Dehalococcoides mccartyi* [82].

Generell ist der mikrobiologische Abbau chlorierter Ethene stark abhängig von den Redox-bedingungen im Aquifer. Dabei sind mit sinkendem Chlorierungsgrad der Chlorethene stärker reduzierende Bedingungen für den Abbau notwendig, sodass beispielsweise die Reduktion von

cis-DCE und Vinylchlorid lediglich unter sulfatreduzierenden und methanogenen Bedingungen abläuft. Der Abbau der niederchlorierten Verbindungen erfolgt wesentlich langsamer als die Reduktion der höher chlorierten Kontaminanten PCE oder TCE, was eine Ursache für die in der Praxis häufig zu beobachtende Akkumulation der toxischen Intermediate ist [5]. Diese kann außerdem durch die mangelnde Verfügbarkeit des Elektronendonators Wasserstoff sowie durch die Anwesenheit alternativer Elektronenakzeptoren, wie Nitrat oder höher chlorierter Ethene verstärkt werden [78].

Neben dem Abbau der chlorierten Ethene über die reduktive Dechlorierung ist vor allem für die niederchlorierten Intermediate der oxidative Abbau relevant. Der cometabolische Abbau ist eingeschränkt für TCE, vor allem aber für *cis*-DCE und Vinylchlorid relevant, während der metabolische Abbau lediglich für *cis*-DCE und Vinylchlorid möglich ist [83]. Dabei entstehen, ohne die Akkumulation toxischer Metabolite, Endprodukte wie Chlorid, Kohlenstoffdioxid und Wasser. Der für die Oxidation notwendige Sauerstoff ist jedoch meist im Bereich der Schadstoffquelle limitiert, sodass der Prozess nur eingeschränkt ablaufen kann. Prinzipiell können aber die mit dem Grundwasserfluss transportierten Intermediate in oxische Bereiche der Fahne gelangen, wo der finale Abbau erfolgen kann.

2.4.2. Einfluss von Eisenpartikeln auf den biotischen Abbau chlorierter Ethene

Mit der Injektion eines eisenbasierten Reagenzes in den Aquifer kommt es aufgrund der hohen Reaktivität des Metalls nicht nur zu Reaktionen mit organischen Schadstoffen, sondern auch zu Wechselwirkungen mit verschiedensten Grundwasserbestandteilen, wodurch potenziell auch der mikrobiologische Schadstoffabbau beeinflusst werden kann. Um idealerweise biologische und chemische Abbauwege miteinander zu kombinieren, aber auch um unerwünschte Folgen zu vermeiden, ist es notwendig, bei einer chemischen Sanierung die ablaufenden mikrobiologischen Vorgänge zu berücksichtigen.

Aktuelle Laborstudien zeigen, dass die Anwesenheit von Nanoeisenpartikeln die mikrobiologische Dechlorierung einerseits beschleunigen, andererseits aber auch inhibieren kann [21,22,84]. Die Hemmung der mikrobiologischen Aktivität ist auf die hohe Reaktivität des Nanoeisens und der daraus resultierenden zytotoxischen Wirkung der Partikel zurückzuführen [85–89]. Als Ursache für die Toxizität werden verschiedene Mechanismen diskutiert,

die meist auf der Zerstörung der Zellmembran sowie der Bildung reaktiver Sauerstoffspezies durch Eisenspezies basieren. Es wird angenommen, dass für die zytotoxische Wirkung der Nanoeisenpartikel der direkte Kontakt mit der Zelle gegeben sein muss. Diese Annahme wird durch die Tatsache unterstützt, dass der negative Effekt meist in Umweltmatrices, durch polymere Beschichtungen des Eisens oder beim Einsatz von Suspensionsstabilisatoren, wie Carboxymethylcellulose vermindert wird [90–93]. Des Weiteren wurde beobachtet, dass die Gegenwart von Nanoeisen bei *Dehalococcoides* spp. zur Senkung von Dechlorierungsraten sowie zur Herunterregulierung der Dehalogenase-Gene *tceA* und *vcrA* führt [91].

Nanoeisen hat wie grobpartikuläres Eisen jedoch auch die Möglichkeit, das Wachstum und die Aktivität von OHRB zu unterstützen [21,22,94–96]. So ist Nanoeisen in der Lage, mit verschiedenen Inhaltsstoffen des Grundwassers zu reagieren und die chemischen Bedingungen im Aquifer zu verändern. Beispielsweise reagieren die Partikel mit dem im Wasser gelösten Sauerstoff, welcher für obligat-anaerobe OHRB, wie z.B. *Dehalococcoides* spp. bereits in minimalen Mengen toxisch wirkt [97]. Außerdem weist Nanoeisen unter anoxischen Bedingungen eine hohe Reaktivität gegenüber Wasser auf, wobei molekularer Wasserstoff gebildet wird, der von OHRB als Elektronendonator verwendet werden kann. Dieser stellt im Aquifer oft einen limitierenden Faktor des mikrobiologischen Schadstoffabbaus dar [98,99]. Entscheidend dabei ist eine langsame und stetige Freisetzung des Elektronendonators, da bei einem geringen Partialdruck des Wasserstoffs OHRB gegenüber Methanogenen wettbewerbsfähiger sind [100]. Durch die Reaktion des Eisens mit leicht reduzierbaren Grundwasserbestandteilen werden außerdem stark reduzierende Bedingungen im Aquifer erreicht, die vor allem für den Abbau niederchlorierter Verbindungen relevant sind. So können die Intermediate *cis*-DCE und Vinylchlorid lediglich unter sulfatreduzierenden und methanogenen Bedingungen reduziert werden [25].

Während es zahlreiche Studien über die Interaktion von Mikroorganismen und Nanoeisen unter Laborbedingungen gibt, ist das Verhalten in der Praxis bislang kaum dokumentiert. In wenigen Feldstudien konnte jedoch gezeigt werden, dass es prinzipiell zu einer Unterstützung der mikrobiologischen Dechlorierung kommen kann [95,96]. In den von Nanoeisen beeinflussten Bereichen konnten ein erhöhtes Vorkommen von *Dehalococcoides* spp., des Vinylchlorid-

Reduktase-Gens sowie eine signifikante Veränderung der mikrobiologischen Gemeinschaft beobachtet werden [95].

Ein in der Literatur noch nicht diskutierter Themenbereich ist die Wechselwirkung von Eisen-Aktivkohle-Systemen wie Carbo-Iron und mikrobiologischem Schadstoffabbau. Im Gegensatz zu Eisenpartikeln stellt sich bei sorptionsaktiven Kompositmaterialien zunächst die Frage nach der biologischen Verfügbarkeit des Schadstoffes. Aufgrund der hohen Sorptionsaffinität werden hydrophobe organische Schadstoffe an der Aktivkohle vor allem in den Mikro- und Mesoporen (ca. 1–50 nm) adsorbiert, die für Mikroorganismen (ca. 1 µm) nicht zugänglich sind. Das Zusammentreffen von Schadstoffen und Mikroorganismen stellt, mit wenigen Ausnahmen, eine Grundvoraussetzung für einen biologischen Abbau dar. Die Studie von Aktaş et al. zeigt jedoch, dass an Aktivkohle sorbierte chlorierte Ethene prinzipiell biologisch verfügbar sind und der bakterielle Abbau stattfinden kann [101]. Auch das Prinzip der Bioregenerierung von Aktivkohle durch Mikroorganismen beweist, dass an der Aktivkohle adsorbierte Schadstoffe biologisch verfügbar sind [102]. Die Fragen, inwiefern der biologische Abbau chlorierter Ethene durch das Eisen-Aktivkohle-Komposit Carbo-Iron beeinflusst werden kann und welche möglichen Interaktionen zwischen *In-situ*-Reagenz und Mikroorganismen auftreten können, ist ein Schwerpunkt der vorliegenden Dissertation.

3. Praktischer Teil – Ergebnisse und Diskussion

Im folgenden Teil der vorliegenden Dissertation werden neue Erkenntnisse zum Verhalten von Eisen-Aktivkohle-Systemen für den Abbau chlorierter Ethene in Wasser beschrieben. Die Ergebnisse der Arbeit liegen in Form von drei Publikationen vor, welche in der Zeitschrift „Science of the Total Environment“ erschienen sind:

I. Acceleration of microiron-based dechlorination in water by contact with fibrous activated carbon

II. Sulfidation of ZVI/AC composite leads to highly corrosion-resistant nanoremediation particles with extended life-time

III. Combined chemical and microbiological degradation of tetrachloroethene during the application of Carbo-Iron at a contaminated field site

Während in der ersten Publikation der Einfluss von Aktivkohle auf die Selektivität und Kinetik der eisenbasierten Dechlorierung thematisiert wird, steht in zwei weiteren Veröffentlichungen das Kompositmaterial Carbo-Iron im Mittelpunkt. In ihnen werden die Optimierung des chemischen Reaktionsverhaltens der Partikel durch reduzierte Schwefelspezies und die Ergebnisse mikrobiologischer Untersuchungen während der praktischen Anwendung des *In-situ*-Reagenzes dargestellt. In den folgenden Absätzen werden die drei Schwerpunkte der Dissertation näher erläutert, bevor die Veröffentlichungen in voller Länge wiedergegeben werden.

I. Einfluss textiler Aktivkohle auf die eisenbasierte Reduktion chlorierter Ethene

In diesem Abschnitt der Arbeit wird der Einfluss von Aktivkohle auf die Kinetik und Selektivität der eisenbasierten Reduktion chlorierter Ethene näher betrachtet. Ziel dieser Untersuchungen ist es, ein besseres Verständnis für das Zusammenspiel der Komponenten zu entwickeln, um möglichst effiziente Eisen-Aktivkohle-Systeme gestalten zu können.

Um Informationen über die Einflussmöglichkeiten der Aktivkohle auf den eisenbasierten Schadstoffabbau zu gewinnen, wurde ein Modellsystem aus mikroskaligen Eisenpartikeln und textiler Aktivkohle untersucht. Dabei liegen die beiden Komponenten im Eisen-Aktivkohle-System in direktem Kontakt miteinander vor, sodass ein Transport reaktiver Spezies über

Partikelgrenzen hinweg vom Eisen zu den an der Aktivkohle sorbierten Schadstoffen möglich ist, der direkte Kontakt von Schadstoff und Eisenpartikel jedoch verhindert wird. Der Abbau von TCE und PCE wurde unter Verwendung verschiedener textiler Aktivkohlearten untersucht und in Verbindung zu ihren chemischen Oberflächeneigenschaften gebracht, wobei ein Schwerpunkt auf die sauerstoffhaltigen funktionellen Gruppen gelegt wurde. Die Quantifizierung des Sauerstoffanteils sowie die Charakterisierung der Gruppen erfolgten mittels temperaturprogrammierter Desorption/Pyrolyse. Anhand der experimentell erhaltenen Daten werden mögliche Reaktionsmechanismen diskutiert und Konsequenzen für die Gestaltung von Eisen-Aktivkohle-Systemen gezogen. Dabei wird erörtert, inwiefern Aktivkohle geeignet ist, die Effizienz der eisenbasierten Dechlorierung zu steigern.

II. Auswirkung reduzierter Schwefelspezies auf die chemische Reaktivität von Carbo-Iron

Die Optimierung von Carbo-Iron hinsichtlich seiner chemischen Reaktivität steht im Mittelpunkt des folgenden Abschnittes der Arbeit. Der unerwünschte Verbrauch von nullwertigem Eisen unter anoxischen Bedingungen im Aquifer durch die Reaktion mit Wasser beeinträchtigt maßgeblich die Effizienz einer Sanierung und tritt bei allen eisenbasierten *In-situ*-Reagenzien auf. Im Gegensatz zu Nanoeisen, welches durch die Reduktion mit Natriumborhydrid synthetisiert wurde, ist Carbo-Iron – als ein Beispiel für ein thermisch reduziertes Eisen-Aktivkohle-Komposit – zwar vergleichsweise korrosionsstabil, jedoch besteht auch für dieses Material der Bedarf einer Optimierung. Einen vielversprechenden Ansatz stellt die Modifizierung der Partikel mit reduzierten Schwefelspezies dar. Erst in kürzlich publizierten Studien konnte gezeigt werden, dass für $nZVI_{NaBH4}$ eine leichte Absenkung der anaeroben Korrosionsrate erzielt werden kann, während die Dechlorierung von TCE beschleunigt wird [19,20]. Es stellt sich die Frage, ob Schwefelspezies ebenfalls das Reaktionsverhalten von Eisen-Aktivkohle-Systemen optimieren können. Ziel dieser Untersuchungen ist es, das Eisen-Aktivkohle-Komposit so zu modifizieren, dass es sich durch eine geringe anaerobe Korrosion, eine hohe Dechlorierungseffizienz sowie durch eine lange Lebensdauer auszeichnet.

Die Auswirkungen von Art und Konzentration ausgewählter Schwefelverbindungen auf das Reaktionsverhalten der Partikel wurden in Batchversuchen in Kurz- und Langzeitexperimenten

untersucht. Dabei wurden der Abbau von PCE sowie die anaerobe Korrosion des enthaltenen Eisens näher betrachtet. Die Anwendung der Röntgenbeugungsanalyse an schwefel-modifizierten Partikeln unterstützt die Interpretation der experimentellen Daten.
Auf Basis der gewonnenen kinetischen Daten werden Dechlorierungseffizienzen bestimmt, welche die Ausnutzung der Reduktionsäquivalente des Eisens zeigen und somit den Einfluss der Modifikation durch Schwefelspezies verdeutlichen.

III. Einfluss von Carbo-Iron auf den mikrobiologischen Schadstoffabbau im Aquifer

In der dritten Publikation werden die mikrobiologischen Prozesse während bzw. nach einer chemischen Sanierungsmaßnahme mit Carbo-Iron näher betrachtet. Der erfolgreiche Einsatz des Eisen-Aktivkohle-Komposits bei einem mit PCE kontaminierten Feldstandort wurde bereits von Mackenzie et al. näher beschrieben [11]. Da der Eintrag des reaktiven *In-situ*-Reagenz in den Aquifer zu einer Veränderung der Grundwasserparameter führt, kann möglicherweise auch der mikrobiologische Schadstoffabbau beeinflusst werden. Während die Wechselwirkung von Nanoeisenpartikeln und Mikroorganismen im Aquifer in wenigen Studien beschrieben wurden [95,96], ist das Zusammenspiel von sorptionsaktiven Eisen-Aktivkohle-Kompositen und biotischen Vorgängen in der Literatur noch nicht dokumentiert. Um zukünftig abiotische und biotische Vorgänge bestenfalls synergistisch miteinander koppeln zu können, aber auch um unerwünschte Folgen auszuschließen, wird in diesem Teil der Arbeit die Interaktion von chemischen und biologischen Abbauvorgängen näher untersucht.
Am Beispiel des Feldstandortes Lohheide wird dargestellt, inwiefern sich die Aquifer-bedingungen nach der Injektion von Carbo-Iron verändern, welche Abbauprodukte innerhalb des Beobachtungszeitraumes von 600 Tagen entstehen und welche schadstoffabbauenden Bakterien damit in Verbindung gebracht werden können. Dabei kamen verschiedene chemisch-analytische Methoden, wie C^{13}/C^{12}-Isotopenanalyse sowie molekularbiologische Techniken, wie z.B. Pyrosequenzierung zur Anwendung. Auf Grundlage der gewonnenen Erkenntnisse werden potenzielle Möglichkeiten des Zusammenspiels von Eisen-Aktivkohle-Kompositen und biotischen Vorgängen diskutiert.

3.1. Acceleration of microiron-based dechlorination in water in contact with fibrous activated carbon

*Maria Vogel, Frank-Dieter Kopinke, Katrin Mackenzie**

Helmholtz Centre for Environmental Research – UFZ, Department of Environmental Engineering, D-04318 Leipzig, Germany

* Corresponding author e-mail: katrin.mackenzie@ufz.de

Abstract

Zero-valent iron (ZVI) is widely applied for reduction of chlorohydrocarbons in water. Since the dechlorination occurs at the iron surface, marked differences in rate constants are commonly found for nanoscale and microscale ZVI. It was already shown for trichloroethene (TCE) adsorbed to activated carbon (AC) that the dechlorination reaction is shifted to the carbon surface simply by contacting the AC with highly reactive nanoscale ZVI particles. Transfer of reactive species to the adsorbed pollutant was discussed.

The present study shows that also very low price and low reactive microscale ZVI can be utilized for an effective dechlorination process. Compared to the reaction rate at the iron surface itself, an enormous acceleration of the dechlorination rate for chlorinated ethenes was observed reaching activity levels such as known for nanoscale ZVI. When fibrous AC is brought into direct contact with microscale ZVI the iron-surface-normalised dechlorination rate constants increased by up to four orders of magnitude. This implies that the dechlorination reaction is fully transferred to the AC surface. Concurrently, the anaerobic corrosion of the same material was not substantially affected. Thus, the utilization of reduction equivalents towards dechlorination of the ZVI particles (dechlorination efficiency) can be considerably enhanced. A screening with various AC types showed that the extent of dechlorination rate acceleration depends strongly on the surface chemistry of the AC. By means of temperature-programmed desorption, it could be shown that concentration and type of oxygen surface groups determine the redox-mediation

properties. Quinone/hydroquinone groups were identified as being the main drivers for electron-transfer processes, but to some extent other redox-active groups such as chromene and pyrone can as well act as redox mediators. AC overall plays the role of a catalyst rather than a reactant. The present study derives recommendations for practical application of the findings in water-treatment approaches.

Keywords: dechlorination in the adsorbed state, zerovalent iron, activated carbon, redox mediator

Highlights

- contact to activated carbon can strongly accelerate of PCE and TCE dechlorination with iron
- low-coast microiron reaches dechlorination rates so far only known from nanoiron
- reactivity increase depends on type and surface concentration of O-functional groups
- quinone/hydroquinone couple at activated carbon surface has catalytic function
- combination of AC and ZVI can optimize iron-based reactive zones or engineered reactors

Graphical abstract

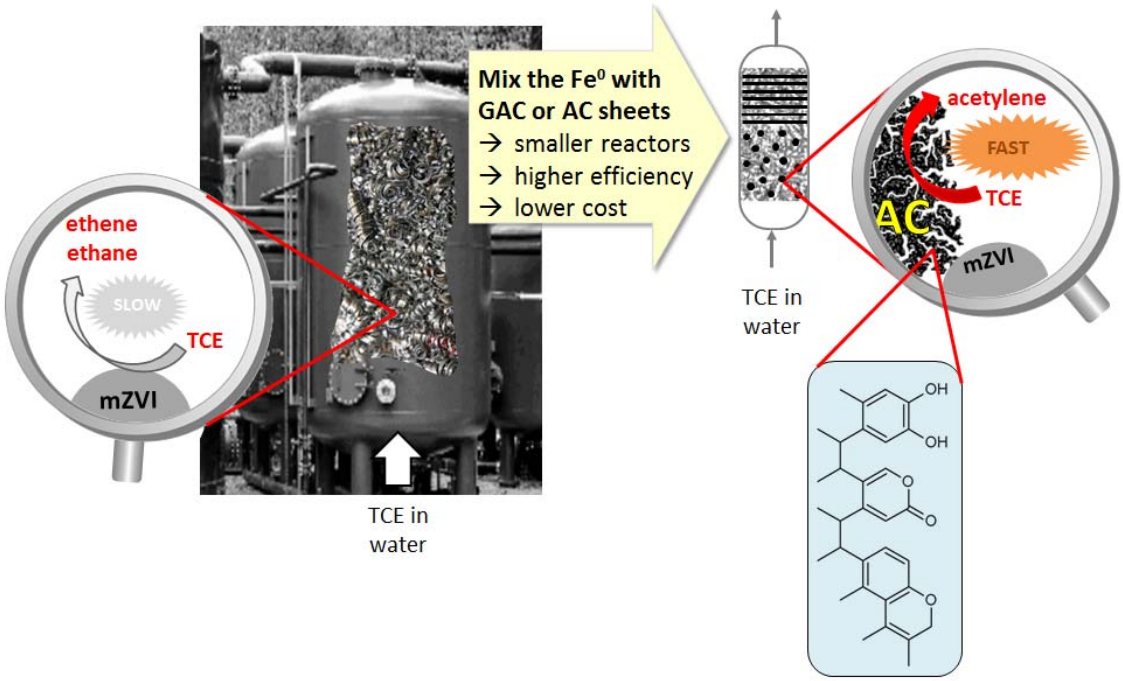

1. Introduction

In the last 20 years, application of ZVI has become the method of choice for *in-situ* and on-site reduction of chlorinated hydrocarbons in aquifers [1,2]. Microscale ZVI (mZVI) and granular iron filings have found application in classical permeable reactive barriers, whereas the more reactive injectable, but cost-intensive, nanoscale ZVI has gained attention in research and field application for *in-situ* installation of reaction zones [3]. However, one remaining restriction for all pristine iron particles is the low affinity of hydrophobic contaminants to the metal surface, which limits the performance of remediation, particularly at low contaminant concentrations [4–8]. One way to overcome this issue is the combination of ZVI with sorption-active carriers, such as activated carbon (AC), forming composite materials [9–18] which allow the sorptive enrichment of organic pollutants in the vicinity of the reactive iron centres, and therefore lead to a more efficient iron utilisation for the target reaction [13]. It is noteworthy that the contaminant degradation in such composites takes place even though the reactive metal surface and the adsorption site for contaminants are spatially separated [14]. Recent studies showed that even in systems with separated AC and nanoscale ZVI particles, which only collide from time to time in an agitated aqueous slurry, a degradation of chlorinated ethenes takes place [19,20]. This raises two questions: (i) how does the transfer of reactive species from their site of origin to the site of contaminant degradation occur, and (ii) what is the role of the carbonaceous sorbent surface.

Generally, carbon materials are known to take an active part in chemical reactions by allowing electron transfer and possibly also hydrogen spill-over [19–22]. It has been found that reaction rates of reductive transformations can be increased, e.g. the reduction of nitroaromatics in the presence of sulfide [23–26] or ZVI [22,27] as reductants. AC is also able to enhance the hydrolysis of 1,1,2,2-tetrachloroethane [28,29] or γ-hexachlorocyclohexane [30]. Furthermore, the microbial degradation of organic contaminants can be mediated and accelerated in the presence of AC [31–33]. Thereby, structural elements, e.g. defect sites of graphitic hexagonal crystallites, unsaturated valences at break lines and edges, and the presence of heteroatoms or different functional groups are discussed and presumed to play a decisive role [21]. However, it was also found that carbonaceous materials have the potential to inhibit chemical reactions at iron metal [5,8]. Graphitic structures at the surface of cast-iron particles

can lead to nonreactive sorption. Consequently, the combination of carbonaceous materials with ZVI offers the chance for efficient contaminant degradation but can also increase the risk of contaminant protection.

The objective of the present study is a closer examination of the mZVI-based dechlorination of typical groundwater contaminants, such as trichloroethene (TCE) and tetrachloroethene (PCE) in the presence of AC with regard to economic optimization. mZVI was chosen instead of nanoscale ZVI as there is a strong gap between the low price on the one hand and the insufficient reactivity towards pollutants on the other hand, due to its low specific surface area (about 0.1-1 m^2 g^{-1}). If this gap could be reduced, the attractiveness of mZVI for practical application in any water treatment approach would be much higher. The present study will examine the combination of AC and mZVI in batch experiments, where various types of AC textiles will be applied in tight contact with mZVI particles in order to ensure a physical contact between the two materials. The role of the textile AC materials for their abilities to influence the dechlorination reaction will be discussed and brought into relation to their surface structural properties with the main emphasis put on oxygen-containing functional groups. In addition, the iron consumption by dechlorination and by the competing anaerobic corrosion, i.e. the progressive loss of reduction equivalents due to the reaction of iron with water, will support the discussion.

2. Experimental section

2.1. Materials

High-purity carbonyl-based mZVI particles ($d_p \approx 10$ µm, $A_{BET} \approx 0.2$ m^2 g^{-1}, $x_{Fe(0)} \geq 99$ wt-%), $NaHCO_3$ (analytical grade) and HNO_3 (65 %) were purchased from Merck, Germany. AC textiles were obtained from Actitex, France. The fibrous AC materials are manufactured from synthetic viscose substrates and processed as cloth and felts. Their physical and chemical properties are listed in Table 1. Ultrapure water (Millipore Simplicity 185, 18.2 MΩ cm) was used for the preparation of the reaction media of all batch experiments. PCE (99 %) and TCE (99 %) were

obtained from Sigma Aldrich, Germany, and directly used without further purification. Methanol (99.7 %) was obtained from Chemsolute, Germany.

Table 1 - Physical and chemical properties of studied AC textiles.

Sample	Layer thickness	Weight per layer surface	BET surface area*	Total pore volume*	Mean pore diameter*	pH at point of zero charge
	[mm]	[g m^{-2}]	[m^2 g^{-1}]	[cm^3 g^{-1}]	[nm]	
FC 10	3	260	1400	0.7	1.9	6.6
FC 15	2	110	1400	0.7	1.9	7.3
FC 12	2.5	140	1100	0.5	1.7	4.6
WKL 20	0.4	100	1100	0.5	1.9	5.9
RS 13	0.5	220	1000	0.5	1.8	7.2
VS 19	0.6	145	2100	1.0	1.8	7.3

* derived from Brunauer-Emmett-Teller (BET) adsorption/desorption isotherms (N_2 at 77 K)

2.2. Analytical methods

The quantitative analysis of chlorine-free C_2-products (acetylene, ethylene and ethane) and the semi-quantitative analysis of C_3- and C_4-coupling products were performed by means of headspace sampling and GC-FID analysis (GC-2010 plus, Shimadzu Corp. equipped with a GS-Q Plot column from Agilent). The analysis of chloride generated during dechlorination was performed by means of ion chromatography (IC 25, Dionex equipped with an IonPacAS15/AG15). The concentrations of the halogenated substances PCE, TCE, dichloroethenes (DCEs) and vinyl chloride (VC) were monitored during the batch experiments by means of headspace sampling and GC-MS analysis (GC-MS-QP2010, Shimadzu, equipped with a HP5 capillary column) taking into account the underlying distribution and sorption equilibria. In order to analyse the chlorinated ethenes, which were adsorbed at the textile AC, solvent extraction using a hexane-propanol mixture (1 : 1, 16 h) with toluene as internal standard was performed, followed by GC-MS analysis of the extracts.

The anaerobic corrosion of mZVI according to the equation $Fe^0 + 2\ H_2O \rightarrow Fe^{2+} + H_2 + 2\ OH^-$ was monitored by measuring the hydrogen concentration in the headspace volume over suspended

particles (with methane as internal standard, allowing extension of the headspace in order to avoid overpressure) using a GC-TCD (HP6850, HP PLOT column).

Temperature-programmed desorption (TPD) of AC samples was performed using a BELCAT-B chemisorption analyser (BEL Japan, Osaka) connected with a mass spectrometer (MKS Cirrus 2). Released gases such as carbon monoxide and dioxide (CO and CO_2) were transferred via a direct-coupling capillary and measured by analysis of their MS signal. The samples were first pre-treated at 150 °C for 30 min in an argon atmosphere. They were then heated up from 150 °C to 1100 °C in a helium flow (50 mL min^{-1}) with a heating rate of 10 K min^{-1}.

The point of zero charge (PZC) of the textile AC samples was determined according to Babic et al. by means of the immersion method. [34].

2.3. Dechlorination studies

The dechlorination experiments with mZVI alone and mZVI in combination with textile AC were performed according to the following procedure: 50 mL of a 5 mM $NaHCO_3$ solution (pH ≈ 8.5) was added to a 120 mL crimped serum bottle and purged with argon. A defined amount of mZVI was placed inside a hand-sewed pouch of textile AC, which was closed and added to the bottle (Figure 1). The pouch varied in its size depending on the applied mass of AC and ranged between 1-3 cm^2 cross-section areas. In all cases, a tight physical contact between the iron particles and the AC felt was ensured.

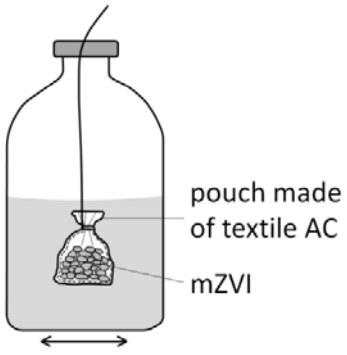

Figure 1- Scheme of the experimental arrangement.

After further purging with argon, the bottles were closed airtight using aluminium crimp caps with PTFE-lined septa and treated for 10 min in an ultrasonic bath. A defined volume of methane was added as internal standard. The reaction was started by injecting a methanolic stock solution of PCE or TCE. The bottles were continuously shaken at room temperature on a horizontal shaker at 90 rpm. The agitation intensity effected a fast mixing of the aqueous phase around the suspended mZVI particles or the AC pouches, whereas the mZVI bed inside the pouches remained largely unaffected ('static'). In order to test the longevity of the catalytic activity of the AC felt FC 10, the batch was prepared as described above, whereby the mZVI-filled AC pouch was pre-conditioned in the argon-purged 5 mM $NaHCO_3$ solution for three days before TCE was added. After one week of reaction time, the bottle was purged with argon and fresh TCE was re-spiked. This procedure was repeated three times.

2.4. Pre-treatment of the carbon felt FC 10

A sample of the AC felt FC 10 (3 g L^{-1}) was pre-treated with mZVI (60 g L^{-1}) for four days in argon-purged 5 mM $NaHCO_3$ aqueous suspension. In order to achieve this, iron particles were placed in a closed AC pouch and slightly shaken as described above. After this conditioning time, the iron particles were removed from the carbon felt and several washing steps with argon-purged, deionised water were performed. The treated AC sample was dried for 45 min at 105 °C under nitrogen atmosphere and analysed by means of TPD analysis.

Furthermore, the surface of the AC felt FC 10 was modified in two ways: (i) by wet oxidation using nitric acid. 1 g of AC was oxidised with 100 mL 5 M HNO_3 under reflux at 90 °C for 24 h. Subsequently, the felt was washed several times with deionised water and dried at 110 °C overnight. (ii) The AC felt FC 10 was heated up to 1100 °C under an inert He-atmosphere and re-exposed to air after cooling. Thereby most of the functional surface groups were removed, however, the re-formation of a small amount of new O-functionalised groups was possible [35].

3. Results and discussion

3.1. Dechlorination of TCE and PCE by mZVI

TCE and PCE were chosen as typical groundwater contaminants for which adsorption to AC is one of the treatment options but which are also subject to chemical reduction by metallic iron in aqueous media. Both substances show very similar dechlorination behaviour with iron and are therefore chosen pari passu in this study. Dechlorination of both substances with mZVI was examined in benchmark experiments. The mZVI under study is a very slow-reacting, high-purity iron which was chosen in order to avoid any effects of trace-level catalytically active metals and carbon impurities. Pre-treatment of mZVI by washing with diluted acids appeared to have no marked influence on neither dechlorination nor corrosion rates and thus was omitted. In duplicate tests, the dechlorination kinetics for TCE and PCE were monitored by means of chlorine-free C_2-hydrocarbons and chloride analysis over a time period of 400 h. For both model contaminants, ethylene and ethane formation was prevalent, whereas acetylene was found only in traces with pure iron as reductant. Partially chlorinated products were formed only in trace amounts, and are not discussed further here. First-order rate constants (k_{obs}) for dechlorination with iron were calculated from the disappearance of chloroethenes and the appearance of products. For TCE and PCE dechlorination, $k_{obs,TCE} = 2.6 \cdot 10^{-4}\ h^{-1}$ and $k_{obs,PCE} = 2.0 \cdot 10^{-4}\ h^{-1}$, respectively, were found (reaction conditions applied: $c_{0,TCE} = 20\ mg\ L^{-1}$ or $c_{0,PCE} = 25\ mg\ L^{-1}$, $c_{mZVI} = 400\ g\ L^{-1}$, 5 mM $NaHCO_3$, $pH_{start} = 8.4$). The reaction selectivity towards the sum of ethylene and ethane formation was roughly constant over the duration of the experiments ($n_{ethylene} : n_{ethane} \approx 1 : 1$). The yields of C_2-hydrocarbons during the reaction were similar: 62 % and 56 % for TCE and PCE, respectively. As commonly performed, the iron-surface normalised (second order) rate constants (k_{SA}) were calculated as the descriptor for the dechlorination activity of ZVI. The obtained values $k_{SA,TCE} = 3.25 \cdot 10^{-6}\ L\ m^{-2}\ h^{-1}$ and $k_{SA,PCE} = 2.5 \cdot 10^{-6}\ L\ m^{-2}\ h^{-1}$ are in the lower range of k_{SA} values cited in the literature for various iron materials, but are in the same order of magnitude as known for other iron samples of high purity grade [36–38] .

3.2. PCE dechlorination in the mZVI+AC system - test of various textile AC types

In contrast to the experiments described in the literature, where AC particles and nanoscale ZVI were brought into lose non-continuous contact [19,20], the textile AC pouches used in the present study allow continuous physical contact between the housed-in mZVI and the AC. The entire system was slightly shaken to ensure mass transport and to avoid stationary hydrogen bubbles at the AC pouches. Thus transport of reactive species is facilitated from the surface of the iron particles to the target compound, which is predominantly located at the internal AC surface [19,20]. After the addition of PCE to the reaction vessel, the major part of the contaminant was rapidly adsorbed by the textile AC. Within 24 h an equilibrium state was approached with an adsorbed fraction of > 99.9 %, such that the share of the reaction of freely dissolved PCE with the iron particles can be considered negligible. In order to exclude any influence of different specific surface areas of the AC textiles on the dechlorination, the offered carbon surface area concentration was kept constant for all batches ($c_{SA,AC}$ = 1800 m² L^{-1}), thus the textile sheet size was adjusted accordingly. The dechlorination progress was monitored by means of headspace analysis of chlorine-free C_2-products, which were, in contrast to the chlorinated educts, not significantly affected by sorption to the AC surface.

Results for PCE degradation in the mZVI+AC system are shown in Figure 2. Although significantly lower amounts of mZVI were applied in the AC pouches (c_{mZVI} = 7 g L^{-1}) compared to the benchmark experiment without AC (c_{mZVI} = 400 g L^{-1}), an accelerated dechlorination of PCE was observed in the presence of four out of the six investigated AC textile samples. The corresponding PCE conversion with the low iron concentration (c_{mZVI} = 7 g L^{-1}) in absence of AC (not shown in Figure 2) amounted to only 0.1 % after 400 h.

This result is markedly different from published data received by particle-particle contact between nanoscale ZVI and AC [19,20]. The AC did decrease the TCE reaction rate. AC can be seen as an adsorption sink for the TCE, which thus is withdrawn from the reactive nanoiron surface. Nevertheless, the authors could show that the dechlorination reaction occurred predominantly at the AC surface. The transfer of reactive species from the iron to the AC surface was, however, slower than the TCE reduction at the bare metal. Differing from these literature findings, in the present study slowly reacting metal particles were applied. We experience for some AC types a strong acceleration of the dechlorination reaction in the mixed particle

suspension compared with the bare metal suspension without AC. Presence of other AC types (e.g. RS 13, VS 19 in Fig. 2) showed only a minor effect. This emphasizes the role of the AC type for the performance of the ZVI+AC system.

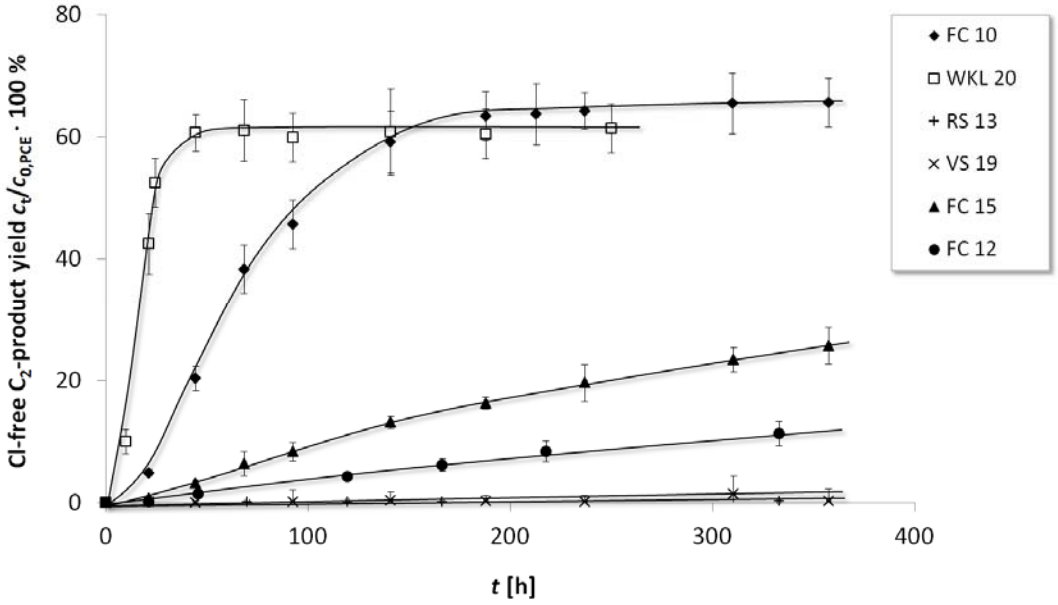

Figure 2 - Kinetics of the PCE dechlorination in the presence of mZVI and various activated carbon textiles ($c_{0,PCE,total}$ = 12.5 mg L^{-1}, c_{mZVI} = 7 g L^{-1}, c_{AC} = 1-2 g L^{-1}, c_{NaHCO3} = 5 mM, pH_{start} = 8.4). The error bar represents the mean deviation of single values from the mean value with n = 3 to 5.

In all cases the product selectivity for mZVI+AC was similar and was characterised by a prevailing acetylene formation. Typically, about 80 % acetylene, 14 % ethylene and 6 % ethane were formed at PCE conversion degrees of about 10 % (primary product selectivities). It has to be pointed out that the AC textiles WKL 20 and FC 10 supported the dechlorination to a higher extent, thus the maximum concentration of chlorine-free C_2-products was already reached after 50 and 200 h, respectively. The solvent extraction of these AC textiles after the reaction (t = 400 h) revealed that only traces of PCE were left, indicating a nearly complete conversion of the contaminant. As generally observed for ZVI as reducing agent of chloroethenes, also the present study showed product selectivities toward chlorine-free C_2-hydrocarbons of less than 100 %. We found a maximum of 65 % of the PCE taking this reaction pathway while 100 % C-Cl bond-breaking was observed (full conversion to chloride). That points to parallel reaction pathways forming higher-molecular-weight dechlorinated products [49]. However, since the

percentage of the headspace-observable formation to C_2 hydrocarbons varies only slightly, this reaction pathway is mostly used here for comparison of the various mZVI+AC systems.

The course of the chlorine-free C_2-product formation in the presence of mZVI in contact with the AC felt FC 10 followed a pseudo-first-order kinetics yielding $k_{obs,PCE} = 1.7 \cdot 10^{-2}\ h^{-1}$, which corresponds formally to an iron-surface-normalised rate constant of $k_{SA,PCE} = 1.2 \cdot 10^{-2}\ L\ m^{-2}\ h^{-1}$. This is a factor of 5000 faster than observed for the same mZVI in the absence of AC. For the AC cloth WKL 20, the acceleration effect is even higher by about one order of magnitude (i.e. a factor of 50,000). On the other hand, in the presence of the woven textile AC types RS 13 and VS 19, nearly no PCE dechlorination activity was detected.

This raises the questions of how the large differences in the chemical activities of these AC textiles in the dechlorination reaction can be explained, and what the mechanism of the interplay between ZVI and AC is. It can be assumed that a multitude of properties of the AC play a role, whereby only a selection is discussed in the present study. The general 'physical' characterisation of the carbon types (see Table 1), including PZC and porosity parameters, did not reveal significant differences in properties which could be responsible for the different chemical behaviour of the AC textiles.

Table 2 - Oxygen content of activated carbon textiles (derived from TPD analysis).

	Oxygen content [wt-%]
FC 10	15.9
FC 15	3.9
FC 12	3.0
WKL 20	13.7
RS 13	5.2
VS 19	2.5

Furthermore, the texture showed overlaps which would not explain the differences in chemical reaction behaviour. When we assume that the reaction site is shifted from the ZVI surface to the AC surface, the chemical composition of the AC surface is more likely to be of importance, e.g. the presence of various oxygen-containing functional groups [21]. Some of them are known to take an active part in chemical reactions, e.g. as redox mediators [21,26]. In order to obtain

information about quantity and quality of these groups at the surface of the various AC textiles, TPD analyses were performed. TPD has been used by several working groups to not only (indirectly) identify but also to quantify the various surface groups in carbon materials by release of carbon oxides at specific temperature ranges. The methods has been applied to prove chemical changes in surface properties and to correlate chemical and catalytic properties of oxidized activated carbon [39-42].

The derived oxygen contents of the analysed carbon samples are shown in Table 2. The high oxygen contents of the two samples FC 10 and WKL 20 correlate with their high chemical activity in the ZVI-driven dechlorination experiments. In addition to the amount of the oxygen-containing functional groups, their type is expected to be relevant for participation in redox reactions. The functional groups present on the AC surface can be derived from the position of CO and CO_2 peaks in temperature-resolved TPD profiles (Figure 3).

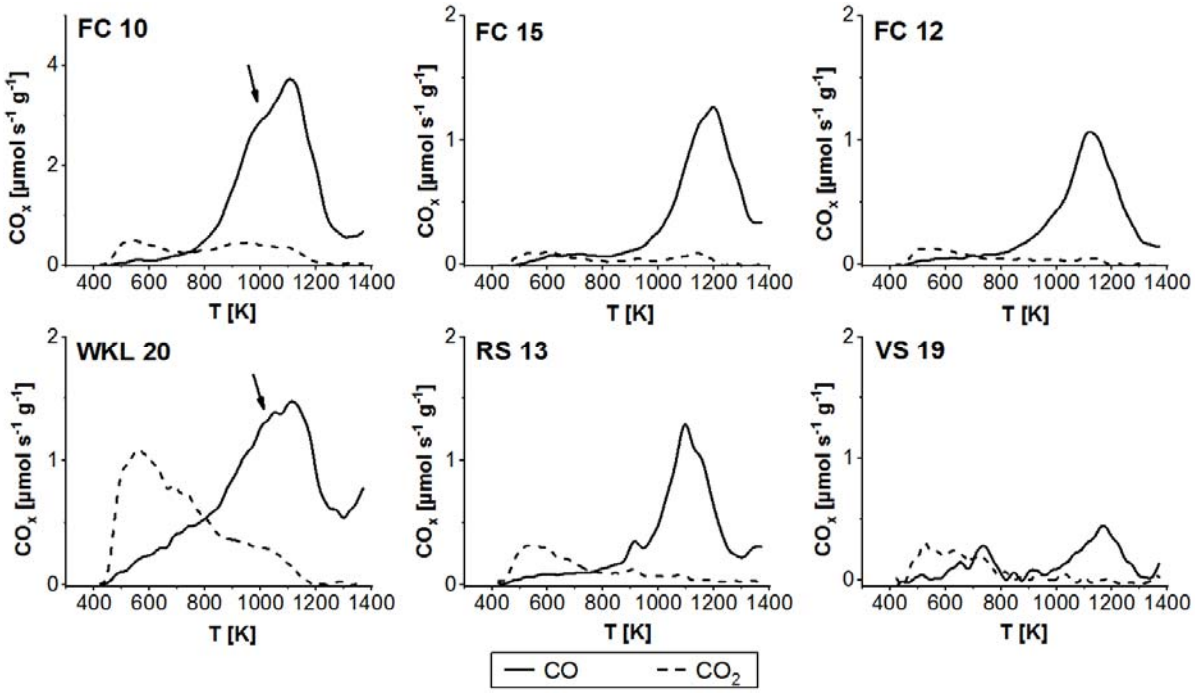

Figure 3 - TPD profiles of activated-carbon textiles under study (heating rate 10 K min^{-1}). The dashed lines represent the release of CO_2, while the solid lines show CO elimination.

The release of CO_2 at about 500 K can be assigned to the decomposition of carboxylic groups. It occurred for all AC samples but to different extents. A correlation between the chemical activity of the AC types and the CO_2 release was not found. Another typical TPD peak at 1100 to 1200 K was also observed for all carbon types. It can be assigned to the destruction of carbonyl groups [39]. Also here, no correlation with the chemical activities is obvious. However, a marked difference between the carbon samples was observed for the release of CO apparent as a shoulder peak at about 1000 K (arrow), indicating phenolic groups [39]. The phenolic groups seem to be especially pronounced for the FC 10 and WKL 20 samples, but less notable for FC 12, FC 15, VS 19 and RS 13. This finding leads to the hypothesis that functional structures with phenolic groups at the carbon surface are involved in the iron-driven dechlorination. It is postulated that a special representative of phenolic groups, the hydroquinone group, acts together with its oxidised quinone form as redox mediator, as is known from literature data for other reduction processes [26,31,32]. In order to obtain further information about the corresponding reaction mechanisms and the involvement of oxygen-containing functional groups, the AC felt FC 10 was chosen for further investigation.

3.3. Study of the mZVI+FC 10 system

3.3.1. TCE dechlorination with mZVI+FC 10

Figure 4 shows results from a typical experiment with mZVI packed in pouches made of the AC felt FC 10 for TCE degradation, whereby educt degradation and formation of all intermediates and final products was monitored over more than five days. PCE and TCE react in a similar way, but TCE was chose for this study in order to avoid overlaps in DCE and VC product formation.

The release of > 96 % of the theoretically expected chloride amount after 140 h indicates an almost complete degradation of the contaminant. Compared to the benchmark experiment without AC at β_{mZVI} = 400 g L^{-1}, in which roughly 4 % of the TCE was dechlorinated by mZVI alone, an approximately 13-fold lower concentration of mZVI in the presence of AC leads to complete TCE reduction within the same time period. After 140 h reaction time, TCE was converted to 62 % acetylene, 13 % ethene, 5 % ethane, > 7 % C_3- and C_4-coupling products and 2 % VC (all data as mol-%). The detected products cover ≥ 90 % of the TCE C-balance. Further coupling

products were probably formed [52], but not detected by headspace analysis. A final extraction of the AC might deliver more information, but was not performed in this study.

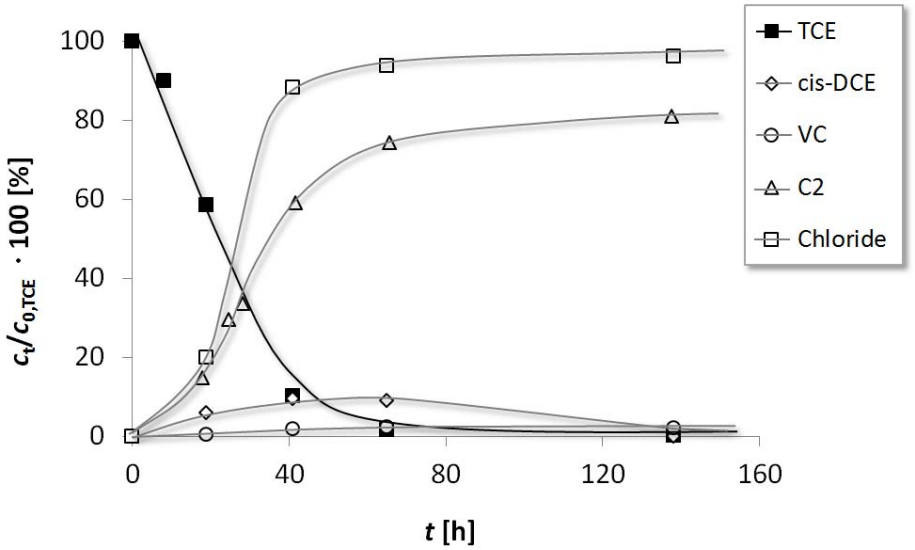

Figure 4 - Kinetics of TCE dechlorination in the presence of mZVI and the activated carbon felt FC 10 ($c_{0,TCE,total}$ = 20 mg L^{-1}, c_{FC10} = 3.4 g L^{-1}, c_{mZVI} = 30 g L^{-1}, c_{NaHCO3} = 5 mM, pH_{start} = 8.4).

One of the plausible reaction pathways is a stepwise dechlorination, since DCEs (max. 10 %) and VC (max. 2.5 %) were detected as intermediates. They undergo further dechlorination and are therefore not regarded as dead-end products here. The appearance of partially dechlorinated intermediates and the dominance of acetylene as final product are indicators for a limitation of active hydrogen as reactive species [20]. In a former study, Kopinke et al. conducted an experiment using a carbon cathode for TCE reduction, which predominantly transferred electrons but no hydrogen species to AC-adsorbed TCE [19]. These conditions led to a similar product spectrum as found in this study for the mZVI+FC 10 system. However, when TCE was degraded in the presence of freely suspended nanoscale ZVI and AC particles, the product spectrum was comparable to those found in systems containing exclusively nanoscale ZVI, indicating the participation of both electrons and active hydrogen in the dechlorination process. In the present study, a limitation in the availability of nascent hydrogen (H*) might occur during the fast dehalogenation, since the available iron surface was substantially smaller than in the study of Kopinke et al. [19]. Increase of ZVI-to-AC ratio leads to a higher hydrogenation

degree. In addition to the availability of reactive species, the nature of attachment of chlorinated ethenes to the different material surfaces could also be responsible for any differences in the product spectrum. While TCE is chemisorbed to the iron surface, forming pi- and di-sigma-bonds [43], the interaction of the chlorinated ethenes to the AC is dominated by physisorption [44].

The reaction of TCE in the mZVI+FC 10 system is characterised by a lag phase during the first ten hours showing a lower dechlorination rate. This phenomenon was not observed for mZVI alone. Hence, a conditioning of the AC surface is a more likely process than an activation of the iron surface. This raises the question of how the AC surface is modified during this initial reaction phase. In order to explain this phenomenon, the carbon felt FC 10 was pre-treated with mZVI in aqueous suspension and then analysed again by means of TPD. The resulting TPD profile is shown in Figure 7A. It clearly reveals the formation of additional groups releasing CO at about 1050 K, which can be ascribed to phenolic groups [39]. At the same time, a decrease of CO-releasing groups between 1100 and 1200 K was observed, which can be interpreted as a decline of carbonyl groups [39]. Based on these observations it can be assumed that during the contact time between mZVI and AC felt in aqueous environment, reduction of quinones to hydroquinone groups may occur at the AC surface, and that the hydroquinone groups in turn are able to take part in reductive dechlorination of the adsorbed chloroethenes. The redox-mediating properties of quinone derivatives in various reactions have been described in the literature [45,46]. In addition, AC-surface-bound quinoid groups are able to support redox reactions, as has been described not only for microbial processes [31,32], but also for the chemical reduction of nitroaromatics with sulfide [26] and the reduction of congo red [47].

3.3.2. Dependence of dechlorination rates on ZVI concentration

When pure ZVI reacts with TCE in aqueous suspensions, the observed first-order rate coefficient k_{obs} strictly depends on the applied ZVI concentration. The second-order surface-normalized dechlorination kinetics is more-or-less a material property. A completely different picture is obtained when ZVI is embedded in AC, forming a new composite material (such as Carbo-Iron), with k_{obs} remaining roughly constant within a wide range of composite concentration [13]. In the present study, various amounts of mZVI were embedded into pouches of the AC felt FC 10

and the resulting k_{obs} were compared. Figure 5 shows the formation of C_2-hydrocarbons over time (A) and the corresponding first-order kinetics plots (B).

For all batch tests, a lag phase (discussed in 3.3.1) was observed at the beginning of the reaction: it lasted up to about 30 hours and decreased with increasing iron concentration. After the lag phase, the product formation followed first-order kinetics, as the resulting linear plots in semi-logarithmic coordinates show. The various slopes of the regression lines, thus the observed dechlorination rate coefficients $k_{obs,}$ were in the range of 0.037 h^{-1} to 0.047 h^{-1} for all applied ZVI concentrations from 10 to 90 g L^{-1}.

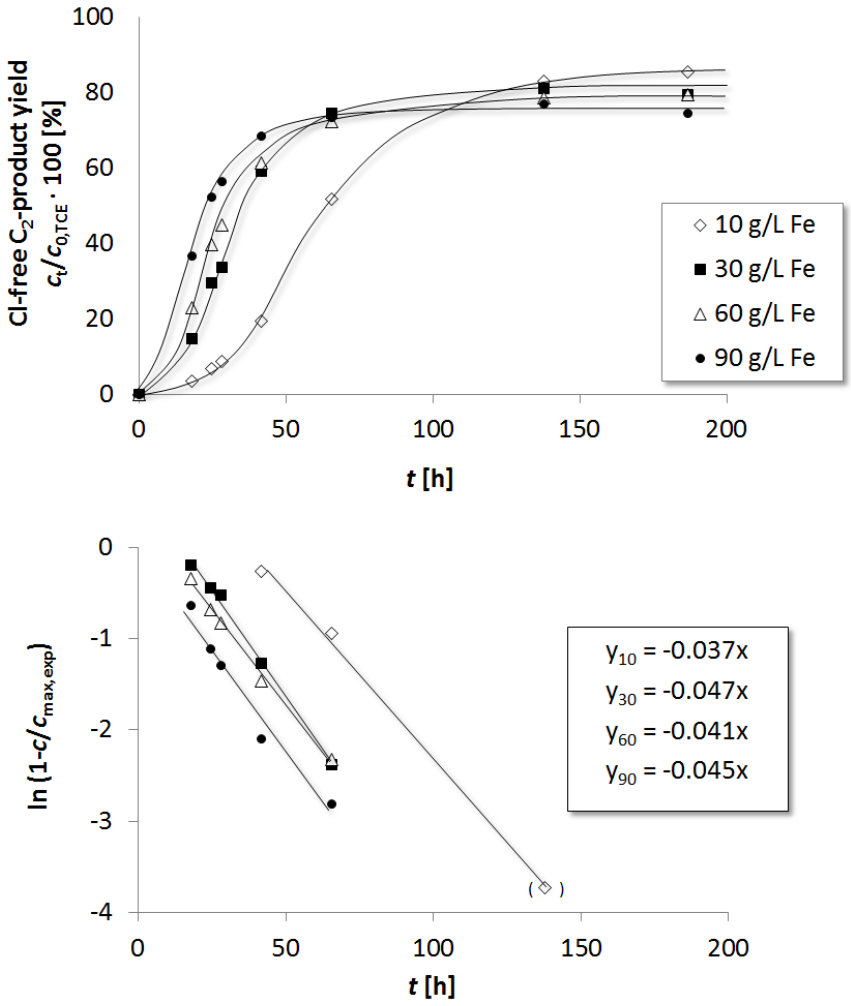

Figure 5 - Kinetics of TCE reduction with various amounts of mZVI embedded into AC-felt pouches. ($c_{0,TCE,total}$ = 20 mg L^{-1}, $c_{Fe(0)}$ = 10 to 90 g L^{-1}, AC: FC 10, $c_{FC\ 10}$ = 3.4 g L^{-1}, c_{NaHCO3} = 5 mM, pH_{start} = 8.4).

This means that the observed TCE dechlorination rates did not depend on the applied iron concentrations under the applied conditions. This can be explained by the fact that the reaction takes place at the carbon surface, where the supply of reactive species (most likely electrons) from the iron particles is not rate-limiting above a certain contact level between ZVI and fibrous AC. The phenomenon appears similar to dechlorination kinetics with Carbo-Iron, where the reaction rate was also observed largely independent of its concentration [13]. However, the mechanistic background may be different in the two systems. As discussed already for Carbo-Iron, the different reaction kinetics make a direct comparison of second-order rate coefficients between carbon-containing and carbon-free ZVI-based systems difficult [13].

While for the activity of different ZVI types the surface-related rate constant k_{SA} is used as general descriptor, for ZVI+AC systems this parameter varies with iron concentration (or in case of Carbo-Iron with iron loading). Characterisation of the performance of ZVI+AC systems by means of the observed rate constant k_{obs} is possibly more conclusive. A value of k_{obs} = 0.04 h^{-1} for the mZVI+AC lies in the same order of magnitude as one knows from nanoscale ZVI as reductant. This is especially remarkable since the mZVI sample applied is otherwise a very slow reductant. However, it is common practice for ZVI users to compare iron performances on a per-mass or per-surface basis. Therefore, k_{SA} values were also used here to evaluate the degradation of TCE in the different systems as $k_{SA,ZVI\text{-}AC}/k_{SA,ZVI}$ formally. The experimental data in this study revealed that bringing mZVI in contact with the AC felt FC 10 results in an immense improvement in reaction rates, by three to four orders of magnitude ($k_{SA,mZVI/AC}/k_{SA,mZVI} \approx 1000$ to 5000).

The obvious difference between the two dechlorination systems is the presumed reaction site. At pristine mZVI, only the iron surface (more precisely its surface oxide layer) can act as attachment and reaction site, whereas in the mZVI+AC system the dechlorination takes place at the carbon surface, which offers a much higher surface area with a (tuneable) number of reactive centres and probably also a different attachment mechanism than that at mZVI surfaces. Almost 100 % of the educt TCE is in the adsorbed (reactive) state in the AC-containing systems studied here, whereas >99 % are in the dissolved (nonreactive) state in pure mZVI suspensions.

3.3.3. Influence of surface modification of the AC sample FC 10 on the dechlorination rate

Table 2 and Figure 3 indicate that the oxygen content and the type of surface functional groups determine the reaction rate and therefore the transfer of reduction equivalents towards the contaminants. Modification of the AC surface should provide more insight into the participation of functional groups in the dechlorination reaction. In this case, the degradation of PCE was examined. Wet oxidation of AC surfaces with nitric acid or hydrogen peroxide is often used to introduce oxygen-functional groups. The method using nitric acid was applied here in order to modify the AC felt FC 10 by wet oxidation. As described in the literature [48-50] and as revealed by the TPD analyses (Figure 7B), nitric acid caused not only a strong increase of acid groups, e.g. carboxylic or phenolic groups, but also a decrease of more thermally stable carbonyl groups, e.g. ketones or redox-active quinones [39]. In the batch experiment with the same amount of mZVI (not shown here), about a ten-fold lower dechlorination rate was found for PCE degradation than for the untreated AC felt. This conforms to our hypothesis that quinoid structures are essential by supporting the dechlorination in Fe+AC systems.

When AC is thermally treated above 1100 °C under inert atmosphere, most of the O-functional groups are split off as CO and CO_2. The thermal treatment in inert atmosphere (He) above 1100 °C was therefore used to modify the AC surface so as to remove the O-functional groups such that its dechlorination performance could be compared with untreated AC. The kinetics of the PCE degradation (as formation of fully dechlorinated C_2-hydrocarbons) before and after the modification are shown in Figure 6.

Surprisingly, the heat-treated sample shows a high reactivity for PCE dechlorination and no pronounced lag phase. This is the opposite of what we expected for an oxygen depleted carbon surface. The TPD profile of the heat-treated FC 10 sample, shown in Figure 7C, reveals a CO peak between 1000 and 1200 K. This can be tentatively assigned to relatively stable carbonyl or ether groups, e.g. chromene or pyrone, which are formed when the AC is re-exposed to air after the thermal treatment [35]. Since the modified carbon felt does not show the typical lag phase, hydroquinones are not likely in this case as the redox mediator. Thus, other redox-active groups may be involved. We hypothesize that pyrone and/or chromene groups at the AC surface can also mediate the electron transfer from ZVI to chlorinated adsorbates [35,51].

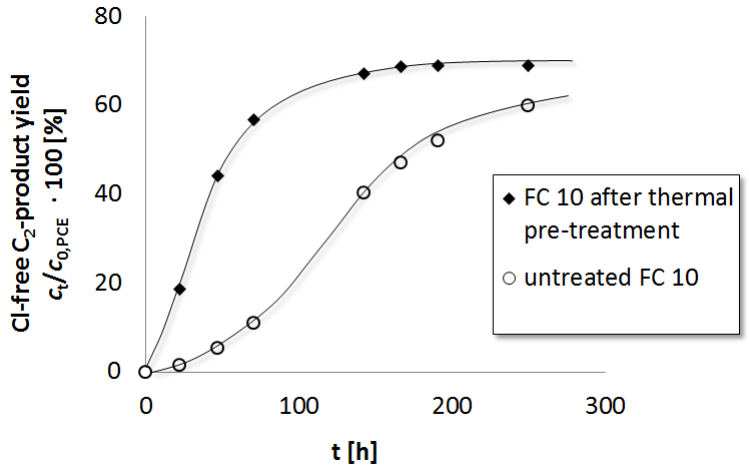

Figure 6 - Kinetics of PCE degradation in the presence of mZVI and AC FC 10 before and after thermal surface modification ($c_{0,PCE,total}$ = 25 mg L^{-1}, c_{FC10} = 1.8 g L^{-1}, c_{ZVI} = 20 g L^{-1}, c_{NaHCO3} = 5 mM, pH_{start} = 8.4).

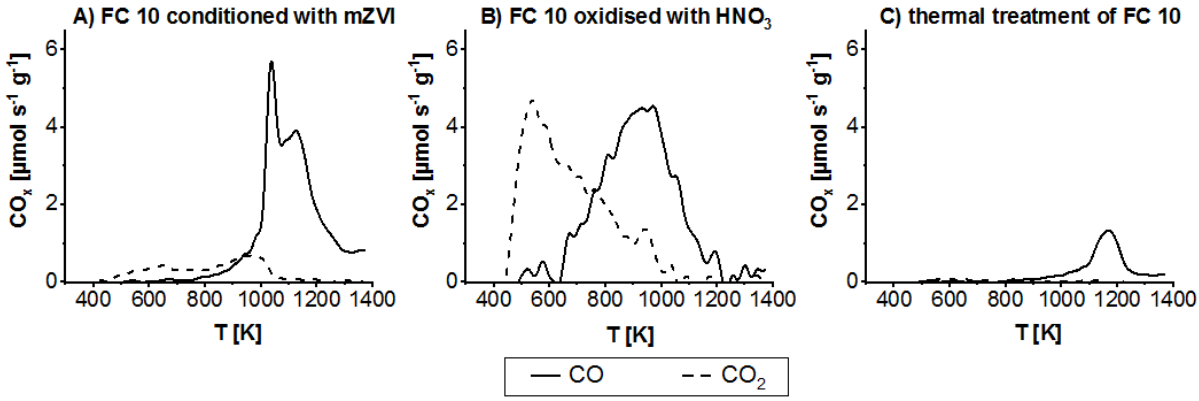

Figure 7 - TPD profiles of the activated carbon FC 10 after various treatments (heating rate 10 K min^{-1}). A) 3 g L^{-1} FC 10 conditioned with 60 g L^{-1} mZVI for 5 days in aqueous environment, B) oxidised with HNO_3 and C) after thermal treatment and re-exposure to air.

3.3.4. Catalytic nature of AC activity

For an efficient utilization of the mZVI+AC system it is important to know whether the participating oxygen-containing functional groups of the AC felt can act catalytically or if they are irreversibly consumed. As shown above, it can be assumed that various surface groups are involved in the electron transfer process, whereby several observations in this study suggest that the quinone/hydroquinone redox couple plays a significant role for the unmodified felt

FC 10. TPD analysis allows a semi-quantitative determination of these groups. The CO peak at about 1050 K can be assigned to phenolic species and was estimated to represent about 13 % of all CO-releasing groups (6.8 mmol g^{-1} AC) in the ZVI-treated sample (see Figure 7A). The participation of pyrones and chromenes plays a relatively minor role in the non-preteated felt, as TPD analysis and the typical lag phase at the beginning of the dechlorination run indicate. In order to test the catalytic activity of the AC felt FC 10, a typical batch experiment was performed, with TCE added in excess compared to the concentration of the quinone/hydroquinone groups at the carbon surface (3.4 moles of TCE per mol of $OH_{hydroquinone}$, corresponding to 10.6 moles of e-acceptor per mol of e-donator). After about 170 and 350 h reaction time, the bottles were extensively purged with argon and spiked again with the same amount of TCE. The reaction progress was monitored via headspace analysis of the chlorine-free C_2-products and chloride analysis of the water phase, thus permitting the conclusion about the total TCE conversion. The results of the experiment are shown in Figure 9, where the derived turnover numbers (TON) over the monitoring period are depicted. The TON is calculated as the molar ratio of converted TCE, referred to the reactive hydroquinone centres (phenolic OH groups), taking into account a 4:1 stoichiometry. It was assumed that two molecules of hydroquinones (2 phenolic OH groups each) are necessary in order to convert one molecule of TCE into acetylene (see Figure 8).

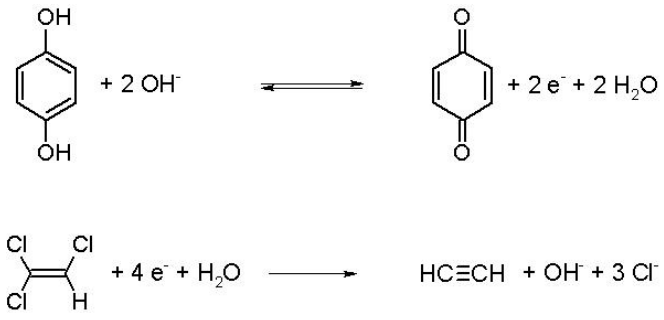

Figure 8 - Assumed stoichiometry of the oxidation of hydroquinone and reduction of TCE.

The degradation apparently followed zero-order kinetics with respect to TCE. Whereas during the first cycle a slightly higher conversion of TCE was observed within the monitoring time, it remained constant for the following two cycles. The slopes of the resulting graphs are similar for

all three cycles. It is possible that oxygen-containing groups other than hydroquinones are also involved in the dechlorination reaction during the first cycle, whereby they are consumed during the reaction with TCE and not regenerated. The resulting overall TON was around 6 after 500 hours reaction time. This experiment proves the catalytic nature of the electron-transfer mediation by AC, rather than a stoichiometric consumption of AC reduction equivalents.

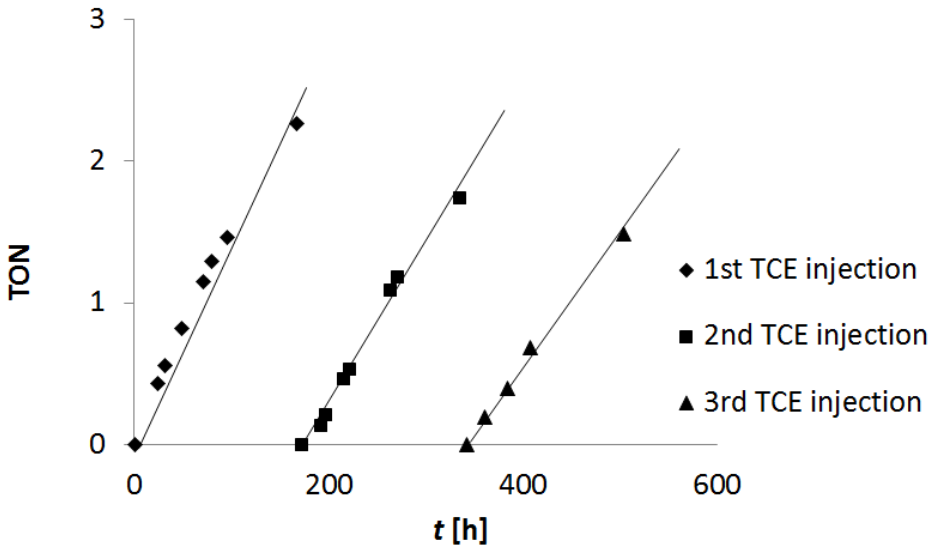

Figure 9 - Turnover numbers (TON) of the TCE dechlorination in the mZVI/AC system ($c_{0,TCE,total}$ = 1.6 g L^{-1}, c_{FC10} = 4.1 g L^{-1}, c_{ZVI} = 80 g L^{-1}, c_{NaHCO3} = 5 mM, pH_{start} = 8.4).

3.3.5. Anaerobic corrosion of mZVI in the presence of the AC felt FC 10

The anaerobic corrosion of ZVI is an undesired electron-consuming reaction competing with the dechlorination reaction for the iron available. In addition, the ageing process of iron leads to precipitations at the metal surface. During field application, even H_2 gas formation can lead to a blockage of groundwater flow, thus by-passing the reaction zone. Dechlorination and anaerobic corrosion often occur concurrently [52,53]. Most importantly, the corrosion rate determines the lifetime of ZVI in an aquifer, which is a crucial performance and cost parameter. This leads to the question of whether the high dechlorination activity of the mZVI+AC system is also accompanied by an increased anaerobic corrosion compared to the mZVI system. In order to elucidate the effect of AC contact for iron corrosion, the production of hydrogen gas was monitored at varying iron concentrations over a time period of 150 h and compared to the pure

mZVI system. First-order rate constants $k_{H2,obs}$ (from $dc_{H2}/dt = k_{H2,obs} \cdot c_{mZVI}$) were calculated for the initial reaction phase and are presented in Figure 10.

In the mZVI+FC10 system the anaerobic iron corrosion is with an average of $k_{H2,obs} = (4.4 \pm 0.9) \cdot 10^{-6}$ h^{-1} slightly higher than in the mZVI system with an average of $k_{H2,obs} = (3.2 \pm 0.6) \cdot 10^{-6}$ h^{-1}. However, both values are in the same range. It is likely that the ZVI+AC system acts as a local element to a small extent, as is known for cast-iron containing graphite [54]. Consequently, for the overall performance in the dechlorination of water pollutants, the combination of mZVI and AC textiles is favourable. The half-life of the investigated mZVI derived from the initial hydrogen formation rates amounts to about 23 years under the applied test conditions. As the corrosion is only increased to a minor extent by physical contact between ZVI and AC, the dechlorination efficiency (defined as ratio between dechlorination and corrosion rates) itself is markedly improved when ZVI is contacted with AC.

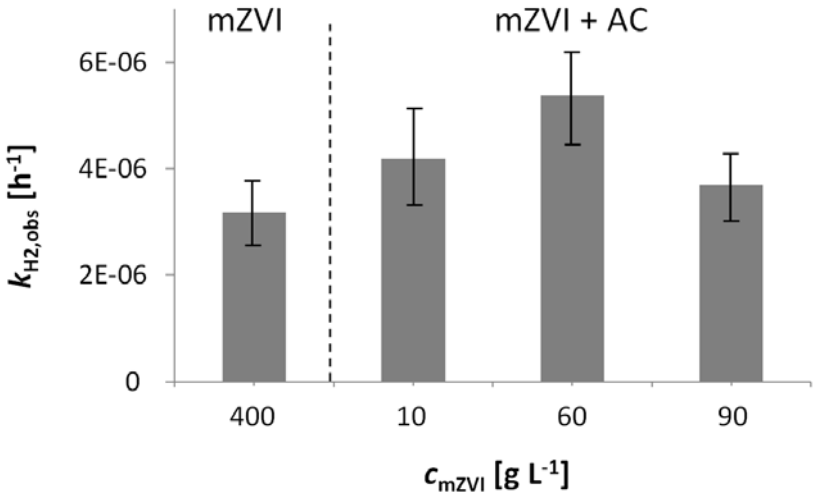

Figure 10 - Anaerobic corrosion of mZVI alone and in the mZVI+AC system (c_{FC10} = 3.4 g L^{-1}, c_{NaHCO3} = 5 mM $NaHCO_3$, pH_{start} = 8.4). The error bar represents the mean deviation of single values from the mean value with n = 3.

4. Conclusions and environmental implications

In the present paper microiron contacting textile AC sheets (as one representative of AC) was inspected on a mechanistic basis using chlorinated ethenes as reaction probe. AC contact with otherwise barely reactive microiron can drastically accelerate the iron-based degradation of chlorinated ethenes by several orders of magnitude. The anaerobic corrosion of ZVI in the

presence of AC is only slightly increased compared to the ZVI system, so that overall greatly increased dechlorination efficiency is achieved. The type of AC matters and determines the extent of rate acceleration. Especially the oxygen surface groups in AC, e.g., the quinone/hydroquinone couple, were recognised as one of the main driver for the redox-mediating activity, whereby AC plays the role of a catalyst rather than a reactant. Iron is "reloading" the redox sites at the surface.

Consequently, the combination represents a method which is easy to apply and which helps to better exploit the reduction capacity of metallic iron. We understand the manuscript as possibility for end users to apply low-cost microiron or filings to reach reactivities close to that of nanoiron, e.g. in on-site treatment plants. But irrespective of the application field, *in-situ* or on-site, a ZVI-based reaction zone can then be designed in such a way that the residence time of the pollutant is sufficiently long to complete degradation. The right choice of carbonaceous materials and its combination with ZVI largely increases the retention time of organic contaminants compared with pure iron barriers / fixed beds. This makes reactive zones or engineered reactors much smaller.

Acknowledgements

The authors thank the integrated project CCF at the Helmholtz Centre for Environmental Research for financial support. Furthermore the authors are grateful for funding from the research projects NanoREM (Project Nr.: 309517, EU 7th FP, NMP.2012.1.2) and Fe-Nanosit (Project Nr.: BMBF 03X0082A). They also thank Maria Balda, Dr. Ulf Trommler and Navid Saeidi for experimental support.

References

[1] F. Fu, D.D. Dionysiou, H. Liu, The use of zero-valent iron for groundwater remediation and wastewater treatment: a review, J. Hazard. Mater. 267 (2014) 194–205.

[2] W. Yan, H.-L. Lien, B.E. Koel, W.-X. Zhang, Iron nanoparticles for environmental clean-up: Recent developments and future outlook, Environ. Sci. Process Impacts 15 (2013) 63–77.

[3] R.A. Crane, T.B. Scott, Nanoscale zero-valent iron: future prospects for an emerging water treatment technology, J. Hazard. Mater. 211-212 (2012) 112–125.

[4] R.M. Allen-King, R.M. Halket, D.R. Burris, Reductive transformation and sorption of cis- and trans-1,2-dichloroethene in a metallic iron-water system, Environ. Toxicol. Chem. 16 (1997) 424–429.

[5] D.R. Burris, T.J. Campbell, V.S. Manoranjan, Sorption of trichloroethylene and tetrachloroethylene in a batch reactive metallic iron-water system, Environ. Sci. Technol. 29 (1995) 2850–2855.

[6] D. Burris, R. Allen-King, V. Manoranjan, T. Campbell, G. Loraine, B. Deng, Chlorinated ethene reduction by cast iron: sorption and mass transfer, J. Environ. Eng. (1998) 1012–1019.

[7] J. Dries, L. Bastiaens, D. Springael, S.N. Agathos, L. Diels, Competition for sorption and degradation of chlorinated ethenes in batch zero-valent iron systems, Environ. Sci. Technol. 38 (2004) 2879–2884.

[8] M. Velimirovic, P.-O. Larsson, Q. Simons, L. Bastiaens, Impact of carbon, oxygen and sulfur content of microscale zerovalent iron particles on its reactivity towards chlorinated aliphatic hydrocarbons, Chemosphere 93 (2013) 2040–2045.

[9] W.-F. Chen, L. Pan, L.-F. Chen, Q. Wang, C.-C. Yan, Dechlorination of hexachlorobenzene by nano zero-valent iron/activated carbon composite: Iron loading, kinetics and pathway, RSC Adv. 4 (2014) 46689–46696.

[10] J. Gao, W. Wang, A.J. Rondinone, F. He, L. Liang, Degradation of trichloroethene with a novel ball milled Fe-C nanocomposite, J. Hazard. Mater. 300 (2015) 443–450.

[11] L. Han, S. Xue, S. Zhao, J. Yan, L. Qian, M. Chen, Biochar supported nanoscale iron particles for the efficient removal of methyl orange dye in aqueous solutions, PLOS One 10 (2015) e0132067.

[12] M. Lawrinenko, Z. Wang, R. Horton, D. Mendivelso-Perez, E.A. Smith, T.E. Webster, D.A. Laird, J.H. van Leeuwen, Macroporous carbon supported zerovalent iron for remediation of trichloroethylene, ACS Sustainable Chem. Eng. 5 (2017) 1586–1593.

[13] Z. Liu, F. Zhang, S.K. Hoekman, T. Liu, C. Gai, N. Peng, Homogeneously dispersed zerovalent iron nanoparticles supported on hydrochar-derived porous carbon: Simple, in Situ Synthesis and Use for Dechlorination of PCBs, ACS Sustainable Chem. Eng. 4 (2016) 3261–3267.

[14] K. Mackenzie, S. Bleyl, A. Georgi, F.-D. Kopinke, Carbo-Iron - An Fe/AC composite - As alternative to nano-iron for groundwater treatment, Water Res. 46 (2012) 3817–3826.

[15] X. Peng, X. Liu, Y. Zhou, B. Peng, L. Tang, L. Luo, B. Yao, Y. Deng, J. Tang, G. Zeng, New insights into the activity of a biochar supported nanoscale zerovalent iron composite and

nanoscale zero valent iron under anaerobic or aerobic conditions, RSC Adv. 7 (2017) 8755–8761.

[16] Y.F. Su, Y.L. Cheng, Y.H. Shih, Removal of trichloroethylene by zerovalent iron/activated carbon derived from agricultural wastes, J. Environ. Manage. 129 (2013) 361–366.

[17] H.-H. Tseng, J.-G. Su, C. Liang, Synthesis of granular activated carbon/zero valent iron composites for simultaneous adsorption/dechlorination of trichloroethylene, J. Hazard. Mater. 192 (2011) 500–506.

[18] Y. Zhou, B. Gao, A.R. Zimmerman, H. Chen, M. Zhang, X. Cao, Biochar-supported zerovalent iron for removal of various contaminants from aqueous solutions, Bioresour. Technol. 152 (2014) 538–542.

[19] F.-D. Kopinke, G. Speichert, K. Mackenzie, E. Hey-Hawkins, Reductive dechlorination in water: Interplay of sorption and reactivity, Appl. Catal., B 181 (2016) 747–753.

[20] H. Tang, D. Zhu, T. Li, H. Kong, W. Chen, Reductive dechlorination of activated carbon-adsorbed trichloroethylene by zero-valent iron: carbon as electron shuttle, J. Environ. Qual. 40 (2011) 1878–1885.

[21] S.-Y. Oh, D.K. Cha, P.C. Chiu, Graphite-mediated reduction of 2,4-dinitrotoluene with elemental iron, Environ. Sci. Technol. 36 (2002) 2178–2184.

[22] F. Rodríguez-Reinoso, The role of carbon materials in heterogeneous catalysis, Carbon 36 (1998) 159–175.

[23] H.J. Amezquita-Garcia, E. Razo-Flores, F.J. Cervantes, J.R. Rangel-Mendez, Activated carbon fibers as redox mediators for the increased reduction of nitroaromatics, Carbon 55 (2013) 276–284.

[24] H. Fu, D. Zhu, Graphene oxide-facilitated reduction of nitrobenzene in sulfide-containing aqueous solutions, Environ. Sci. Technol. 47 (2013) 4204–4210.

[25] W. Xu, K.E. Dana, W.A. Mitch, Black carbon-mediated destruction of nitroglycerin and RDX by hydrogen sulfide, Environ. Sci. Technol. 44 (2010) 6409–6415.

[26] W. Xu, J.J. Pignatello, W.A. Mitch, Reduction of nitroaromatics sorbed to black carbon by direct reaction with sorbed sulfides, Environ. Sci. Technol. 49 (2015) 3419–3426.

[27] S.-Y. Oh, D.K. Cha, B.J. Kim, P.C. Chiu, Reduction of nitroglycerin with elemental iron - pathway, kinetics, and mechanisms, Environ. Sci. Technol. 38 (2004) 3723–3730.

[28] W. Chen, Y. Li, D. Zhu, S. Zheng, W. Chen, Dehydrochlorination of activated carbon-bound 1,1,2,2-tetrachloroethane: Implications for carbonaceous material-based soil/sediment remediation, Carbon 78 (2014) 578–588.

[29] K. Mackenzie, J. Battke, R. Koehler, F.-D. Kopinke, Catalytic effects of activated carbon on hydrolysis reactions of chlorinated organic compounds, Appl. Catal., B 59 (2005) 171–179.

[30] K. Mackenzie, J. Battke, F.-D. Kopinke, Catalytic effects of activated carbon on hydrolysis reactions of chlorinated organic compounds, Catal. Today 102-103 (2005) 148–153.

[31] L. Li, Q. Liu, Y.-X. Wang, H.-Q. Zhao, C.-S. He, H.-Y. Yang, L. Gong, Y. Mu, H.-Q. Yu, Facilitated biological reduction of nitroaromatic compounds by reduced graphene oxide and the role of its surface characteristics, Sci. Rep. 6 (2016) 30082.

[32] R.A. Pereira, M.F.R. Pereira, M.M. Alves, L. Pereira, Carbon based materials as novel redox mediators for dye wastewater biodegradation, Appl. Catal., B 144 (2014) 713–720.

[33] Van der Zee, F., I.A.E. Bisschops, G. Lettinga, J.A. Field, Activated carbon as an electron acceptor and redox mediator during the anaerobic biotransformation of azo dyes, Environ. Sci. Technol. 37 (2003) 402–408.

[34] B.M. Babic, S.K. Milonji, M.J. Polovina, B.V. Kaludierovi, Point of zero charge and intrinsic equilibrium constants of activated carbon cloth, Carbon 37 (1999) 477–481.

[35] M.A. Montes-Morán, D. Suárez, J.A. Menéndez, E. Fuente, On the nature of basic sites on carbon surfaces: An overview, Carbon 42 (2004) 1219–1225.

[36] S.M. Hassan, Reduction of halogenated hydrocarbons in aqueous media: I. Involvement of sulfur in iron catalysis, Chemosphere 40 (2000) 1357–1363.

[37] Y. Sun, J. Li, T. Huang, X. Guan, The influences of iron characteristics, operating conditions and solution chemistry on contaminants removal by zero-valent iron: A review, Water Res. 100 (2016) 277–295.

[38] M. Velimirovic, L. Carniato, Q. Simons, G. Schoups, P. Seuntjens, L. Bastiaens, Corrosion rate estimations of microscale zerovalent iron particles via direct hydrogen production measurements, J. Hazard. Mater. 270 (2014) 18–26.

[39] M.S. Shafeeyan, W.M.A.W. Daud, A. Houshmand, A. Shamiri, A review on surface modification of activated carbon for carbon dioxide adsorption, J. Anal. Appl. Pyrolysis 89 (2010) 143–151.

[40] G.S. Szymański, Z. Karpiński, S.Biniak, A. Świątkowski, The effect of the gradual thermal decomposition of surface oxygen species on the chemical and catalytic properties of oxidized activated carbon. Carbon, 40 (2002) 2627-2639.

[41] A. Dandekar, R.T.K. Baker, M.A. Vannice, Characterization of activated carbon, graphitized carbon fibers and synthetic diamond powder using TPD and DRIFTS. Carbon, 36 (1998) 1821-1831.

[42] J.L. Figueiredo, M.F.R. Pereira, M.M.A. Freitas, J.J.M. Orfao, Modification of the surface chemistry of activated carbons. Carbon, 37 (1999) 1379-1389.[43] W.A. Arnold, A.L. Roberts, Pathways and kinetics of chlorinated ethylene and chlorinated acetylene reaction with Fe(0) particles, Environ. Sci. Technol. 34 (2000) 1794–1805.

[44] D.S. He, C.P. Liu, Y.F. Yuan, X.Y. Li, Study on the adsorption of trichloroethylene in water on activated carbon and activated carbon fibers, Adv. Mat. Res. 113-116 (2010) 1021–1024.

[45] J. López, F. de La Cruz, Y. Alcaraz, F. Delgado, M.A. Vázquez, Quinoid systems in chemistry and pharmacology, Med. Chem. Res. 24 (2015) 3599–3620.

[46] A.E. Wendlandt, S.S. Stahl, Quinone-catalyzed selective oxidation of organic molecules, Angew. Chem. Int. Ed. Engl. 54 (2015) 14638–14658.

[47] L.H. Alvarez, I.C. Arvizu, R.B. García-Reyes, C.M. Martinez, D. Olivo-Alanis, Y.A. Del Angel, Quinone-functionalized activated carbon improves the reduction of congo red coupled to the removal of p-cresol in a UASB reactor, J. Hazard. Mater. 338 (2017) 233–240.

[48] J.L. Figueiredo, M.F.R. Pereira, M.M.A. Freitas, J.J.M. Órfão, Modification of the surface chemistry of activated carbons, Carbon 37 (1999) 1379–1389.

[49] J.L. Figueiredo, M.F.R. Pereira, M.M.A. Freitas, J.J.M. Órfão, Characterization of active sites on carbon catalysts, Ind. Eng. Chem. Res. 46 (2007) 4110–4115.

[50] J. Jaramillo, P.M. Álvarez, V. Gómez-Serrano, Oxidation of activated carbon by dry and wet methods, Fuel Process. Technol. 91 (2010) 1768–1775.

[51] E. Fuente, J.A. Menéndez, D. Suárez, M.A. Montes-Morán, Basic surface oxides on carbon materials: A Global View, Langmuir 19 (2003) 3505–3511.

[52] Y. Liu, S.A. Majetich, R.D. Tilton, D.S. Sholl, G.V. Lowry, TCE dechlorination rates, pathways, and efficiency of nanoscale iron particles with different properties, Environ. Sci. Technol. 39 (2005) 1338–1345.

[53] Y. Liu, G.V. Lowry, Effect of particle age (Fe0 content) and solution pH on nZVI reactivity: H2 Evolution and TCE Dechlorination, Environ. Sci. Technol. 40 (2006) 6085–6090.

[54] J.R. Davis, Corrosion: Understanding the basics, ASM International, Materials Park, Ohio, 2000.

[55] A.D. Henderson, A.H. Demond, Long-term performance of zero-valent iron permeable reactive barriers: A Critical Review, Environ. Eng. Sci. 24 (2007) 401–423.

3.2. Sulfidation of ZVI/AC composite leads to highly corrosion-resistant nanoremediation particles with extended life time

*Maria Vogel, Anett Georgi, Frank-Dieter Kopinke, Katrin Mackenzie**

Helmholtz Centre for Environmental Research – UFZ, Department of Environmental Engineering, D-04318 Leipzig, Germany

* Corresponding author e-mail: katrin.mackenzie@ufz.de

Abstract

Nanoscale zero-valent iron (nZVI) is a powerful reductant for many water pollutants. The lifetime of nZVI in aqueous environments is one of its limitations. Sulfidation of the nZVI surface by reduced sulfur species is known to significantly modify the particle properties. In the present study we examined various post-synthesis sulfidation methods applied on Carbo-Iron, a composite material where iron nanostructures are embedded in colloidal activated carbon (AC) particles. In such cases, where ZVI is surrounded by carbon, sulfidation largely inhibits the anaerobic corrosion of ZVI in water whereas its dechlorination activity was slightly increased. Even at a very low molar S/Fe ratio of 0.004 a strong decrease of the corrosion rate by a factor of 65 was achieved, while concurrently dechlorination of tetrachloroethene (PCE) was accelerated by a factor of three compared to the untreated particles. As a consequence, over 98 % of the reduction equivalents of the sulfidated ZVI were utilized for the reduction of the target contaminant (33 mg L^{-1} PCE) under simulated groundwater conditions. In a long-term experiment over 160 days the extended life-time and the preservation of the reduction capacity of the embedded ZVI were confirmed. Reasons for the modified reaction behavior of Carbo-Iron after sulfidation compared to previously studied nZVI are discussed. We hypothesize that the structure of the carbon-embedded iron is decisive for the observed reaction behavior. In addition to reaction rates, the product pattern is vastly different compared to that of sulfidated nZVI. The triple combination of ZVI, AC and sulfur makes the composite particle very suitable for practical *in-situ* applications.

Keywords: Carbo-Iron, zero-valent iron, dechlorination, anaerobic corrosion, sulfidation

Highlights

- Substantial decrease of anaerobic corrosion of Carbo-Iron's ZVI by sulfide treatment
- Long-term study over 160 days verifies the preservation of ZVI activity by sulfidation
- The ZVI/AC/S system shows a ZVI utilization towards dechlorination close to 100 %

Graphical abstract

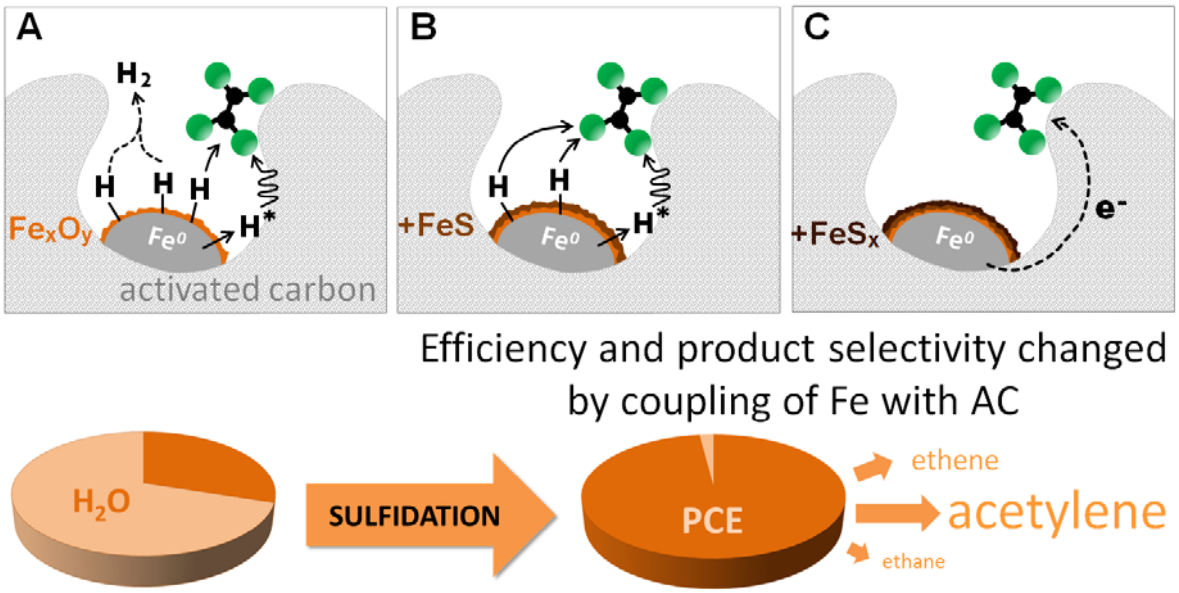

1. Introduction

Iron-based materials are widely used for the reductive *in-situ* destruction of groundwater contaminants, e.g. chlorinated ethenes (Fu et al., 2014; Yan et al., 2013, Dong et al., 2018). Especially nanoscale zero-valent iron (nZVI) with its large specific surface area and the associated high reactivity towards organic pollutants received considerable attention in the last decades. One development trend for ZVI-based *in-situ* reagents led to composite materials, consisting of nZVI combined with sorption-active carbonaceous carriers, such as activated carbon (AC), which allow the collection of organic pollutants in the vicinity of reactive iron centers (Chen et al., 2014; Han et al., 2015; Liu et al., 2016; Mackenzie et al., 2012; Peng et al., 2017). The application of such materials in permeable reaction zones within a contaminated aquifer means an increased retention of the pollutants in this zone and more efficient iron utilization for contaminant reduction, which is pronounced especially for low-concentrated pollutants. Although the supported iron systems show in comparison to pure ZVI a similar ability to degrade organic contaminants, the distinct reaction mechanisms might differ due to the different sorption properties of the systems (Kopinke et al., 2016; Mackenzie et al., 2012; Tang et al., 2011). In case of pure ZVI, both adsorption and reaction of the pollutants take place at the iron surface, while in the case of ZVI/AC composite materials the contaminants are predominantly adsorbed at the inner AC surface and are therefore spatially separated from ZVI as the production site of reactive species (Kopinke et al., 2016; Tang et al., 2011).

A general obstacle against a wider utilization of nZVI and iron-based composite materials in the field is their limited longevity. With the high reactivity of such materials also a high susceptibility to undesired electron-consuming reactions such as anaerobic corrosion according to $Fe^0 + 2\ H_2O \rightarrow Fe^{2+} + H_2 + 2\ OH^-$ are associated (Tratnyek and Johnson, 2006). The extent of this “parasitic” reaction depends on the particle properties and the chemical composition of the water, but is never a negligible side reaction. Recent studies showed that over 95 % of the reduction equivalents of ZVI can be consumed due to the reaction with water (Fan et al., 2016; Schöftner et al., 2015). Omnipresent groundwater constituents, such as bicarbonate or natural organic matter, but also a low pH value can accelerate the iron consumption (Klausen et al., 2003; Liu and Lowry, 2006; Nurmi and Tratnyek, 2008; Reardon, 1995), leading to particle lifetimes of only

a few hours to several weeks (Agrawal et al., 2002; Eglal and Ramamurthy, 2014; Liu et al., 2005b; Liu et al., 2005a; Schöftner et al., 2015; Velimirovic et al., 2014).

A promising method to improve the performance of ZVI is the addition of reduced sulfur compounds, e.g. sulfide or dithionite during or after the synthesis of the particles (Fan et al., 2017; Li et al., 2017b, Dong et al. 2018). An acceleration of the contaminant removal and a simultaneous decrease of the anaerobic corrosion rate could be achieved, which brings a double positive effect for the utilization of the metal (Hassan, 2000; Butler and Hayes, 2001; Kim et al., 2011; Rajajayavel and Ghoshal, 2015; Han and Yan, 2016; Fan et al., 2016; Tang et al., 2016; Fan et al., 2017; Gu et al., 2017). Unfortunately, long-term studies of the reaction behavior of sulfidated nZVI are missing.

Besides the reports on selectivity enhancement in the desired direction (dechlorination versus corrosion), there are also some studies where the presence of sulfide leads to an increased corrosion rate of ZVI (Turcio-Ortega et al., 2012; Hansson et al., 2008). Also other iron-based structures, such as pipelines and storage tanks can undergo accelerated anaerobic corrosion due to biogenically formed sulfide ("chemical microbially influenced corrosion") (Enning and Garrelfs, 2014). These studies show how complex the consequences of a sulfidation on iron are and that the sulfur treatment can lead to a highly protective, but in some cases also to a corrosion-promoting effect.

Some of the most recent reviews on sulfidation of iron-based materials (Fan et al., 2017; Li et al., 2017b, Dong et al., 2018) reveal another limitation of the present state of knowledge: most experimental studies with nZVI have been conducted with borohydride-reduced materials. Such materials are less suitable to represent full-scale applications, due to their high cost of preparation.

For us the question arose which influence a sulfidation treatment would have on the reactivity behavior of the ZVI/AC composite particles, which might differ from that of bare nZVI. The present study focused on the composite material Carbo-Iron, which consists of AC and embedded nanoscale ZVI structures and has been successfully applied at laboratory and field scale (Bleyl et al., 2012; Bleyl et al., 2013; Mackenzie et al., 2012; Mackenzie et al., 2016). With its carbon carrier and the embedded crystalline iron the composite has possibly other ways to interact with the sulfidation reagent compared to the previously studied nZVI, which was

synthesized by reduction of iron salts with $NaBH_4$ (Fan et al., 2017; He et al., 2018). In batch experiments the influence of different post-synthesis sulfidation methods on the dechlorination of tetrachloroethene (PCE) and the anaerobic iron corrosion of Carbo-Iron's ZVI were investigated, considering the dependence of the applied sulfur amount and its interaction with the omnipresent groundwater constituent bicarbonate. In contrast to previous reports, we also performed a long-term study over 160 days and tested the residual dehalogenation activity of the sulfur-treated particles. In order to gain information about the alteration of mineral phases of the iron, X-ray diffraction (XRD) analysis of sulfidated Carbo-Iron particles was performed.

2. Experimental section

2.1. Chemicals and reagents

PCE (99 %) and 1,2-dibromoethane (DBA) (98 %) were purchased from Sigma Aldrich and ABCR, respectively, and used without further purification. $Na_2S \cdot 9\ H_2O$, Na_2SO_3, Na_2SO_4, $Na_2S_2O_3$, $Na_2S_2O_4$, $Na_2S_2O_8$ and $NaHCO_3$ (all p.a.), H_2S (> 99.5 %), L-cysteine (97 %) were obtained from Sigma Aldrich. Methanol (99.7 %) was provided by Chemsolute. Deionized water (Millipore Simplicity 185, 18.2 MΩ cm) was used for the preparation of the reaction media of all batch experiments.

The synthesis of Carbo-Iron was carried out by the carbothermal method which is described in detail in a former study (Bleyl et al., 2012). Briefly, AC particles were loaded with $Fe(NO_3)_3$ from aqueous solution, dried and thermally converted at 700 to 850°C ($Fe_2O_3 + C \rightarrow Fe^0 + CO/CO_2$). The prepared particles consisted of approximately 20 wt-% nanoscale ZVI and 55 wt-% AC and (even though stable at dry air) were stored under argon atmosphere in order to avoid moisture contact. A specific surface area (SSA) of nanostructured ZVI particles in Carbo-Iron of about 15.5 $m^2\ g^{-1}$ was estimated based on the mean ZVI cluster size which was derived from transmission electron microscopy (TEM) and X-ray diffraction analysis (XRD) (Mackenzie et al., 2012). The SSA of Carbo-Iron, determined by nitrogen adsorption, is about 600 $m^2\ g^{-1}$ (Mackenzie et al., 2012).

Commercially available Nanofer Star was supplied by NANO IRON, s.r.o. Czech Republic, stored under aerobic conditions at 4°C and utilized within five months after arrival. At the time of utilization, the sample contained 75 wt-% Fe^0. According to the technical data sheets from NANO IRON s.r.o. the SSA amounts to 20 - 25 $m^2\ g^{-1}$ and the primary particle size is about 50 nm.

2.2. Analytical methods

The X-ray diffraction (XRD) pattern of sulfidated Carbo-Iron was studied at room temperature using a Bruker D8-Advance diffractometer (LynxEye), equipped with a one-dimensional silicon strip detector and operated with Cu-Kα radiation (step size of 0.02°). Energy dispersive X-ray analysis (EDX) was conducted by using a scanning electron microscope (Zeiss Merlin VP Compact) equipped with a Bruker Quantax X-ray detector (XFlash 5060F). Transmission electron microscopy (TEM) was used to depict Carbo-Iron. Particles were embedded into glue (M-Bond 610) and cut by Ar+ ion thinning.

The TEM examinations were carried out in a Philips CM 200 STEM equipped with a super twin objective lens (point resolution 0.23 nm).

In XPS studies Fe and S pattern were measured using an ESCALAB 220i-XL with monochromatic Al *Kα* radiation.

Headspace gas chromatography was chosen for analysis of the fully dechlorinated products ethane, ethene and acetylene using a GC-FID device (GC-2010 plus, Shimadzu Corp., equipped with a GS-Q PLOT-column).

The reaction products chloride and bromide were analyzed by ion chromatography (IC25, Dionex, equipped with an IonPacAS15/AG15 column).

Anaerobic corrosion was monitored by measuring the formation of molecular hydrogen by GC-TCD (HP6850, HP PLOT 30 m x 0.32 mm).

For analysis of the Fe^0 content of the particles, the reaction of ZVI in acidic suspension forming molecular hydrogen according to $Fe^0 + 2\ H^+ \rightarrow Fe^{2+} + H_2$ was utilized. The H_2 evolved was measured by means of GC-TCD as described above.

2.3. Sulfidation procedure

The sulfidation of Carbo-Iron was performed after the synthesis of the particles by applying three different methods: i) a dry pre-treatment of the particles with gaseous H_2S in a nitrogen stream, ii) the addition of an anoxic solution of the sulfur substance to the reaction medium, which contained suspended Carbo-Iron, and iii) a separate wet pre-treatment of the composite material with sulfur species prior to dechlorination tests. This was performed as follows: the particles were conditioned for 24 h in a 50 mM bicarbonate solution, which contained the sulfur species. Subsequently, sulfidated Carbo-Iron was separated from the supernatant by centrifugation under anoxic conditions, re-suspended in a fresh sulfur-free bicarbonate solution and shaken for two hours on a horizontal shaker. After this washing step was repeated three times in order to remove soluble sulfur species, the particles were re-suspended in the fresh reaction medium.

The sulfidation of Carbo-Iron was performed after the synthesis of the particles by applying gas-solid and aqueous-solid phase sulfidation processes. Gas-solid sulfidation was performed by a dry treatment of the particles with gaseous H_2S (diluted with N_2) at room temperature (g/s sulfidation). Aqueous-solid phase sulfidation (aq/s sulfidation) involved the addition of an anoxic solution of the sulfur substance to the anoxic bicarbonate solution, which contained suspended Carbo-Iron particles. In the latter process the duration of sulfidation was varied. The sulfur species were allowed to remain in solution during the entire dechlorination reaction. In a third sulfidation variant, the particles were conditioned with sulfur species for 24 h in 50 mM bicarbonate solution (aq/s pre-treatment). The sulfidated Carbo-Iron was separated in that case from the supernatant by centrifugation under anoxic conditions, re-suspended in a fresh sulfur-free bicarbonate solution and shaken for two hours on a horizontal shaker. After the washing step was repeated three times in order to remove soluble sulfur species, the particles were re-suspended in fresh reaction medium and used as reactant.

Unless otherwise noted, the sulfidation was performed as aq/s sulfidation process where the sulfur species remained in the reaction medium.

2.4. Reactivity tests

Batch experiments were performed to study the influence of sulfidation treatments on the reaction behavior of Carbo-Iron, considering PCE dechlorination and anaerobic corrosion of the composite's ZVI. The reactivity of the composite material was tested after the sulfidation procedures (see 2.3), with variation of the kind of sulfur species (Na_2S, Na_2SO_3, $Na_2S_2O_3$, $Na_2S_2O_4$, Na_2SO_4, $Na_2S_2O_8$ or cysteine were used), their concentration and the concentration of bicarbonate in the reaction medium.

The batch experiments were commonly performed as follows: 60 mL of a bicarbonate solution was added to a 120 mL crimped serum bottle and purged with argon. After the addition of a defined mass of (sulfidated) Carbo-Iron or nZVI, the suspension was further purged with argon. If specified, an anoxic solution containing sulfur compounds was added. The bottle was crimped and particles were dispersed for 20 min in an ultrasonic bath. Then a defined volume of methane was added as internal standard for the headspace analysis and the reaction was started by injecting an aliquot of a methanolic stock solution of PCE ($t_{reaction}$ = 0). The bottles were continuously shaken on a horizontal shaker (90 rpm) at room temperature.

In long-term experiments over 160 days the effect of a sulfidation on the anaerobic corrosion of Carbo-Iron and the residual reduction capacity of the remaining ZVI after the monitoring period were examined. The sulfidation treatment of the composite material was performed as described in section 2.3. by direct addition of an anoxic Na_2S solution to the Carbo-Iron suspension (S/Fe = 0.003 moles mol^{-1}, aq/s sulfidation), by aq/s pre-treatment in bicarbonate solution with washing steps prior use (S/Fe = 0.003 and 0.33) and of dry composite particles with H_2S (g/s sulfidation S/Fe ≈ 0.33). The sulfide-treated samples were compared to a sulfur-free batch. At the end of the monitoring period after 160 days, the residual reduction capacity of Carbo-Iron was measured by adding DBA in excess (35 g L^{-1}) as dehalogenation probe. This substance was previously identified for its fast reaction with ZVI, forming almost completely ethene and only traces of ethane (observed first-order rate constant $k_{obs,DBA}$ = 0.03 h^{-1} at $c_{Carbo\text{-}Iron}$ = 5 g L^{-1}) with a reaction selectivity close to 100 % towards the bromine-free C_2 hydrocarbons. This method offers a fast quantification of the remaining ZVI content without separation of the solid fraction.

2.5. Calculation of dechlorination efficiency

In the literature there exist several approaches to describe the relation between dechlorination and anaerobic corrosion of ZVI. Terms such as “particle efficiency” or “electron efficiency” are often used in a similar meaning, but the definitions vary widely between the various studies (Fan et al., 2016; Gu et al., 2017; Liu et al., 2005b; Liu et al., 2013; Schöftner et al., 2015; Tang et al., 2017, Dong et al., 2018). In the present work, we define two types of dechlorination efficiencies to describe the relation between the two parallel occurring reactions. Firstly, the dechlorination efficiency ε_1 is defined in accordance to Gu et al. (2017) as the ratio of iron amount used for dechlorination ($n_{ZVI,dechlor}$) and the overall consumed amount of iron, considering dechlorination and the anaerobic corrosion ($n_{ZVI,corr}$) within a certain time interval. It was calculated according to eq. (1), where n_i is the molar quantity of the dechlorination product *i* (e.g. ethene), n_{H2} is the molar quantity of H_2 formed and ν_i are stoichiometric factors of the respective half reactions.

$$\varepsilon_1 = \frac{n_{ZVI,dechl}}{n_{ZVI,dechl} + n_{ZVI,corr}} \cdot 100\ \% = \frac{\sum_i \nu_i n_i}{\sum_i \nu_i n_i + \nu_{H2} n_{H2}} \cdot 100\ \% \qquad (1)$$

The stoichiometric factor per converted molecule PCE varied depending on the spectrum of products formed. For the formation of acetylene, ethene and ethane stoichiometric factors of ν_i = 3, 4 and 5 were applied, respectively (according to the PCE reduction equation $C_2Cl_4 + (4 + n)\ e^- + (4 + n)\ H_2O \rightarrow C_2H_n + (4 + n)\ OH^- + 4\ Cl^-$, with n = 2, 4 or 6), while for the residual fraction of higher molecular weight hydrocarbons a mean stoichiometric factor of ν_i = 4 was assumed. For the hydrogen formation ($2\ H^+ + 2\ e^- \rightarrow H_2$) a stoichiometric factor ν_i = 1 was applied ($Fe \rightarrow H_2 + 2\ e^-$). In the batch system the value for ε_1 depends on the initial concentration and the conversion degree of the chlorocompound. The calculated value has therefore only a limited significance for general comparisons and conclusions, although it is a plausible percentage value.

Alternatively, we propose the calculation of the dechlorination efficiency ε_2 by comparing second-order rate constants (in L mol^{-1} h^{-1}) of the dechlorination (k''_{dechl}) and the anaerobic corrosion (k''_{corr}), which should be independent of the applied reactant concentrations. The

overall iron consumption can be described by eq. (2) with n_{ZVI} as the molar amount of ZVI in the reaction batch, $c_{PCE,pore}$ in mol L^{-1} as the pore volume ("local") concentration of PCE in the pore volume of Carbo-Iron. The idea of eq. (2) is that the reaction rates are controlled by the local reactant concentrations rather than those in the suspension bulk phase (Mackenzie et al., 2012). The concentration of the reactant water c_{H2O} is independent of the place of reaction, i.e. $c_{H2O,bulk} = c_{H2O,pore} = c_{H2O} = 55.6$ mol L^{-1}.

$$-\frac{dn_{ZVI}}{dt} = k''_{corr} \cdot c_{H2O} \cdot n_{ZVI} + k''_{dechl} \cdot c_{PCE,pore} \cdot n_{ZVI} \qquad (2)$$

The local PCE concentration at the reactive iron centers can be calculated from the total PCE concentration $c_{PCE,bulk}$ (moles of PCE per volume of reaction suspension) by eq. (3), under conditions where PCE adsorption is quite dominant ($n_{PCE,adsorbed} >> n_{PCE,freely\ dissolved}$) with $c_{Carbo\text{-}Iron}$ as the Carbo-Iron concentration in the bulk phase (suspension) in g L^{-1} and p as the Carbo-Iron intraparticle porosity in L g^{-1} (0.8 mL g^{-1}, Bleyl et al. 2012).

$$c_{PCE,pore} = \frac{c_{PCE,bulk}}{c_{Carbo\text{-}Iron} \cdot p} \qquad (3)$$

We are aware of the fact that $c_{PCE,pore}$ considers PCE as dissolved in the pore water, whereas actually it is adsorbed on the AC surface. The calculation of the second-order rate constants k_i'' was performed on the basis of eqs. (4) and (5) using initial reaction rates ($t \rightarrow 0$) and with n_i and ν_i as molar amounts and stoichiometric factors of the dechlorination products.

$$k''_{corr} = \frac{\nu_i}{n_{ZVI} \cdot c_{H2O}} \cdot \left(\frac{dn_{H2}}{dt}\right)_{t \rightarrow 0} \qquad [L\ mol^{-1}\ h^{-1}] \qquad (4)$$

$$k''_{dechl} = \frac{\sum_i \nu_i}{n_{ZVI} \cdot c_{PCE,pore,0}} \cdot \left(\frac{dn_i}{dt}\right)_{t \rightarrow 0} \qquad [L\ mol^{-1}\ h^{-1}] \qquad (5)$$

$$\varepsilon_2 = \frac{k''_{dechl}}{k''_{corr}} \qquad [-] \qquad (6)$$

The dechlorination efficiency ε_2, as ratio of the second-order rate constants for dechlorination and corrosion (eq. (6)) is a dimensionless number with some general significance and can be used for comparing properties of unsulfidated and sulfidated materials.

3. Results and discussion

3.1. XRD analysis of sulfidated Carbo-Iron

Previous studies on nZVI showed that different sulfidation treatments of iron particles lead to the formation of FeS at the metal surface, which is considered as reason for the improved reaction behavior of nZVI (Fan et al., 2017, Dong et al., 2018). Beside the formation of FeS, also the generation of other iron-sulfur minerals (e.g., greigite Fe_3S_4 or pyrite FeS_2) or iron polysulfides was observed (Fan et al., 2017, Heift et al, 2018).

The sulfidation methods used in this study had similar impacts on the Carbo-Iron samples. No substantial differences in reaction behavior as aqueous suspensions were found. Dechlorination and corrosion studies were carried out using all three sulfidation methods (see 3.2.). In order to avoid a drying step, which could alter the sample surfaces, we decided to use samples generated by g/s sulfidation for surface analysis. In order to gain information about the modification of the particle surface and the mineral phases of Carbo-Iron's ZVI during a sulfidation treatment, H_2S-treated Carbo-Iron (g/s sulfidation) was analyzed by XPS, EDX and XRD analysis.

Unfortunately, the analysis of the porous composite by XPS did not reveal any information about the oxidation state of the sulfur, which could be possibly explained by the low amount of sulfur species at the surface. However we gain the qualitative information by EDX analysis that sulfide distributes between the iron and the activated carbon surfaces. Figure 1 shows EDX data which were taken in iron-rich and carbon-rich regions of the composite particle surface before (Fig. 1A and B) and after sulfidation (g/s sulfidation; Fig. 1C and D). A typical TEM image of Carbo-Iron generated by carbothermal synthesis is added in Fig. 1E.

The XRD pattern of sulfidated Carbo-Iron is shown in Fig. 2 (g/s sulfidation) and reveals dominant signals which are characteristic of α-Fe. This verifies the high crystallinity of the

incorporated ZVI. A rather high degree of iron crystallinity has to be expected for Carbo-Iron due to the thermal synthesis of the particles at temperatures ≥ 700°C.

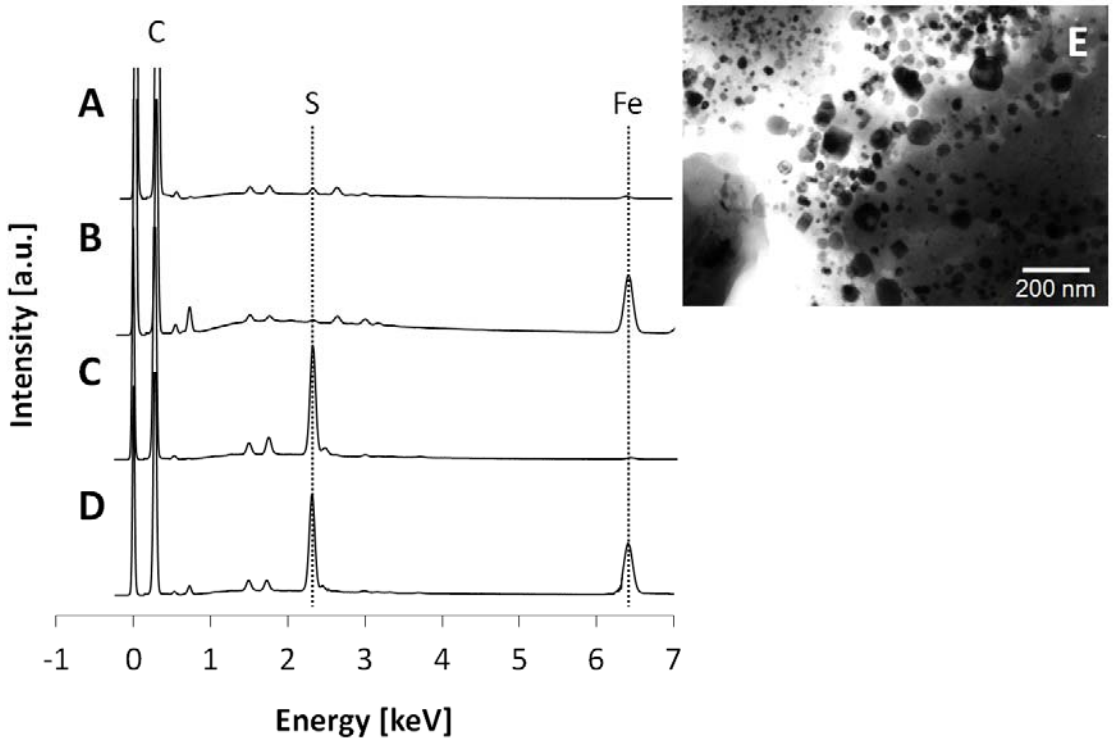

Fig. 1 - Stacked depiction of EDX analysis date of A) untreated Carbo-Iron (focus on region rich in carbon); B) untreated Carbo-Iron (focus on region rich in iron); C) Carbo-Iron, treated with gaseous H_2S (focus on region rich in carbon); D) Carbo-Iron, treated with gaseous H_2S (focus on region rich in iron); E) TEM bright-field image of a thin cut of resin-embedded Carbo-Iron particles.

Next to those of α-Fe, reflections of mackinawite (crystalline FeS) at 18°, 31° and 39° (2θ) were observed. Despite the high noise in the spectrum, FeS signals are assignable. For sulfidated nZVI which was synthesized by reduction with sodium borohydride ($nZVI_{NaBH4}$) also the formation of FeS at the iron surface is described in literature (Kim et al., 2011; Rajajayavel and Ghoshal, 2015). In contrast to Carbo-Iron, which has at least partially a crystalline FeS shell, the formed FeS phase at the surface of $nZVI_{NaBH4}$ is characterized by a low degree of crystallinity, which could potentially lead to a somewhat different reaction behavior of the particles.

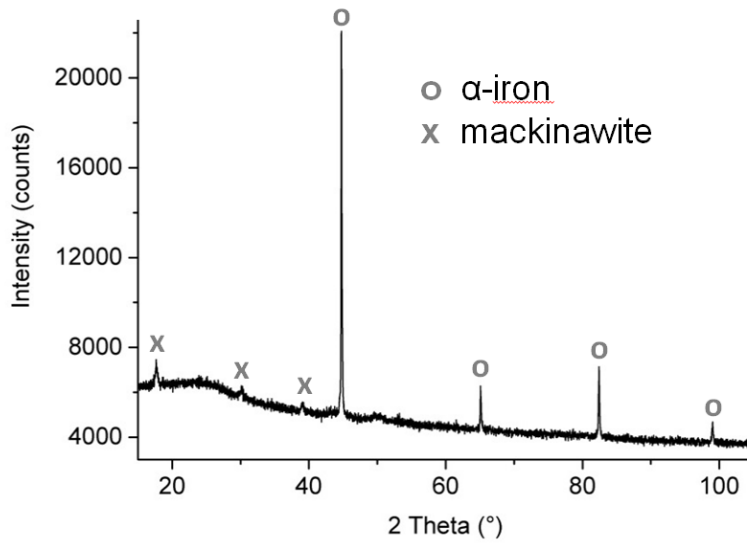

Fig. 2 - XRD pattern of Carbo-Iron particles pre-treated with gaseous H2S in a nitrogen stream.

3.2. Influence of sulfide and bicarbonate on the reactivity of Carbo-Iron

Former studies demonstrated that the effect of sulfur on the nZVI reactivity is concentration dependent (Fan et al., 2017; Li et al., 2017b). Therefore, also a variation in properties has to be expected for the ZVI/AC-composite Carbo-Iron when treated with different amounts of reduced sulfur. In a first set of experiments, the sulfidation was performed after the synthesis of the particles in the reaction medium by adding an anoxic sodium sulfide solution (aq/s sulfidation). Although being aware that bisulfide (HS^-) is the dominant species under the applied conditions (pH = 8.5, pK_{a,HS^-} = 12), we use the term sulfide when describing the interaction with Carbo-Iron for reasons of convenience. For an accurate comparison of literature data with various iron samples, the ratio of sulfur atoms applied to the iron surface atoms would be the most appropriate parameter. However, as the surface area of the investigated particles is not always given in the various data sets, the introduced molar S/Fe ratio remains as reasonable compromise as a comparative measure of sulfur doses.

3.2.1. Anaerobic corrosion of Carbo-Iron's ZVI

The anaerobic corrosion of Carbo-Iron's ZVI was studied by analyzing the formation of molecular hydrogen over a time period of 5 to 20 days varying the S/Fe ratio (aq/s sulfidation) and the

bicarbonate concentration of the reaction medium. Bicarbonate concentrations of 0.2 mM represent very soft water, 5 mM are in the range of very hard water and 50 mM can be seen as worst case scenario. For sulfide, we chose a S/Fe ratio up to 0.33 which is in a range where the effect of sulfidated nZVI can already reach a plateau (Fan et al., 2017). With S/Fe = 0.004 we chose a sulfidation degree which is an order of magnitude lower than that used as the lower limit in other studies. In order to compare the corrosion activity of different samples, the hydrogen evolution rate at the beginning of the reaction was used and a ZVI-mass-normalized rate constant $k_{m,corr}$ [µmol h^{-1} g^{-1}] was determined as a parameter which is frequently reported in literature. In Fig. 3A the results for the anaerobic corrosion of Carbo-Iron's ZVI in the presence of various S/Fe ratios and bicarbonate concentrations are depicted. Note that $k_{m,corr}$ is related to k''_{corr} in eq. (7) by

$$k_{m,corr} = k''_{corr} \cdot \frac{c_{H2O}}{M_{Fe}} \qquad (7)$$

with M_{Fe} as molecular weight of Fe. PCE dechlorination follows pseudo-first order kinetics and the respective rate constants ($k_{obs,dechl}$) are shown in Fig. 3B. They can be converted into second-order rate constants k''_{dechl} as used in eq. (5) by eq. (8):

$$k''_{dechl} = \frac{c_{Carbo\text{-}Iron} \cdot p}{c_{ZVI}} \cdot k_{obs,dechl} \qquad (8)$$

Generally, a strong corrosion-inhibiting effect of sulfide on the embedded ZVI was observed (note the divided Y axis). Although bicarbonate accelerates the iron corrosion, the protecting sulfur effect was significant even for the lowest sulfide concentration (factor of 30 to 65).

Under the applied conditions a maximum coverage of 20 % of the iron surface with a FeS monolayer would be achieved when we assume that the sulfide is exclusively attached to the Fe surface and the Fe surface is provided by 50 nm spherical clusters (Mackenzie et al., 2012). We assumed body-centered cubic structure for the iron species and a 1:1 Fe:S stoichiometry. In practice the sulfide coverage will be much lower due to partial distribution of sulfide to the AC surface (see Fig. 1).

However, the low sulfide coverage seems to be sufficient for deactivation of the corrosion-sensitive sites. The presence of higher sulfide concentrations led to a further slight decrease of hydrogen evolution reaching a minimum when 0.2 mM $NaHCO_3$ and S/Fe of 0.33 were applied (pH = 7.6, while at higher $NaHCO_3$ concentrations the system shows a slight buffer effect reaching a pH value of 8.5).

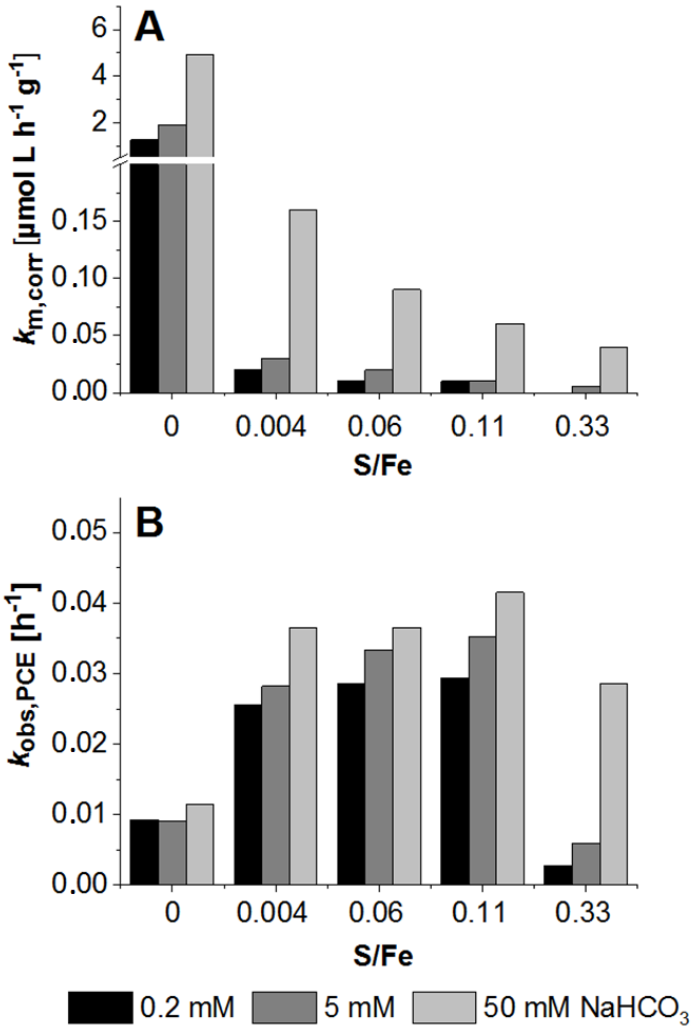

Fig. 3 - A) Mass-normalized rate constants for anaerobic corrosion of Carbo-Iron's ZVI km,corr and B) observed first-order rate constants for PCE dechlorination kobs,dechl by Carbo-Iron in the presence of different bicarbonate and sulfide concentrations ($c_{0,PCE}$ = 33 mg L^{-1}, $c_{Carbo\text{-}Iron}$ = 4 g L^{-1}).

Under these conditions essentially no hydrogen evolution was detected within 18 days (detection limit ≈ 1 µmol H_2). This finding corresponds to an upper limit of the corrosion rate coefficient $k_{ZVI,corr} < 3 \times 10^{-6}$ h^{-1} or an estimated half-life of the ZVI of more than 25 years. Under these conditions, the applied sulfide concentration would be theoretically sufficient to 6-fold cover the iron surface with a monolayer of FeS. Consequently, it can be assumed that under sulfide excess conditions beside FeS, also FeS_2 and polysulfides are generated at the iron surface (Heift et al., 2018), which can have passivating effects. However, this complete corrosion inhibition is reached at the expense of the dechlorination activity. Therefore, such a high sulfidation degree is not our preferred layout.

Generally, the sulfide-induced suppression of the anaerobic corrosion of nZVI is a known effect, which is described in literature and is explained by an inhibition of the recombination reaction of surface-attached hydrogen atoms (Iyer et al., 1990; Oudar, 1980). However, the corrosion-inhibiting effect found in the present study for Carbo-Iron is much higher than observed for non-supported nZVI with comparable S/Fe ratios. Rajajayavel and Ghoshal (2015) observed a decrease in the hydrogen generation rate by a factor of 2 to 3 at S/Fe ratios between 0.02 to 0.07 compared to the untreated particles. Han and Yan (2016) achieved a suppression of the corrosion rate constant by a factor of four from $k_{m,corr}$ = 50 to 13 µmol g^{-1} h^{-1} at S/Fe ratios of 0.05 and 0.25, while at a S/Fe ratio of 0.01 nearly no inhibition effect was observed. Fan et al. (2016) demonstrated that the presence of higher amounts of reduced sulfur species (S/Fe ratio ≥ 0.33) leads to a stronger inhibition of the hydrogen evolution. However, the presented data do not allow derivation of quantitative parameters for the remaining corrosion rates.

This leads to the question why Carbo-Iron's ZVI showed such a high corrosion inhibition (about one to two orders of magnitude) at even low S/Fe ratios and how the differences compared to the previously studied nZVI particles can be explained. Firstly, the morphology of the iron particles is different. In previous studies, mostly nZVI synthesized by reduction with $NaBH_4$ was applied, which has an amorphous structure with more surface defects in contrast to ZVI in Carbo-Iron, which has a crystalline structure due to high temperature reduction (Liu et al. 2005b). It is known that $nZVI_{NaBH4}$ particles undergo dissolution during aging (Liu et al., 2005a), so that corrosion-sensitive fresh subjacent ZVI is consistently exposed to the water phase. Crystalline nZVI, as it is present in Carbo-Iron, rather forms more stable core-shell-structures,

protecting the iron core from corrosion much better (Liu et al., 2005a). In order to evaluate the influence of the crystallinity of ZVI particles on the response behavior towards a sulfidation treatment, the thermally reduced and commercially available nZVI Nanofer Star was examined regarding its corrosion activity in absence and presence of sodium sulfide. While untreated Nanofer Star showed a comparably high corrosion rate of 238 ± 15 µmol h^{-1} g^{-1} in a 50 mM bicarbonate solution (pH = 8.5), the presence of sodium sulfide (S/Fe = 0.06) decreased the anaerobic corrosion by a factor of about 7 ($k_{m,corr}$ = 33.3 ± 1.3 µmol L h^{-1} g^{-1}). This inhibition effect is substantially lower compared to Carbo-Iron's ZVI thus indicating that crystallinity of ZVI is not the only relevant property. Rather, carbon enrichment in the ZVI crystallites and the AC backbone itself could play a role in the different reaction behavior. Another possible benefit of the ZVI/AC-system could be the protection of FeS layers against mechanical stress due to their intrapore position. As a consequence a more uniform FeS shell could be formed, protecting the underlying ZVI better.

3.2.2. PCE dechlorination

The effect of a sulfidation on TCE dechlorination by nZVI has been described in several publications (He at al., 2018; Fan et al., 2016; Han and Yan, 2016; Kim et al., 2011; Rajajayavel and Ghoshal, 2015), while the impact on PCE dechlorination has not been examined so far. It is reasonable to expect similar effects. In the present study, the degradation of PCE in absence and presence of sulfide was studied by analyzing the chlorine-free C_2-hydrocarbons and chloride over a time period of 5 to 20 days. Both products offer the advantage of only marginal sorption to the AC surface in contrast to the educt PCE, which facilitates the kinetic evaluation of the measured data. The obtained first-order rate constants $k_{obs,dechl}$ are not converted into the metal surface-normalized second-order rate constant k_{SA} as commonly applied for pure ZVI systems. The normalization is inappropriate for ZVI/AC composites like Carbo-Iron, since k_{obs} for pollutant reduction is more or less independent of the applied total ZVI concentration (Mackenzie et al., 2012). The more suitable parameter for comparing material reactivities is $k_{obs,dechl}$.

The $k_{obs,dechl}$ values obtained for Carbo-Iron in the presence of various sulfide and bicarbonate concentrations are shown in Fig. 3B. Sulfidation of Carbo-Iron leads in most cases to an enhancement of the PCE dechlorination rate by a factor of about three over a wide range of S/Fe ratios between 0.004 and 0.11 at all applied bicarbonate concentrations. Only for the highest S/Fe ratio tested (S/Fe = 0.33) the dechlorination rate decreased again. Such an 'over-sulfidation' effect was not observed for TCE (Fan et al., 2016; Han and Yan, 2016; Kim et al., 2011; Rajajayavel and Ghoshal, 2015). Along with the sulfide-induced altered PCE dechlorination rates we observed a significant change of the product pattern towards less hydrogenated products. In Fig. 4 exemplary the product distribution for C_2-hydrocarbons and chloride over time is shown in absence and presence of sodium sulfide (S/Fe = 0.06). Ethene and ethane are the main products in nearly equal ratios for dechlorination with untreated Carbo-Iron. The addition of sulfide led to a dominant formation of acetylene, which was then subsequently hydrogenated. In the presence of high sulfide concentrations (S/Fe = 0.33) in a 0.2 mM bicarbonate solution, acetylene was the sole C_2-hydrocarbon, while hydrogenation to ethene and ethane was largely suppressed (data not depicted in Fig. 4).

The changed reaction behavior of sulfidated Carbo-Iron in the PCE dechlorination could be explained by the modified surface properties of the embedded ZVI, as shown schematically in Fig. 5. While untreated ZVI is characterized by an oxide shell (Fig. 5A), a low degree of sulfidation leads to the formation of a thin and uncomplete FeS shell (Fig. 5B) (Fan et al., 2017; Li et al., 2017a; Li et al., 2017b). In the literature, it is generally assumed that the FeS layer at the iron surface can accelerate the degradation of the TCE as it i) improves the adsorption of the pollutant at the cluster surface and ii) has advantageous electron-conducting properties compared to iron oxides (Fan et al., 2017; Li et al., 2017b). iii) The contribution of an increased availability of reactive hydrogen for pollutant degradation, due to suppression of hydrogen recombination by sulfide was suggested but is controversially discussed (Fan et al., 2017).

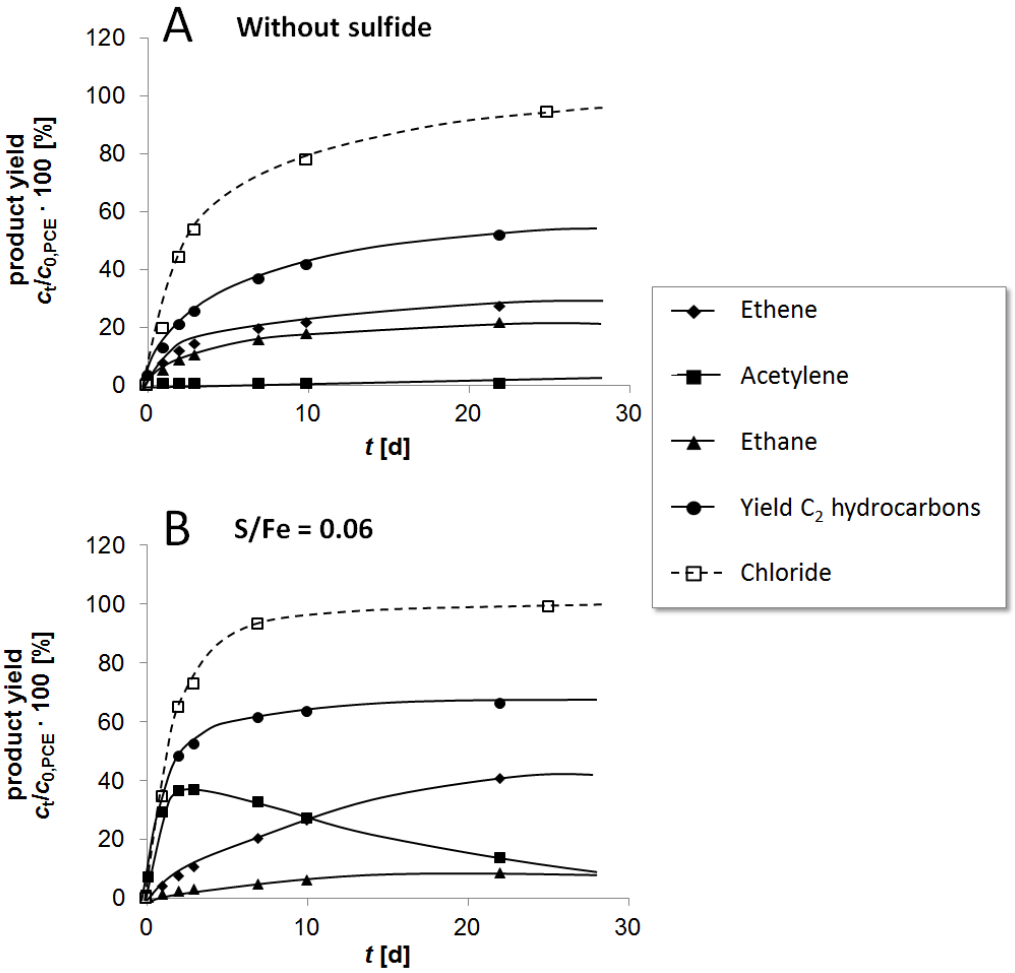

Fig. 4 - Kinetic evaluation of the PCE dechlorination with Carbo-Iron A) without Na2S and B) in the presence of Na_2S with S/Fe = 0.06 ($c_{0,PCE}$ = 33 mg L^{-1}, $c_{Carbo\text{-}Iron}$ = 4 g L^{-1}, c_{NaHCO3} = 50 mM, pH_{start} = 8.5).

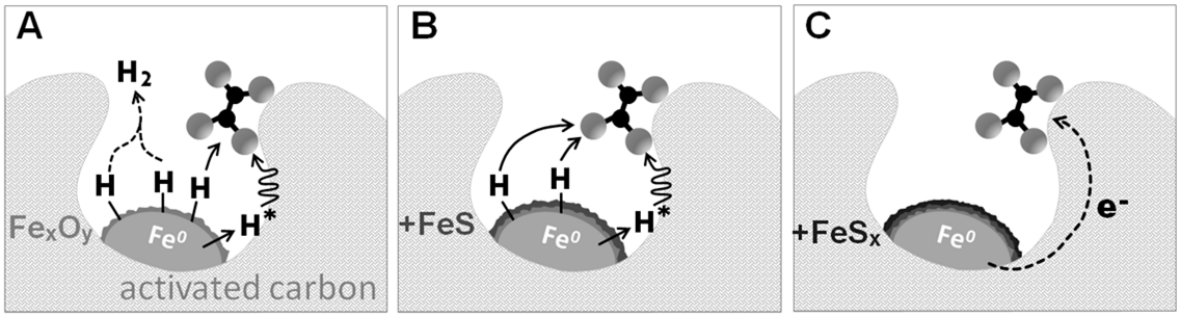

Fig. 5 - Scheme of sulfidation states and their effects on ZVI reactions in Carbo-Iron pores (AC backbone in light gray with embedded ZVI in core-shell-structure); A) untreated Carbo-Iron, B) low S/Fe ratios and C) high S/Fe ratios.

For the ZVI/AC composite Carbo-Iron an improved sorption of the chlorinated compound at a sulfidated ZVI surface should not play a dominant role, as the contaminant is adsorbed at the much larger AC surface, where the dechlorination reaction is supposed to take place. This assumption is based on dechlorination experiments where the two reactants, TCE adsorbed on AC particles and suspended nZVI particles, were spatially separated (Kopinke et al., 2016; Tang et al., 2011). This however poses the question, how the sulfidation of ZVI does affect the dechlorination reaction at the carbon surface. Generally, carbonaceous materials are known to take an active part in chemical reactions by allowing electron transfer and most likely also hydrogen spill-over (Kopinke et al., 2016; Oh et al., 2002; Tang et al., 2011). The product pattern of the PCE dechlorination, which is shifted from ethene plus ethane to acetylene upon sulfidation, indicates that the ratio of electrons and reactive hydrogen available at the reaction site (i.e. the carbon surface) is increased if sulfide is present. This could be explained by the improved electron conductivity of FeS (Li et al., 2017b) which facilitates the electron transfer from ZVI to carbon and therefore accelerates the PCE dechlorination. Beside the modified iron surface, also the alteration of the carbon surface by sulfide could be a possible reason for the observed dechlorination acceleration. Previous studies on the reduction of nitroaromatic compounds showed that carbonaceous materials can mediate the reaction in the presence of sulfide as reductant. As reduction mechanisms (i) the electron transfer from sulfides through the carbon phase to the target compound and (ii) mediation by sulfur-based intermediates at the carbon surface were discussed (Amezquita-Garcia et al., 2013; Fu and Zhu, 2013; Xu et al., 2010; Xu et al., 2015).

A higher sulfidation degree (Fig. 5C) will proceed to modify the iron surface in such a way that electrons but not atomic hydrogen are available. Inhibition of PCE degradation at high sulfidation degree (S/Fe = 0.33) might be due to a passivation process of the ZVI surface, e.g. by FeS_2 or polysulfides, which are less conductive compared to FeS, leading to an insulation of the iron core. In this context, the tendency of crystalline nZVI to form stable sulfidation shells can be disadvantageous. In particular, the inhibited formation of reactive hydrogen may slow down the PCE dechlorination (Jayalakshmi and Muralidharan, 1992). Nevertheless, long-living particles with a sufficient dechlorination activity are created. What does this scenario mean for ZVI embedded in an AC matrix for its field relevance? The chlorinated pollutants are “trapped”

within the AC pores, providing a long residence time within a treatment zone. Hence, even a reduced chemical reactivity of sulfidated (long-lived) ZVI may be sufficient for the contaminant degradation in Carbo-Iron. The advantage of markedly improved longevity might outcompete the disadvantage of lower reactivity by means of the outstanding sorption affinity of the AC support toward chlorohydrocarbons.

3.2.3. Dechlorination efficiency

The efficient utilization of the reduction equivalents of ZVI is decisive for the particle longevity and their impact on the intended treatment goal. With the iron 'dechlorination efficiency' we evaluate the two main iron consumption pathways occurring in parallel, the dechlorination of PCE and the anaerobic corrosion of the ZVI in Carbo-Iron (see eq. (1)). In former studies the focus was often placed on chemical reactivity for contaminant degradation alone. However, it is plausible that for field applications the ratio between dechlorination and corrosion rates is a more conclusive parameter. The calculated dechlorination efficiencies ε_1 for the reduction of PCE by various concentrations of untreated and sulfidated Carbo-Iron are shown in Fig. 6. Note that the efficiency parameter ε_1 as defined in eq. (1) is not a unique material property but depends on the experimental conditions, in particular on reactant concentrations, e.g. c_{PCE}. For untreated Carbo-Iron, the dechlorination efficiency is the highest for its lowest concentration. This can be explained by means of the local concentrations of the reactants PCE and water (eq. (2) and Mackenzie et al., 2012). PCE is almost completely adsorbed to Carbo-Iron (at the applied concentration of $c_{\text{Carbo-Iron}} \geq 1.25$ g L^{-1}). This means, the loading of Carbo-Iron with PCE, expressed by $c_{\text{pore,PCE}}$ in eq. (2), is the highest for the lowest Carbo-Iron concentration. In contrast, c_{H2O} is independent of the Carbo-Iron concentration (as long as its loading with PCE is low, i.e. the AC pores are filled with water). Hence, the dechlorination reaction (represented by the second summand in eq. (2)) can better compete for electrons from ZVI. For the case of sulfide absence, the dechlorination efficiency was calculated to be about 27 to 60 %. This means that a significant part of the ZVI is 'wasted' by the corrosion pathway.

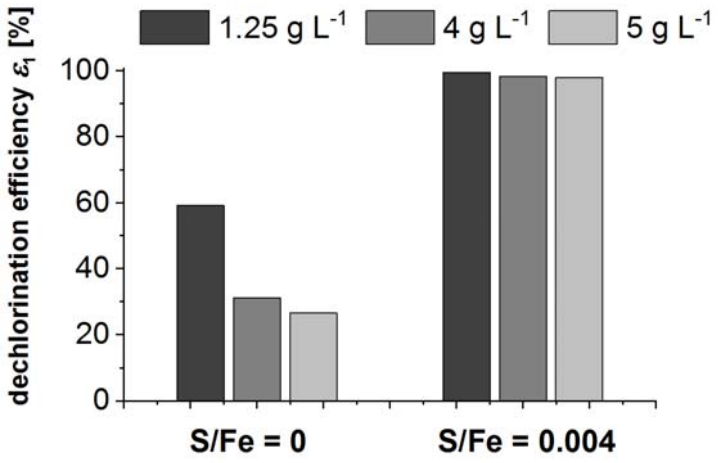

Fig. 6 - Dechlorination efficiencies ε1 of original and sulfide-treated particles at three Carbo-Iron concentrations ($c_{Carbo\text{-}Iron}$ = 1.25 - 5 g L^{-1}, $c_{0,PCE}$ = 33 mg L^{-1}, c_{NaHCO3} = 0.2 mM, pH_{start} = 8.5, S/Fe = 0 and 0.004 mol mol^{-1}).

The tendency that a majority of the reduction equivalents are consumed by anaerobic corrosion is already described for nZVI (Fan et al., 2016; Gu et al., 2017; Liu et al., 2013; Schöftner et al., 2015). This is highly undesired from the economic point of view, especially against the background of the high costs and effort for nanoparticle synthesis. The sulfidation of Carbo-Iron particles led already for the lowest sulfidation degree (S/Fe = 0.004) to a vast increase of the dechlorination efficiency up to 97 to 99 %. This means that sulfidation of Carbo-Iron can dramatically improve the performance of the particles, as the majority of the electrons are used for dechlorination. In literature the enhanced dechlorination efficiency of sulfidated ZVI is described by several working groups, but a direct comparison between the different studies is difficult. Fan et al. (2016) only showed a scheme to illustrate the change in usage of reducing equivalents, but specific calculations are missing. Gu et al. (2017) determined in their study the dechlorination efficiency to 0.2 % for mZVI (at 90 % TCE conversion) and to 10 % for S-mZVI (at 40 % TCE conversion) when ZVI was applied in excess ($c_{0,TCE}$ = 76 µM, $c_{0,mZVI}$ = 10 g L^{-1}). At these specific contaminant conversion degrees for Carbo-Iron a dechlorination efficiency ε_1 = 16 % for the untreated and ε_1 = 98 % for the sulfidated particles are calculated ($c_{0,PCE}$ = 200 µM, $c_{Carbo\text{-}Iron}$ = 4 g L^{-1}).

The dechlorination efficiency ε_2, defined by eq. (6), was calculated to about 420 for the untreated particles and 53,600 for sulfidated Carbo-Iron. The shift in the ratio by two orders of magnitude demonstrates the improved utilization of iron for the target reaction.

3.3. Influence of various sulfur species

In the literature, treatment of iron with sodium sulfide (S^{2-}, HS^-) but also with dithionite ($S_2O_4^{2-}$) or thiosulfate ($S_2O_3^{2-}$) showed beneficial effects on the iron dechlorination activity (Fan et al., 2017; Han and Yan, 2016; Kim et al., 2011; Li et al., 2017b; Rajajayavel and Ghoshal, 2015). Within the present study also other sulfur species were studied for their abilities to optimize the reactivity of Carbo-Iron. We tested Na_2S, Na_2SO_3, $Na_2S_2O_4$, $Na_2S_2O_3$ and cysteine bearing S in the oxidation states -2, +4, +3, +5 and -1, and -2, respectively. As sulfur substances in the oxidation state +6 Na_2SO_4 and $Na_2S_2O_8$ were also selected. The applied S/Fe molar ratios were 0.04 for sulfate, sulfite, sulfide and cysteine and 0.08 for peroxodisulfate, dithionite and thiosulfate. The resulting $k_{obs,dechl}$ for PCE dechlorination and $k_{m,corr}$ for anaerobic corrosion of Carbo-Iron's ZVI in the presence and absence of sulfur species are shown in Fig. 7. The addition of 'reduced' sulfur species (i.e., with S in oxidation states <6) to Carbo-Iron causes a significant decrease in the corrosion rate by a mean factor of more than 50 compared to untreated Carbo-Iron, while the dechlorination rates increased by a factor of about three.

The presence of sulfate and peroxodisulfate had no impact on the performance of the ZVI in Carbo-Iron. It is remarkable that a broad pattern of different sulfur compounds produces quite similar effects. It was shown before for $nZVI_{NaBH4}$ particles that several reduced sulfur species are able to influence the iron reactivity in a similar way (Fan et al., 2016; Han and Yan, 2016; Kim et al., 2011). As mechanisms it has been assumed that the applied sulfur compounds are able to *in-situ* generate sulfide species with ZVI via several pathways, which finally precipitates as FeS at the iron surface. Kim et al. (2011) and Han and Yan (2016) assumed that dithionite and thiosulfate are converted to sulfide by hydrolysis and disproportionation, whereby the participation of nZVI was neglected.

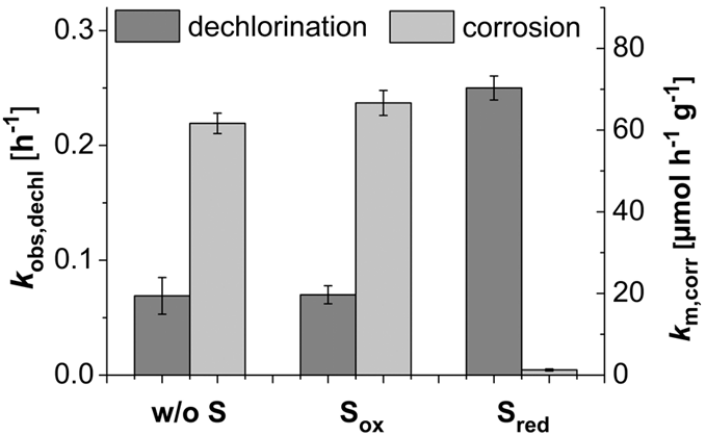

Fig. 7 - Influence of sulfur species in various oxidation states on the observed rate constants for PCE dechlorination ($k_{obs,dechl}$) and the mass-related rate constants for anaerobic corrosion of ZVI in Carbo-Iron ($k_{m,corr}$ in µmol H_2 per g ZVI per hour). The rate constants in the presence of reduced species (Na_2S, Na_2SO_3, $Na_2S_2O_3$, $Na_2S_2O_4$, and cysteine) and oxidized species (Na_2SO_4, $Na_2S_2O_8$) are presented as mean values. The error bars represent the average deviation of the single values from the mean value. ($c_{0,PCE}$ = 33 mg L^{-1}, $c_{Carbo\text{-}Iron}$ = 4 g L^{-1}, c_{NaHCO3} = 50 mM, pH_{start} = 8.5; S/Fe = 0.04 mol mol^{-1} for Na_2S, Na_2SO_3, Na_2SO_4, cysteine and S/Fe = 0.08 for $Na_2S_2O_3$, $Na_2S_2O_4$ and $Na_2S_2O_8$).

However, sulfide formation by reduction of the various sulfur compounds consumes reduction equivalents of ZVI. This assumption is supported by data of Fan et al. (2016), which revealed that at a S/Fe molar ratio of 0.33 more than 70 % of nZVI was consumed when dithionite was applied, while sulfide did not consume a significant part of nZVI. Consequently, the direct application of sulfide is more favorable. In our study we found that the treatment of Carbo-Iron with sodium sulfide (S/Fe = 0.04) in aqueous solution led to a negligible loss of ZVI of less than 5 %.

3.3.1. Influence of medium exchange on the activity of sulfidated Carbo-Iron

In order to evaluate the stability of sulfur modification, the Carbo-Iron particles were thoroughly washed several times with bicarbonate solution and suspended in fresh, anoxic media. The obtained reaction rate constants before and after exchange of the reaction medium are shown in Fig. 8.

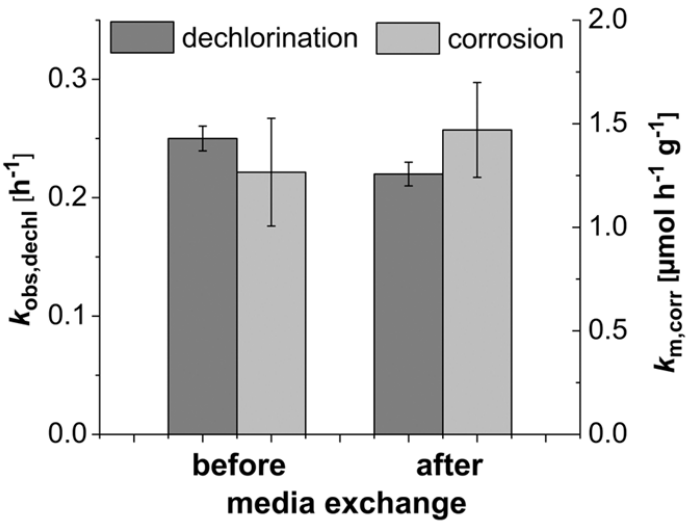

Fig. 8 - Observed rate constants for the dechlorination of PCE ($k_{obs,dechl}$) and mass-related rate constant for the anaerobic corrosion of ZVI in Carbo-Iron ($k_{m,corr}$) in the presence of reduced sulfur species and after exchange of the reaction medium ($c_{0,PCE}$ = 33 mg L^{-1}, $c_{Carbo\text{-}Iron}$ = 4 g L^{-1}, c_{NaHCO3} = 50 mM, pH_{start} = 8.5). The mean values are derived from the obtained reaction rate constants in the presence of the sulfur species Na_2S, Na_2SO_3, cysteine (S/Fe = 0.04) and $Na_2S_2O_3$, $Na_2S_2O_4$ (S/Fe = 0.08). The error bars represent the average deviations of the single values from the mean values.

No significant changes in the reaction behavior were observed after the reaction media were exchanged. This confirms that the sulfur-induced surface modification is not only chemically resistant but also resistant against mechanical stress. Due to the low solubility of FeS (solubility product $K_{L,FeS} = 8 \cdot 10^{-19}$ mol^2 L^{-2}), the proportion of FeS which undergoes dissolution in neutral aqueous media is negligible (Hummel et al., 2002). This is of relevance especially for placement of sulfidated particles in a flow-through aquifer system. In case of sulfidated $nZVI_{NaBH4}$, the surface modification by Na_2S was found to be less stable due to a rather brittle structure of FeS, which led to a decrease in protection after a washing step (Rajajayavel and Ghoshal, 2015). There are two plausible reasons for the higher stability of the FeS surface coating in Carbo-Iron: (i) the crystallinity of the ZVI clusters in Carbo-Iron and (ii) their placement inside the rigid pore structure of the AC particles. Furthermore, it is hypothesized that AC can provide sulfide in low concentrations over a longer time interval and can thus act as a sulfur reservoir which provides steadily low amounts of the passivating species to the neighboring iron.

3.4. Long-term effects of sulfidation treatments

Any application-relevant sulfide effect of corrosion suppression is desired to last as long as iron is still present as zero-valent metal. Therefore, the long-term effect of different sulfidation treatment methods on the anaerobic corrosion of Carbo-Iron was examined over 160 days. Then the ability of the residual metal to act as dehalogenation reagent was measured by adding the fast-reacting 1,2-dibromoethane as probe. Carbo-Iron samples were differently treated with sodium sulfide: (i) by direct addition of an O_2-free Na_2S solution to the Carbo-Iron suspension (S/Fe = 0.003 mol mol^{-1}), (ii) by an aqueous pre-treatment in bicarbonate solution, containing sulfide (S/Fe = 0.003 and 0.33 mol mol^{-1}) with subsequent exchange of the aqueous phase by a S-free bicarbonate solution, and (iii) via the gas phase as H_2S pre-treatment of dry Carbo-Iron particles. As a "worst case" scenario in terms of corrosion, a 50 mM bicarbonate solution was chosen for the long-term tests as reaction medium. The kinetics of the anaerobic corrosion of sulfide-treated and unmodified Carbo-Iron over 160 days alteration time are shown in Fig. 9A.

For all sulfidated samples a similar extent of corrosion suppression was observed. Based on the measured H_2 formation, only 20 – 25 % of the ZVI underwent anaerobic corrosion within 160 days, while the untreated sample had lost already 70 % of its reduction capacity within the first 15 days due to corrosion. The observation that all sulfide-treated samples showed similar stabilities can be explained by the fact that the degree of corrosion suppression does not strongly depend on the applied sulfide amount (see section 3.2.1 and Fig. 3). Qin et al. (2018) reported a biphasic kinetics for corrosion of sulfidated and non-sulfidated ZVI samples with a higher initial rate (first 8-10 h) and a slower second stage (10-120 h). However, Fig. 9A shows that corrosion of the sulfidated Carbo-Iron samples runs with a constant rate over the whole observation period of 160 d. Also for corrosion of non-sulfidated Carbo-Iron no indication on a deviation from pseudo-first-order kinetics was observed even in experiments with higher initial time resolution of sampling (data not shown).

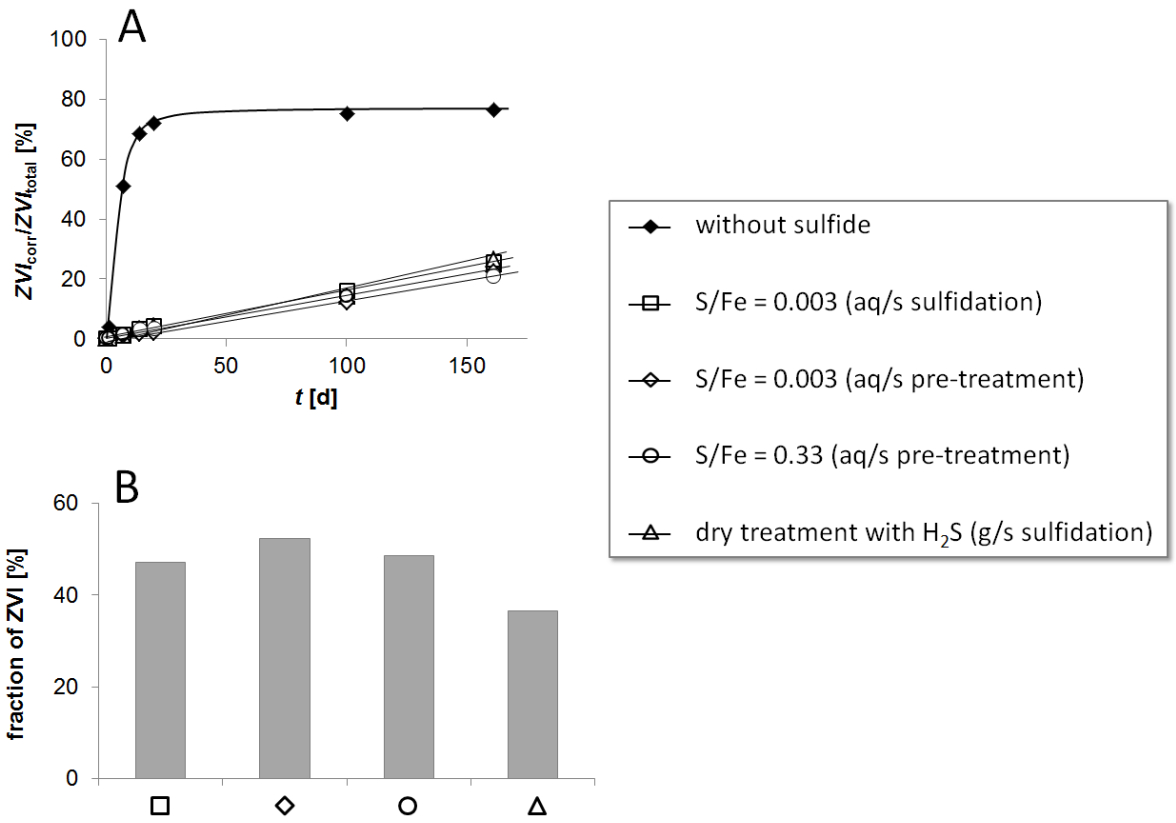

Fig. 9 - Long-term monitoring of the anaerobic ZVI corrosion in Carbo-Iron, which was modified by different sulfidation methods. A) Fraction of corroded iron based on H_2 formation within 160 d and B) fraction of residual metallic ZVI after 160 d determined by conversion of 1,2-dibromoethane. The following reaction conditions were used: $\beta_{Carbo\text{-}Iron}$ = 4 g L^{-1}, c_{NaHCO3} = 50 mM, pH_{start} = 8.5, $\beta_{DBA,0}$ = 35 g L^{-1}.

After 160 days reaction time the residual dehalogenation activity of sulfidated Carbo-Iron was examined. We developed an easy to use and reliable method to analyze low-concentrations of Fe(0) in suspension. 1,2-Dibromoethane (DBA) reacts fast and completely to ethene/ethane with 100% selectivity towards the fully debrominated C_2 hydrocarbons. Fe(0) can be quantified from their yield. We recommend this method as an excellent means for Fe(0) determination in highly diluted suspensions. In order to examine the residual Fe(0) content in the sulfidated Carbo-Iron sample after 160 days, a large excess of DBA was added to the batches. The conversion of DBA was monitored by analysis of bromide and C_2-hydrocarbons over a period of eight days and used to calculate the residual fraction of reactive ZVI. The results for the sulfidated Carbo-Iron particles are presented in Fig. 9B.

For the sulfidation treatments in the aqueous phase similar residual iron fractions of about 50 % were observed, while the lowest was found for particles, which where pre-treated by gaseous H_2S (37 %). It can be assumed that the very low amount of sulfide during the aqueous sulfidation is sufficient to induce the desired effect on a minimal expense of iron content, while the dry sulfidation using gaseous H_2S consumed more reduction equivalents of the embedded ZVI. A closed balance of ZVI reduction equivalents (for H_2 formation and DBA reduction) was not reached which could possibly be explained by side reactions, e.g. with residual oxygen penetrating slowly into the system. Nevertheless, such a remaining high availability of nZVI (as directly confirmed by DBA conversion) after 160 days under corrosion-promoting conditions (50 mM $NaHCO_3$) is promising for the *in-situ* application of the particles in the field. In the presence of soft water (0.2 mM $NaHCO_3$) an about 16-fold and in the presence of very hard water (5 mM $NaHCO_3$) an even 3-fold lower corrosion rate can be expected (see section 3.2.1 and Fig. 3), which would be associated with an even more extended life-time of the particles ($t_{1/2} \geq$ 2-8 a in absence of halogenated pollutants). To the best of our knowledge, such a long life-time has never been demonstrated for conventional $nZVI_{NaBH4}$.

4. Conclusions

In the present study we were able to show that sulfidation has a very positive effect on the reaction behavior of the ZVI/AC composite material Carbo-Iron. In contrast to previously studied $nZVI_{NaBH4}$ the composite particles showed already at low molar S/Fe ratios of 0.004 a 30 to 65-fold decrease of the anaerobic corrosion rate, which ensured a prolonged metal life-time. Under the same conditions, the PCE dechlorination could be accelerated by a factor of about three leading to an overall dechlorination efficiency of the Carbo-Iron particles of > 98 % (at $c_{PCE,0}$ = 200 µM and pH = 8.5). As reasons for the strong sulfidation effects, the high degree of crystallinity of the embedded ZVI and the participation of the AC as “sulfide buffer” are discussed. The combination of ZVI, AC and sulfide leads to efficient and long-living particles, which are perfectly suitable for aquifer *in-situ* applications.

Acknowledgements

This research was supported by the integrated project 'Controlling Chemical's Fate' at the Helmholtz Centre for Environmental Research and by the research projects NanoREM (Project Nr.: 309517, EU 7th FP, NMP.2012.1.2) and Fe-Nanosit (Project Nr.: BMBF 03X0082A). The authors also thank Dr. Roberto Köferstein for support in XRD analysis. The authors also thank Dr. Roberto Köferstein for support in XRD analysis, ClaudiaWöckel for XPS analysis andMatthias Schmidt for EDX analysis.

References

Agrawal A, Ferguson WJ, Gardner BO, Christ JA, Bandstra JZ, Tratnyek PG. Effects of carbonate species on the kinetics of dechlorination of 1,1,1-trichloroethane by zero-valent iron. Environmental Science & Technology 2002;36(20):4326–33.

Amezquita-Garcia HJ, Razo-Flores E, Cervantes FJ, Rangel-Mendez JR. Activated carbon fibers as redox mediators for the increased reduction of nitroaromatics. Carbon 2013;55:276–84.

Bleyl S, Kopinke F-D, Mackenzie K. Carbo-Iron - Synthesis and stabilization of Fe(0)-doped colloidal activated carbon for in situ groundwater treatment. Chemical Engineering Journal 2012;191:588–95.

Bleyl S, Kopinke F-D, Georgi A, Mackenzie K. Carbo-Iron - ein maßgeschneidertes Reagenz zur *In-situ*-Grundwassersanierung. Chemie Ingenieur Technik 2013;85(8):1302–11.

Butler EC, Hayes KF. Factors influencing rates and products in the transformation of trichloroethylene by iron sulfide and iron metal. Environmental Science & Technology 2001;35(19):3884–91.

Chen W-F, Pan L, Chen L-F, Wang Q, Yan C-C. Dechlorination of hexachlorobenzene by nano zero-valent iron/activated carbon composite: iron loading, kinetics and pathway. RSC Advances 2014;4(87):46689–96.

Dong, H., Zhang, C., Deng, J., Jiang, Z., Zhang, L., Cheng, Y., ... & Zeng, G. (2018). Factors influencing degradation of trichloroethylene by sulfide-modified nanoscale zero-valent iron in aqueous solution. Water research, 135, 1-10.

Eglal MM, Ramamurthy AS. Nanofer ZVI: Morphology, particle characteristics, kinetics, and applications. Journal of Nanomaterials 2014;2014(2):1–11.

Enning D, Garrelfs J. Corrosion of iron by sulfate-reducing bacteria: new views of an old problem. Applied and Environmental Microbiology 2014;80(4):1226–36.

Fan D, Lan Y, Tratnyek PG, Johnson RL, Filip J, O'Carroll DM et al. Sulfidation of Iron-Based Materials: A review of processes and implications for water treatment and remediation. Environmental Science & Technology 2017;51(22):13070–85.

Fan D, O'Brien Johnson G, Tratnyek PG, Johnson RL. Sulfidation of nano zerovalent iron (nZVI) for improved selectivity during *in-situ* chemical reduction (ISCR). Environmental Science & Technology 2016;50(17):9558–65.

Fu H, Zhu D. Graphene oxide-facilitated reduction of nitrobenzene in sulfide-containing aqueous solutions. Environ. Sci. Technol. 2013;47(9):4204–10.

Fu F, Dionysiou DD, Liu H. The use of zero-valent iron for groundwater remediation and wastewater treatment: a review. Journal of Hazardous Materials 2014;267:194–205.

Gu Y, Wang B, He F, Bradley MJ, Tratnyek PG. Mechanochemically sulfidated microscale zero valent iron: Pathways, Kinetics, Mechanism, and Efficiency of Trichloroethylene Dechlorination. Environmental Science & Technology 2017;51(21):12653–62.

Han L, Xue S, Zhao S, Yan J, Qian L, Chen M. Biochar supported nanoscale iron particles for the efficient removal of methyl orange dye in aqueous solutions. PloS One 2015;10(7):e0132067.

Han Y, Yan W. Reductive dechlorination of trichloroethene by zero-valent Iron nanoparticles: reactivity enhancement through sulfidation treatment. Environmental Science & Technology 2016;50(23):12992–3001.

Hansson EB, Odziemkowski MS, Gillham RW. Influence of Na2S on the degradation kinetics of CCl4 in the presence of very pure iron. Journal of Contaminant Hydrology 2008;98(3-4):128–34.

Hassan SM. Reduction of halogenated hydrocarbons in aqueous media: I. Involvement of sulfur in iron catalysis. Chemosphere 2000;40(12):1357–63.

He F, Li Z., Shi S, Xu W, Sheng H, Gu Y, Jiang Y, Xi B. Dechlorination of Excess Trichloroethene by Bimetallic and Sulfidated Nanoscale Zero-Valent Iron. Environmental Science & Technology 2018;52(15): 8627–8637.

Heift, D., Lacroix, L. M., Lecante, P., Fazzini, P. F., & Chaudret, B. (2018). Controlling the Sulfidation Process of Iron Nanoparticles: Accessing Iron− Iron Sulfide Core-Shell Structures. ChemNanoMat, 4(7), 663-669.

Hummel W, Berner U, Curti E, Pearson FJ, Thoenen T. Nagra/PSI Chemical thermodynamic data base 01/01. Radiochimica Acta 2002;90(9-11).

Iyer RN, Takeuchi I, Zamanzadeh M, Pickering HW. Hydrogen sulfide effect on hydrogen entry into iron— a mechanistic study. Corrosion 1990;46(6):460–8.

Jayalakshmi M, Muralidharan VS. Influence of sulfur on passivation of iron in alkali solutions. Corrosion 1992;48(11):918–23.

Kim E-J, Kim J-H, Azad A-M, Chang Y-S. Facile synthesis and characterization of Fe/FeS nanoparticles for environmental applications. ACS Applied Materials & Interfaces 2011;3(5):1457–62.

Klausen J, Vikesland PJ, Kohn T, Burris DR, Ball WP, Roberts AL. Longevity of granular iron in groundwater treatment processes: solution composition effects on reduction of organohalides and nitroaromatic compounds. Environmental Science & Technology 2003;37(6):1208–18.

Kopinke F-D, Speichert G, Mackenzie K, Hey-Hawkins E. Reductive dechlorination in water - interplay of sorption and reactivity. Applied Catalysis B: Environmental 2016;181:747–53.

Li D, Zhu X, Zhong Y, Huang W, Peng P'a. Abiotic transformation of hexabromocyclododecane by sulfidated nanoscale zerovalent iron: kinetics, mechanism and influencing factors. Water Research 2017a;121:140–9.

Li J, Zhang X, Sun Y, Liang L, Pan B, Zhang W et al. Advances in sulfidation of zerovalent iron for water decontamination. Environmental Science & Technology 2017b.

Liu Y, Choi H, Dionysiou D, Lowry GV. Trichloroethene hydrodechlorination in water by highly disordered monometallic nanoiron. Chemistry of Materials 2005a;17(21):5315–22.

Liu Y, Majetich SA, Tilton RD, Sholl DS, Lowry GV. TCE dechlorination rates, pathways, and efficiency of nanoscale iron particles with different properties. Environmental Science & Technology 2005b;39(5):1338–45.

Liu Y, Lowry GV. Effect of particle age (Fe 0 content) and solution pH on nZVI reactivity: H2 evolution and TCE dechlorination. Environmental Science & Technology 2006;40(19):6085–90.

Liu H, Wang Q, Wang C, Li X-Z. Electron efficiency of zero-valent iron for groundwater remediation and wastewater treatment. Chemical Engineering Journal 2013;215-216:90–5.

Liu Z, Zhang F, Hoekman SK, Liu T, Gai C, Peng N. Homogeneously dispersed zerovalent iron nanoparticles supported on hydrochar-derived porous carbon: Simple, in Situ Synthesis and Use for Dechlorination of PCBs. ACS Sustainable Chemistry & Engineering 2016;4(6):3261–7.

Mackenzie K, Bleyl S, Georgi A, Kopinke F-D. Carbo-Iron - an Fe/AC composite - as alternative to nano-iron for groundwater treatment. Water Research 2012;46(12):3817–26.

Mackenzie K, Bleyl S, Kopinke F-D, Doose H, Bruns J. Carbo-Iron as improvement of the nanoiron technology: from laboratory design to the field test. The Science of the Total Environment 2016;563-564:641–8.

Nurmi JT, Tratnyek PG. Electrochemical studies of packed iron powder electrodes: effects of common constituents of natural waters on corrosion potential. Corrosion Science 2008;50(1):144–54.

Oh S-Y, Cha DK, Chiu PC. Graphite-mediated reduction of 2,4-dinitrotoluene with elemental iron. Environmental Science & Technology 2002;36(10):2178–84.

Oudar J. Sulfur adsorption and poisoning of metallic catalysts. Catalysis Reviews 1980;22(2):171–95.

Peng X, Liu X, Zhou Y, Peng B, Tang L, Luo L et al. New insights into the activity of a biochar supported nanoscale zerovalent iron composite and nanoscale zero valent iron under anaerobic or aerobic conditions. RSC Advances 2017;7(15):8755–61.

Qin, H., Guan, X., Bandstra, J. Z., Johnson, R. L., & Tratnyek, P. G. (2018). Modeling the Kinetics of Hydrogen Formation by Zerovalent Iron: Effects of Sulfidation on Micro-and Nano-Scale Particles. Environmental science & technology, 52(23), 13887-13896.

Rajajayavel, Ghoshal S. Enhanced reductive dechlorination of trichloroethylene by sulfidated nanoscale zerovalent iron. Water Research 2015;78:144–53.

Reardon EJ. Anaerobic corrosion of granular iron: measurement and interpretation of hydrogen evolution rates. Environmental Science & Technology 1995;29(12):2936–45.

Schöftner P, Waldner G, Lottermoser W, Stöger-Pollach M, Freitag P, Reichenauer TG. Electron efficiency of nZVI does not change with variation of environmental parameters. The Science of the Total Environment 2015;535:69–78.

Tang H, Zhu D, Li T, Kong H, Chen W. Reductive dechlorination of activated carbon-adsorbed trichloroethylene by zero-valent iron: carbon as electron shuttle. Journal of Environmental Quality 2011;40(6):1878–85.

Tang F, Xin J, Zheng T, Zheng X, Yang X, Kolditz O. Individual and combined effects of humic acid, bicarbonate and calcium on TCE removal kinetics, aging behavior and electron efficiency of mZVI particles. Chemical Engineering Journal 2017;324:324–35.

Tang J, Tang L, Feng H, Zeng G, Dong H, Zhang C et al. pH-dependent degradation of p-nitrophenol by sulfidated nanoscale zerovalent iron under aerobic or anoxic conditions. J Hazard Mater 2016;320:581–90.

Tratnyek PG, Johnson RL. Nanotechnologies for environmental cleanup. Nano Today 2006;1(2):44–8.

Turcio-Ortega D, Fan D, Tratnyek PG, Kim E-J, Chang Y-S. Reactivity of Fe/FeS nanoparticles: electrolyte composition effects on corrosion electrochemistry. Environmental Science & Technology 2012;46(22):12484–92.

Velimirovic M, Carniato L, Simons Q, Schoups G, Seuntjens P, Bastiaens L. Corrosion rate estimations of microscale zerovalent iron particles via direct hydrogen production measurements. Journal of Hazardous Materials 2014;270:18–26.

Xu W, Dana KE, Mitch WA. Black carbon-mediated destruction of nitroglycerin and RDX by hydrogen sulfide. Environ. Sci. Technol. 2010;44(16):6409–15.

Xu W, Pignatello JJ, Mitch WA. Reduction of nitroaromatics sorbed to black carbon by direct reaction with sorbed sulfides. Environ. Sci. Technol. 2015;49(6):3419–26.

Yan W, Lien H-L, Koel BE, Zhang W-X. Iron nanoparticles for environmental clean-up: recent developments and future outlook. Environmental Science: Processes & Impacts 2013;15(1):63–77.

3.3. Combined chemical and microbiological degradation of PCE during the application of Carbo-Iron at a contaminated field site

Maria Vogel[a], Ivonne Nijenhuis[b], Jonathan Lloyd[c], Christopher Boothman[c], Marlén Pöritz[b], Katrin Mackenzie[a]*

[a] *Helmholtz Centre for Environmental Research – UFZ, Department of Environmental Engineering, D-04318 Leipzig, Germany*

[b] *Helmholtz Centre for Environmental Research – UFZ, Department of Isotope Biogeochemistry, D-04318 Leipzig, Germany*

[c] *School of Earth and Environmental Sciences, University of Manchester, Manchester* M13 9PL*, United Kingdom*

[*] Corresponding author e-mail: katrin.mackenzie@ufz.de

Abstract

After the injection of Carbo-Iron® in a PCE contaminated aquifer, combined chemical and microbiological contaminant degradation processes were found in a long-term study of a field site in Lower Saxony (Germany). The applied composite material Carbo-Iron, which consists of colloidal activated carbon and embedded nanoscale zero-valent iron (ZVI) structures, functioned as intended by accumulating the pollutants and promoting their reductive dechlorination. Furthermore the particles decreased the redox potential of the groundwater due to their reaction with oxygen and the ZVI corrosion-induced formation of molecular hydrogen up to 190 days after the injection, the latter promoting sulfate-reducing conditions. The emergence of *cis*-dichloroethene (*cis*-DCE), which was found only in traces before the injection of Carbo-Iron, and the presence of organisms related to *Sulfospirillum multivorans*, *Desulfitobacterium* spp. and *Dehalococcoides mccartyi*, indicate that Carbo-Iron is also able to support microbial

degradation of PCE. However, *cis*-DCE did not accumulate in the present case study although it is often observed at sites with active microbial dechlorination. The results of compound-specific isotope analysis in combination with pyrosequencing data suggested the oxidative degradation of *cis*-DCE by an organism related to *Polaromonas* sp. strain JS666. Consequently, the formation of the carcinogen degradation intermediate vinyl chloride was circumvented. Overall, the moderate and slow change of environmental conditions mediated by Carbo-Iron supported organohalide-respiring bacteria, but also created the basis for a subsequent microbial oxidation step.

Key words: Carbo-Iron, nanoiron, field test, PCE dechlorination, organohalide respiration, *Polaromonas* JS666

Graphical abstract

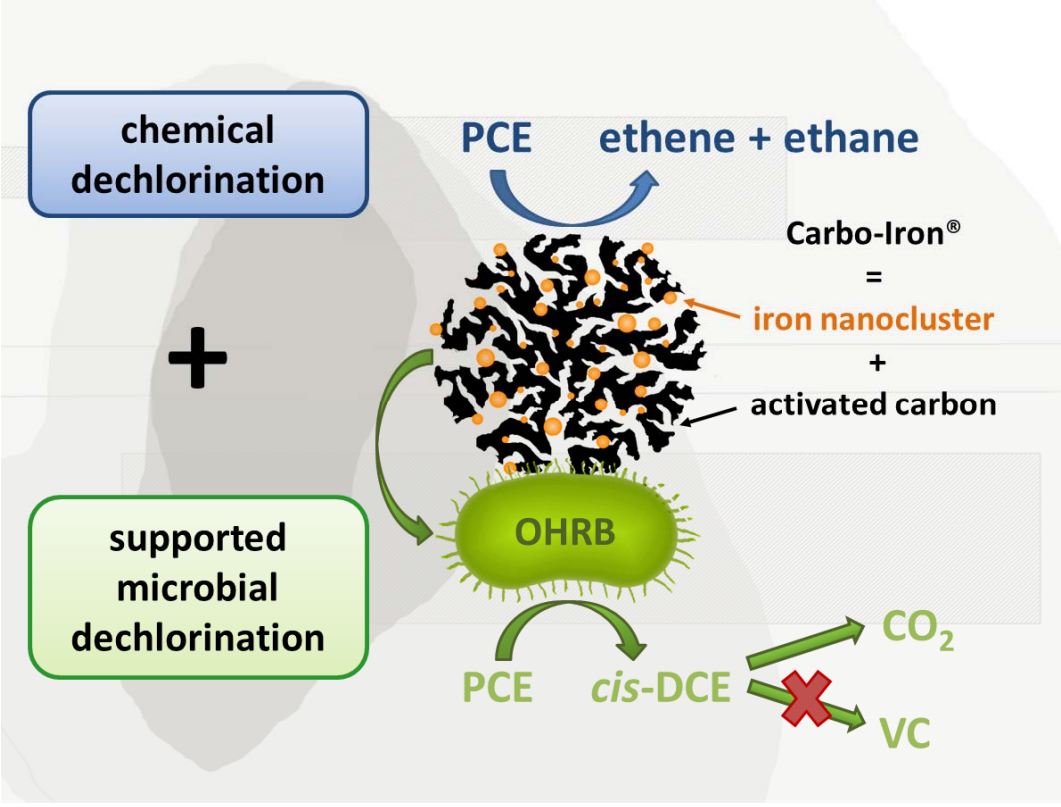

1. Introduction

The application of nanoscale zero-valent iron particles (nZVI) is an emerging innovative technology for the *in-situ* remediation of aquifers which are contaminated with toxic and persistent chlorinated ethenes (Fu et al., 2014; Yan et al., 2013). Recently, the material Carbo-Iron was developed, which consists of colloidal activated carbon (d_{50} < 1 µm) containing embedded nanoscale zero-valent iron structures. Due to its composite structure, Carbo-Iron overcomes some of the limitations of conventional nZVI (Mackenzie et al., 2012). Its composition and particle size lead to colloid particles with favourable transport and surface properties, and a high chemical reactivity coupled with the ability to strongly adsorb hydrophobic organic contaminants at the carbon surface (Bleyl et al., 2013; Mackenzie et al., 2012). After successful laboratory tests, the first pilot study with Carbo-Iron was started in 2012 as a two-step field test at a site in Lower Saxony (Germany), which was contaminated with tetrachloroethene (PCE) from a large dry cleaning facility. The pilot test comprised of a single-well injection of 20 kg Carbo-Iron (≙ 4 kg ZVI) followed 16 months later by a two-dimensional injection of 110 kg Carbo-Iron (≙ 22 kg ZVI) into the main contamination zone (Mackenzie et al., 2016). Besides the expected chemical degradation of PCE to ethene and ethane, the emergence of the intermediate *cis*-dichloroethene (*cis*-DCE) approximately one year after the first injection raised the question whether microbial transformation of PCE could have been triggered by the injected particles. Microbial reductive dechlorination is currently seen as a common attribute of anoxic groundwater systems, whereby the efficiency of dechlorination is highly variable under field conditions, and depends on the number of chlorine substituents of the pollutant (Adrian and Löffler, 2016; Bradley, 2003). The process involves organohalide-respiring bacteria (OHRB), which are able to couple electron transfer from H_2 or other electron donors to halogen removal from organohalides (Wang et al., 2016). Organisms of diverse genera, e.g. *Sulfurospirillum, Desulfitobacterium, Geobacter* or *Dehalobacter* can dechlorinate PCE to *cis*-DCE, but only *Dehalococcoides* is known to be capable of completely dechlorinating chlorinated ethenes to ethene, which includes the critical reduction steps via vinyl chloride (Adrian and Löffler, 2016).

As remediation actions driven abiotically by ZVI cannot be considered separately from microbial processes, a deeper understanding of the interaction of these two processes is necessary. The question of how nZVI particles and OHRB interact with each other has been already investigated

under laboratory conditions (Xie et al., 2017). It was shown that nZVI has the potential to support dechlorinating organisms by e.g. providing molecular hydrogen, which can be used by OHRB as an electron donor for reductive declorination (Xiu et al., 2010b). However, nZVI was also found to have toxic effects on microorganisms and to cause oxidative stress as well as cell membrane disruption at elevated ZVI concentrations (Diao and Yao, 2009; Fajardo et al., 2013). Exposure of *Dehalococcoides* spp. to nZVI led to decreased dechlorination rates and downregulation of the reductive dehalogenase genes *tceA* and *vcrA,* when normalised to 16S rRNA (Xiu et al., 2010a). This negative impact is usually reduced in environmental matrices (Chen et al., 2011) or when polymeric coatings inhibit the direct contact of the cells to the metal, e.g. when suspension stabilisers such as carboxymethyl cellulose (CMC) are applied (Li et al., 2010; Zhou et al., 2014). Besides influencing the growth and activity of OHRB, nZVI particles also have the potential to influence the composition and activities of the microbial community in the aquifer. Several studies have assessed this effect in laboratory experiments, and here only relatively short time periods ranging between a few hours and less than one month were considered (Fajardo et al., 2012; Fajardo et al., 2015; Kirschling et al., 2010; Kumar et al., 2014; Ma et al., 2015; Pawlett et al., 2013; Sacca et al., 2014; Tilston et al., 2013; Wu et al., 2013). nZVI was shown to cause a shift in the community composition or variations in gene expression. The effect depended strongly on the ZVI concentrations applied, and the characteristics of the tested soil and its microbial community. In contrast to the high number of laboratory studies, only a few publications have addressed the interactions of nZVI and microbial degradation activity in aquifers which are contaminated with chlorinated ethenes (He et al., 2010; Kocur et al., 2015; Kocur et al., 2016). These studies have shown that CMC-stabilised nZVI particles can affect microbial populations significantly, and that the growth and activity of OHRB, e.g. *Dehalococcoides* can be supported by their addition.

The aim of this study was to examine the impact of Carbo-Iron treatment on microbial processes at a previously described chloroethene contaminated field site in Lower Saxony (Germany) (Mackenzie et al., 2016). The effect of Carbo-Iron amendment on aquifer conditions after the injection of the composite material, and the influence on the microbial degradation of PCE were investigated. In addition to basic groundwater parameters, e.g. oxidation reduction potential (ORP) and pH value, the fate of the chlorinated ethenes and their reaction products

were examined within a monitoring period of around 600 days. The degradation state of the chlorinated ethenes was derived by compound-specific stable isotope analysis (CSIA). PCR-based 16S rRNA gene amplicon pyrosequencing, in combination with taxon and functional gene specific PCR were implemented to obtain information about the presence of dechlorinating bacteria, reductive dehalogenases and changes in the overall bacterial community.

2. Material and Methods

2.1. Description of the field site

The field site studied in Lower Saxony (Germany) has already been described (Mackenzie et al., 2016) focusing on the chemical activity of Carbo-Iron. The site was a former military area, which was contaminated by a dry-cleaning facility with chlorinated ethenes, mainly PCE. The dry-cleaning activities ended twenty years before the start of the field test. Mass calculations carried out previously gave an estimate of about 1,100 kg of chlorinated hydrocarbons contaminating an overbuilt area of about 10,000 m². A simplified map with the plume extension and the wells, which are relevant for the present study, is shown in Fig. 1. A more detailed map can be found in Mackenzie et al. (2016). In the hot spot area, PCE concentrations up to 720 µM were found, but a distinct source of undissolved solvent was not detected. The site is characterised by a hydraulic variability, showing a mean flow velocity of 30 cm d^{-1} for the southern part and 6 cm d^{-1} for the northern part. Upstream the groundwater level of the site is about 4 m, downstream about 6 m below ground level (bgl). The chemical composition of the groundwater is summarised in Table SI 3). The aquifer consists of an artificial infill of sand down to 0.5 m bgl, which is followed by a 25–30 m thick interbedded sequence of quaternary mixed sands and some clayey silt layers. The highest PCE concentration was found in the upper sandy layers at around 6 m bgl, which decreased down-gradient.

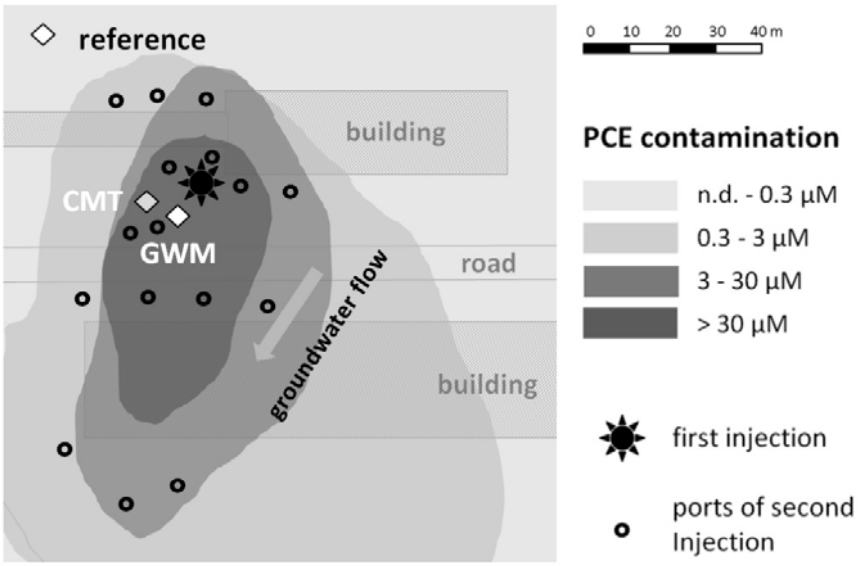

Fig. 1 - Site overview with plume extension, selected monitoring wells and injection ports within the demonstration test area according to Mackenzie et al., 2016.

2.2. Synthesis and injection of Carbo-Iron

Carbo-Iron particles used for the field test were synthesised according to Bleyl et al., 2012 and consisted of 21 wt% ZVI, 55 wt% activated carbon and 24 wt% iron oxides. The effective density of the water-filled porous particles was calculated to be about 1.7 g cm^{-3}. Detailed information on the physical and chemical properties of Carbo-Iron were given previously (Bleyl et al., 2012; Mackenzie et al., 2016). For the first stage of the pilot-scale field study, 20 kg of Carbo-Iron were suspended into 2 m^3 nitrogen-flushed, deoxygenised tap water (c_{ZVI} = 2 g L^{-1}), stabilised with 4 kg of low viscous carboxymethyl cellulose (CMC) (Antisol FL 30 from Wolff Cellulosics, molecular weight about 70,000 g mol^{-1}, substitution degree 0.85, viscosity 20-60 mPas Brookfield LVT at 25°C and 2 g L^{-1}) and injected into a depth of 6 m bgl, where the highest pollution concentration was measured (Mackenzie et al., 2016). One additional m^3 of water was used for subsequent rinsing. The second injection was delivered 450 days later using 110 kg Carbo-Iron ($c_{Carbo\text{-}Iron}$ = 15 g L^{-1}, c_{CMC} = 1.5 g L^{-1}), whereby the suspension was divided at 18 wells as shown in Fig. 1.

2.3. Sampling and analysis of groundwater parameters

Fig. 1 shows the location of the monitoring wells at the field site, which were selected for the present study. Information on all installed sampling wells can be found in Mackenzie et al. (2016). The Carbo-Iron-impacted monitoring wells named GWM (groundwater monitoring well with a sampling depth of 8.5 m bgl) and CMT (continuous-multi-channel-tubing monitoring well with seven ports in depths between 6 m and 25 m bgl), as well as the reference well (sampling depth of 8.5 m bgl), were chosen as sampling locations. The latter well was located within the PCE-contaminated area, but considered to be outside the radius of influence of the Carbo-Iron. Groundwater samples were taken using direct push technology, before injection and then frequently over a time frame of 600 days after the initial injection. During sampling 40 mL glass vials were completely filled with groundwater and airtight closed with PTFE-coated rubber septa and crimping with aluminium caps. The samples were stored at 4 °C. At the end of the 600 days monitoring period, sediment samples were collected by percussion drilling to a depth of 5 to 9 m bgl close to the GWM well and at the reference well (distance from well < 1 m). The 40 mL glass vials were filled with sediment, closed with screw caps, which were lined with PTFE-septa and stored at -18 °C.

On-site groundwater parameters were collected using multi-meter measurement devices (WTW, Germany) equipped with multiple probes, including SenTri 41 (pH value), TetraCon 325 (electrical conductivity), SenTix ORP (oxidation reduction potential) and CellOx 325 (oxygen level). Analysis of chloride, nitrate, nitrite, sulfate, sulphide, iron and total organic carbon was performed according to DIN standards or Golder standard operation procedures as listed in Table SI 1.

For the analysis of chlorinated ethenes and the non-chlorinated C_2-hydrocarbons ethane, ethene and acetylene, 1 mL of groundwater from the sampling vials was replaced by 1 mL of argon headspace. After equilibration of the headspace and water phase, headspace analysis was performed by a gas chromatograph coupled with a mass spectrometer (GC-MS). For measurement of the chlorinated ethenes a DB-624 capillary column (Agilent GC 5860/ MSD 5875C; measurement conditions: $T_{injector}$ = 200 °C; T_{oven} = 120 °C; $T_{detector}$ = 230 °C) was used. For measurement of the non-chlorinated products a DB-1 column (Shimadzu QP2010; measurement conditions: $T_{injector}$ = 80°C; T_{oven} = 27°C; $T_{detector}$ = 230°C) was applied.

2.4. Compound-specific isotope analysis (CSIA)

Stable carbon isotope composition of chlorinated ethenes in selected groundwater samples was determined by gas chromatography combined with a combustion isotope ratio mass spectrometer (Thermo GC Trace 1320 in combination with Thermo-Finnigan MAT 253 IRMS; Bremen, Germany). Samples were injected via the solvent vent method (Herrero-Martin et al., 2015) and chromatographically separated by a GC column ZB- 624 (60 m, 0.32 mm internal diameter, 1.8 µm film thickness). The carbon isotope composition is reported in δ-notation (‰) relative to the Vienna Pee Dee Belemnite standard (International Atomic Energy Agency, Vienna, Austria), as follows in equation (1) (Coplen, 2011):

$$\delta^{13}C\,[‰] = \left(\frac{(^{13}C/^{12}C)_{\text{sample}}}{(^{13}C/^{12}C)_{\text{standard}}} - 1\right) \cdot 1000 \qquad (1)$$

$(^{13}C/^{12}C)_i$ is the atomic ratio of carbon-13 and carbon-12 in the component *i.* As only a limited sample volume was available for CSIA, the analysis was performed only once per sample. A method standard deviation of 0.5 ‰ was estimated.

2.5. Organism specific 16S rRNA and functional gene-targeted PCR

For organism-specific 16S rRNA- and functional gene-targeted PCR, a groundwater sample from the monitoring well CMT and sediment samples in the vicinity of the reference and GWM wells were used. DNA isolation from sediment samples (1 g) was performed using the UltraClean™ Soil DNA extraction kit (Mo Bio Laboratories, USA) according to manufacturer's instructions. DNA from groundwater was obtained by filtration of 250 mL sample using sterile filters (0.2 µm pore diameter, cellulose acetate membrane) and extraction using the PowerWater DNA Isolation Kit (Mo Bio Laboratories, USA). Isolated DNA was stored at -20°C. 16S rRNA genes were amplified by PCR using HotStar Taq DNA Polymerase (Qiagen) and specific primers as shown in Table SI 2). The thermocycler program used during PCR amplification was as follows: initial denaturation at 95 °C for 15 min, followed by 40 cycles of primer annealing at 46 to 65 °C for 30 s, chain extension at 72 °C for 14 to 90 s, denaturation at 94 °C for 30 s and a final

extension at 72 °C for 10 min. The annealing temperature was calculated in accordance with the melting point of the primer (see equation SI 1). To check the length of the PCR products, they were separated by electrophoresis in a 1 – 2 % agarose gel and stained with ethidium bromide.

2.6. Broad-specificity 16S rRNA gene amplicon pyrosequencing and data analysis

In addition to the use of primers targeting specific taxonomic groups and their functional genes, broad-specificity 16S rRNA gene primers were also used for amplicon pyrosequencing analysis of key samples. Sediment samples from the vicinity of the reference and GWM well were used, which were taken according to the procedure described in 2.2. Furthermore, a groundwater sample of the monitoring point CMT (at 25 m bgl) was analysed. The samples were taken around 600 days after the first particle injection. The bacterial community structure was examined by analysis of DNA extracted from groundwater and sediment samples. DNA was extracted from 0.2 g of sediment using the MoBio PowerLyzer™ PowerSoil DNA Isolation Kit and 50 mL of ground water sample using the MoBio Power Water DNA Isolation Kit (MoBio Laboratories, Inc., Carlsbad, CA, USA). PCR for amplicon pyrosequencing was performed using tagged fusion bacterial primers 27F (Lane, 1991) and 907R (Muyzer, 1995), targeting the V1-V5 hypervariable region of the bacterial 16S rRNA gene. Pyrosequencing PCR was performed using Roche's 'Fast Start High Fidelity PCR system' as described previously (Bassil et al., 2015). The pyrosequencing run was performed by using a Roche 454 Life Sciences GS Junior system. The 454 pyrosequencing reads were analysed using Qiime 1.8.0 release (Caporaso et al., 2010), and denoising and chimera removal was performed in Qiime during OTU picking (at 97 % sequence similarity) with usearch (Edgar, 2010). Taxonomic classification of all reads was performed in Qiime using the Ribosomal Database Project (RDP) at 90 % confidence threshold (Cole et al., 2009), while the closest GenBank match for the OTUs that contained the highest number of reads (the representative sequence for each OTU was used) was identified by BLASTn nucleotide search. In addition, Qiime was used to show the rarefaction curves.

2.7. Confocal laser scanning microscopy (CLSM)

Groundwater samples from the well GWM, which contained Carbo-Iron particles were examined by CLSM using a TCS SP5X system (Leica, Germany) equipped with an upright

microscope and a super continuum laser source. The CLSM was controlled by the LASAF ver. 2.7.3 software. The particles were stained using the nucleic acid specific fluorochrome SybrGreen (Molecular Probes, Oregon). The laser line at 483 nm was selected for excitation and used in combination with a 63x NA 1.2 objective lens. Emission signals were collected from 478-488 nm (reflection) and 500-550 nm (nucleic acid stain). Image stacks were recorded at a 0.5 µm step size and presented as maximum intensity projections.

3. Results and discussion

3.1. Particle transport and change of aquifer conditions after the first injection of Carbo-Iron

As described by Mackenzie et al. (2016), CMC-stabilised particles can be transported with the groundwater flow up to a range of ten meters. Thereby the wells GWM and CMT, which are considered in the present study, could be reached. Besides the transport of the particles within the groundwater flow, a marked vertical descent from the injection depth of 6 m was also observed. The wide distribution of the Carbo-Iron particles in the contaminated sandy aquifer is a decisive key property for a combined chemical and biological remediation approach. The radius, where Carbo-Iron particles and microorganisms can potentially interact with each other is substantially larger compared to that of conventional low-mobile nZVI (Grieger et al., 2010; Wang et al., 2016). Carbo-Iron therefore has the capacity to improve the conditions for growth and activity of OHRB over a larger area.

At the present field site the initial mild anoxic conditions of the aquifer were not favourable for OHRB. As shown in Fig. 2 at the wells GWM and the reference (8.5 m bgl) values up to 300 mV were detected, whilst at the CMT well (22 m bgl) values of -50 mV were recorded. Sulphide was not found under these conditions. The more or less anoxic milieu can possibly be attributed to the influent of oxygen-containing surface water, which could easily pass through the sandy layers.

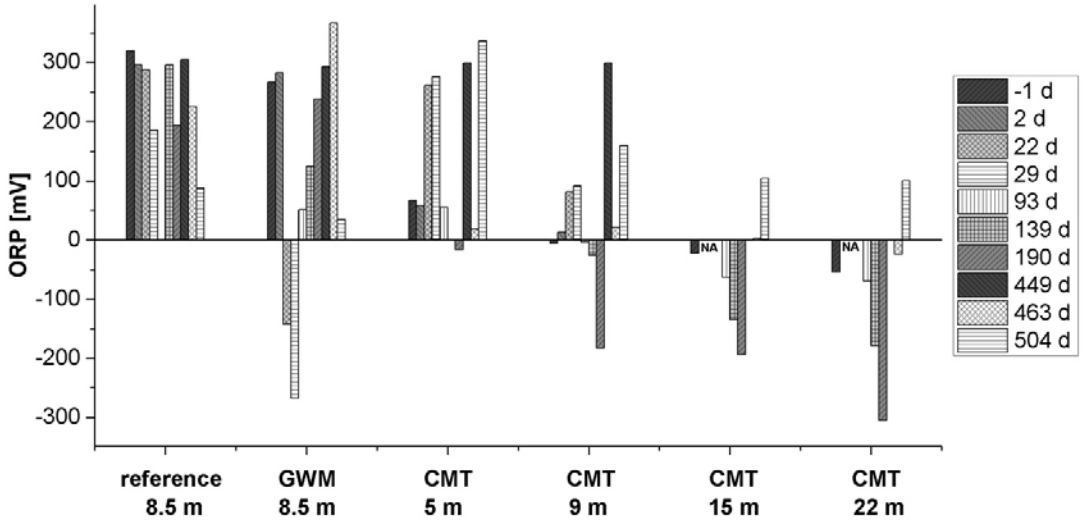

Fig. 2 - Oxidation-reduction potential (ORP) of groundwater from the Carbo-Iron-influenced wells GWM and CMT and at the reference well at different sampling depths before the injection (-1 d) and maximal 504 days after the first injection of Carbo-Iron. NA = not analysed.

The presence of CMC-stabilised Carbo-Iron particles led to a clear decrease of the ORP of the groundwater over time as shown in Fig. 2, whereby a large zone with improved conditions for OHRB was created. At the GWM well, which is close to the injection point, Carbo-Iron induced a decrease of the ORP, reaching -300 mV 30 days after the injection. Following this however, an increase of the ORP was observed, reaching positive redox values about 70 days later. Due to the geological conditions of the aquifer, the intrusion of oxygen-containing surface water can easily occur, leading to the oxidation of Carbo-Iron's embedded ZVI. In contrast, at all CMT sampling ports at and below 9 m bgl, the CMC-stabilised particles led to a decrease of the ORP of about 200 mV within 190 d, reaching -200 to -300 mV. Here the presence of traces of sulphide indicates that sulfate-reducing conditions were reached, which is favourable for growth and activity of OHRB. The delayed impact of Carbo-Iron at this monitoring well could possibly be explained by the slow transport of the Carbo-Iron suspension or single particles within the aquifer, and their density-induced descent to lower depths over time. Notable is the gradual, but continuing reducing effect of the injected particles, indicating a mild and long-term reactivity of the embedded ZVI nanostructures. In contrast, in the former studies from Kocur et al. (2015) and He et al. (2010) the redox milieu of the aquifer was affected very quickly and

strongly, with ORP reaching as low as -400 mV, but after some days to a few weeks the ORP values had returned to the pre-injection levels (He et al., 2010; Kocur et al., 2015; Kocur et al., 2016). Thereby $nZVI_{NaBH4}$ was used, which is characterised by a high dechlorination activity, but also by a high susceptibility to anaerobic corrosion, leading to a short life-time (Liu et al., 2005). In contrast, Carbo-Iron with its more crystalline nanostructured ZVI seems to have an extended life-time, which would be accompanied by a slower corrosion rate of the particles. The long lasting reducing effect of Carbo-Iron is a key property to support microbial dehalogenation efficiently, as growth and activity of these microorganisms occurs relatively slowly under environmental conditions.

The decrease of the ORP in the aquifer after the injection of Carbo-Iron can be associated with the reaction of the embedded ZVI with various groundwater components, e.g., molecular oxygen or other electron acceptors, which often impede microbial dechlorination (Bradley, 2003). Furthermore Carbo-Iron's ZVI reacts with water itself, forming molecular hydrogen via anaerobic corrosion. Hydrogen can be used by OHRB as terminal electron donor and is often limited in contaminated aquifers. Due to the gradual, but continuing reducing effect of the injected Carbo-Iron particles, a steady and long-term release of low amounts of hydrogen can be assumed, which is a large advantage over the short-living non-supported nZVI. Also the delivery of low amounts of hydrogen is desired for an efficient remediation as the competition of OHRB at low hydrogen partial pressures against methanogens is favourable (Fennell et al., 1997).

Beside the change of the ORP of the groundwater, the pH is also partially influenced by the injection of CMC-stabilised Carbo-Iron particles (see Fig. SI 1). At both, the reference and the monitoring GWM wells, where the groundwater was already slightly acidic (pH = 5.5), no substantial changes were observed. In contrast, at the CMT monitoring well between 5 m and 15 m bgl, a decrease of pH from around 7 to 6 occurred, which could be related to the metabolism of CMC by fermenting organisms (He et al., 2010; Kocur et al., 2016).

3.2. Monitoring of PCE and its degradation products

Before the injection of Carbo-Iron in the hot spot area of the field site, PCE concentrations up to 720 µM were found, but a distinct source of undissolved solvent was not detected. The

concentration of TCE amounted to < 2 µM, while *cis*-DCE was found only in trace quantities and vinyl chloride (VC) was not detected at all. The fact that the partially chlorinated products did not appear in significant concentrations could be an indication that complete reductive dechlorination by organisms such as *Dehalococcoides* spp. only played a minor role before Carbo-Iron was injected.

To gain further information about the extent of the transformation of PCE at the field site, CSIA was performed. Before the Carbo-Iron injection, the carbon isotope signature of PCE in groundwater of the CMT well amounted to δ_{PCE} = -25.5 ± 0.5 ‰ from 5 m down to 15 m bgl, while in zones at and below 18 m bgl an isotope signature of δ_{PCE} = -21 ± 0.5 ‰ was measured (see Fig. 4B). As the typical carbon isotope signature of PCE, produced by light petrol in Europe is typically in the range of -25 to -26 ‰ (Nijenhuis et al., 2013; van Warmerdam et al., 1995), it can be assumed that in the upper aquifer no degradation had occurred. This means that the main area of PCE contamination, located at around 6 m bgl (Mackenzie et al., 2016) was not accessible for microbial degradation, so that biological remediation of the field site was rather improbable under normal conditions. In the lower aquifer the carbon isotope signature of PCE indicates a degradation of the pollutant. Since both, microbial dechlorination and iron-mineral induced chemical reduction can lead to a strong fractionation, it is not possible to differentiate between these two processes (Nijenhuis et al., 2005; Zwank et al., 2005). However, since the degradation occurred predominantly in regions which are especially favourable for organohalide-respiring organisms, it implies that also microbial activity is involved in the degradation of the pollutant.

After the injection of Carbo-Iron, PCE depletion and the peak-like and long-lasting formation of high amounts of ethene and ethane were observed at the Carbo-Iron-influenced monitoring wells, while at the reference site no degradation products were found (Mackenzie et al., 2016).

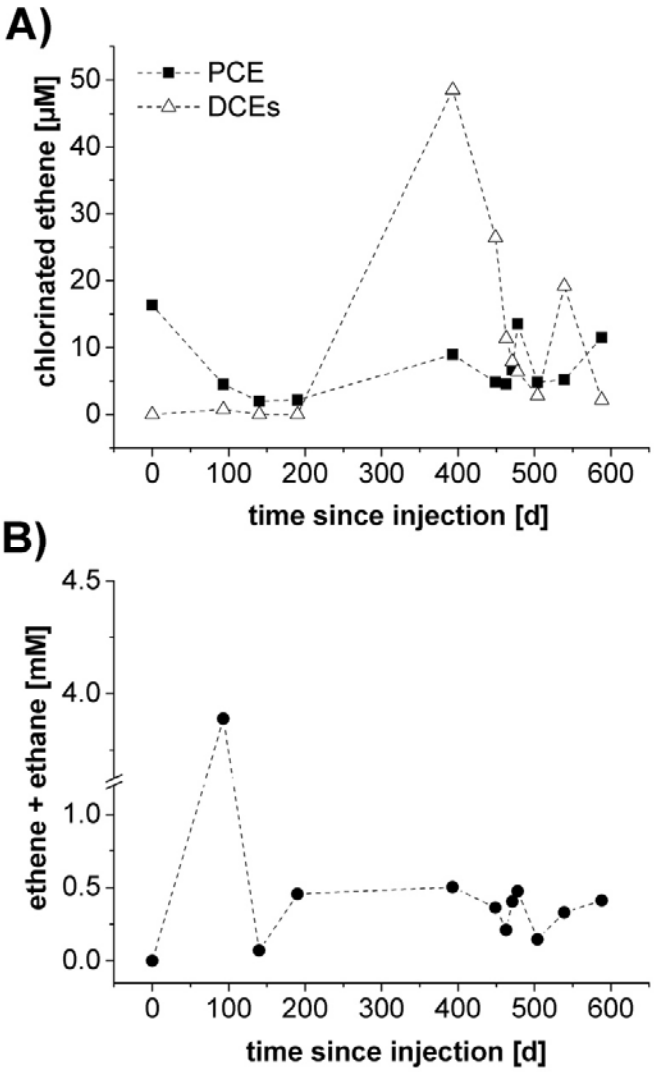

Fig. 3 - A) Concentration courses of chlorinated C_2-hydrocarbons and B) dechlorination products ethene and ethane over time at the monitoring well CMT at a depth of 22 m bgl.

In Fig. 3 the concentrations of the chlorinated hydrocarbons PCE and DCE and of the chlorine-free C_2-products at the CMT well at a depth of 22 m bgl over the monitoring period are depicted. Over the whole observation time no VC was detected (detection limit < 2 nM). Until 200 days after the injection of Carbo-Iron DCEs were found only in traces (≈ 50 nM). The presence of ethene, ethane and only negligible partially dechlorinated products corresponds to the product spectrum of the PCE degradation found under laboratory conditions (Mackenzie et al., 2012; Sunkara et al., 2015), which implies that the observed degradation is primarily

attributed to the chemical activity of Carbo-Iron. The long-term formation of ethene and ethane was notable and indicates in combination with the ORP decrease of the groundwater (see section 3.1) the extended life-time of ZVI in the injected particles. A possible explanation for the remarkable long life-time could be the high crystallinity of the embedded ZVI, but also its interaction with sulphide from the groundwater, leading to a corrosion-inhibiting FeS shell, as could be shown for $nZVI_{NaBH4}$, is conceivable (Fan et al., 2016; Vogel et al., 2018).

At the GWM and monitoring well no partially dechlorinated products were found in the long-term, while significant concentrations of DCEs (mainly *cis*-DCE) were detected around one year after the injection at the CMT well in depths between 12.5 m and 25 m bgl (see Fig. 3A and Fig. 4A). Unfortunately, there were no sampling campaigns during the winter months (day 200 to 380), so the course of degradation during this time period cannot be elucidated. As the sole formation of *cis*-DCE by ZVI is unlikely and DCE formation occurs most notably in regions which are favourable for OHRB, microbial participation seems to be plausible. Within the following 100 days after the highest *cis*-DCE concentration occurred, the intermediate disappeared gradually. To understand if *cis*-DCE disappeared due to dilution or degradation processes, CSIA was performed. The results of the carbon isotope analysis of groundwater samples from different sampling ports of the monitoring well CMT are shown in Fig. 4B. An enrichment of the heavier carbon isotope was observed over time with decreasing *cis*-DCE concentrations, which indicates a degradation process. The maximal change of the carbon isotope signature of *cis*-DCE was detected between day 393 and 449 at a depth of 12.5 m bgl from δ_{DCE} = -26.5 ± 0.5 ‰ to -24.7 ± 0.5 ‰. The 'real' isotope fractionation of the degradation process could be even higher, but is possibly masked by the parallel formation of *cis*-DCE. As a degradation process, the microbial reductive dechlorination by OHRB is rather unlikely, as VC was not detected. A dechlorination of the intermediate by Carbo-Iron is in principle possible, but would not lead to an isotope fractionation, as is known from sorption-dominated processes (Bombach et al., 2010; Braeckevelt et al., 2012). A possible degradation pathway could be the microbial oxidation of *cis*-DCE.

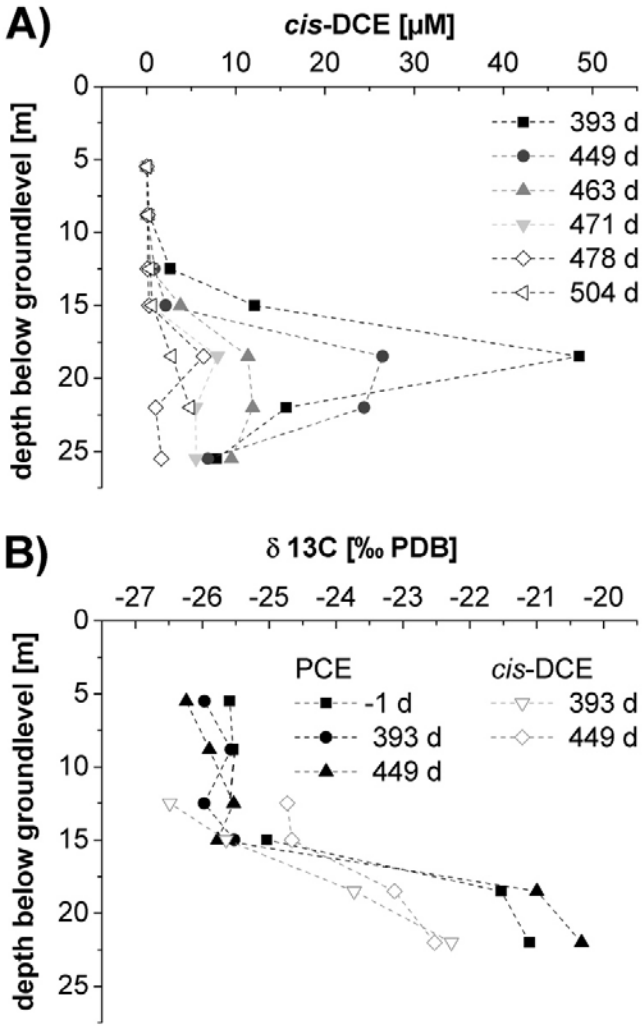

Fig. 4 - A) Lateral concentration profile of *cis*-DCE at the monitoring well CMT between 393 days up to 504 days after the injection of Carbo-Iron. B) Lateral isotope signature of PCE and *cis*-DCE at the monitoring well CMT before the injection (- 1 d) and up to 449 days after the injection of Carbo-Iron. The standard deviation of the method was estimated to about ± 0.5 ‰.

3.3. Detection of contaminant-degrading organisms

3.3.1. Organohalide-respiring bacteria

At the end of the monitoring period after around 600 days, groundwater from the CMT well and sediment samples in the vicinity of all the monitoring wells were collected and analysed by

broad-specificity 16S rRNA gene amplicon pyrosequencing. The analysis did not reveal the presence of known OHRB, which could be possibly explained by the low abundance of these organisms in the microbial community. For a more specific analysis of OHRB, specific 16S rRNA and functional gene-targeted PCR was performed. DNA was extracted from the samples and amplified by PCR targeting both the 16S rRNA gene present in all bacteria and the more specific dehalogenase genes *bvcA*, *pceA*, *tceA* and *vcrA*. The results are summarised in Table 1.

Table 1 - Summary of collected data from different monitoring points.

	reference	**influenced by Carbo-Iron**	
		GWM	**CMT**
depth bgl [m]	8.5	7 - 8.5	25
Carbo-Iron particles detected	no	yes	yes
detection of *cis*-DCE	no	traces	yes
presence of OHRB	no	no	*Sulfurospirillum multivorans* spp. *Desulfitobacterium* spp. *Dehalococcoides*
relative abundance of OTU most closely related to *Polaromonas* sp., strain JS666 [%]	5	1	1

In the monitoring well CMT at a depth of 25 m bgl, the presence of relatives to the dechlorinating bacteria *Sulfurospirillum multivorans* and *Desulfitobacterium* spp. was confirmed using primers specific for the 16S rRNA genes of these organisms. The dechlorinating *Dehalococcoides mccartyi* could also be detected; however, detection of dehalogenase genes was not successful. One reason for the missing evidence of dehalogenase genes could be the low abundance of this organism, but also other unknown, not analysed genes could be involved in the dechlorination. The presence of the detected OHRB at the monitoring well CMT, combined with the formation of *cis*-DCE between 12.5 and 25 m bgl supports the assumption that Carbo-Iron is able to support the microbial dechlorination of PCE. At the reference and the GWM well, at a depth down to 8.5 m bgl, no dechlorinating microorganisms could be detected using the genus specific primers noted in SI Table 1. A possible reason could be the intrusion of

oxygen-containing surface water into the upper aquifer, which is not favourable for the growth and activity of OHRB (Bradley and Chapelle, 2010).

3.3.2. Organism related to Polaromonas sp. strain JS666

The use of broad-specificity 16S rRNA gene amplicon pyrosequencing revealed the presence of an organism related to *Polaromonas* sp. strain JS666 at the field site (98 % identities). It is the only microorganism known thus far to be capable of oxidizing *cis*-DCE by using it as sole carbon and energy source (Jennings et al., 2009; Mattes et al., 2008). For the metabolic degradation of *cis*-DCE by *Polaromonas* sp. strain JS666 an enrichment of carbon-13 is described in literature (Abe et al., 2009; Jennings et al., 2009), which could be associated with isotope fractionation of the intermediate at the CMT monitoring well (see 3.2). The presence of this species at the different monitoring wells is shown in Fig. 5. A notably high abundance of the operational taxonomic unit (OTU) related to *Polaromonas sp.* (up to 18 % of the 16S rRNA genes detected) was found at the reference point in the upper levels of the aquifer. In sediments affected by Carbo-Iron (GWM well) the abundance of this OTU was even more pronounced. Both sampling spots were frequently affected by fresh rain water run-off, and subsequent intrusion of oxygenated water into the upper aquifer. However, more surprisingly the organism could also be detected in a low percentage range in the CMT monitoring well at a depth of 25 m bgl, where anoxic conditions prevail.

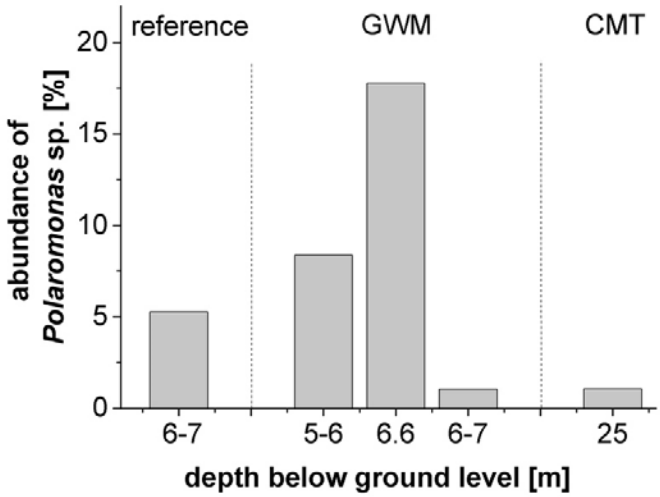

Fig. 5 - Abundance of OTUs related to Polaromonas sp. strain JS666 at the reference point and Carbo-Iron influenced wells GWM and CMT.

Although it is assumed that growth-coupled oxidation of *cis*-DCE is not common at field sites (Giddings et al., 2010), we have shown here that relatives of a known *cis*-DCE -degrading *Polaromonas* strain can be a dominant species in the microbial community. As proposed by Giddings et al., 2010 JS666 is a prime candidate for bioaugmentation at sites where *cis*-DCE has migrated into aerobic zones. Despite the high potential of this organism for complete degradation of chlorinated ethenes, until now there is still a lack of knowledge, especially in terms of field data. Further investigation is necessary and advised.

In our field study the oxidative degradation of *cis*-DCE most likely complemented the Carbo-Iron-supported microbial degradation of PCE. An advantage of this degradation pathway is the prevention of VC formation. Possibly, the mild and long-term reducing activity of Carbo-Iron could have been advantageous, as it helps to create conditions for OHRB, but still leaves the possibility of a subsequent oxidative step.

3.4. General bacterial community at the field site after Carbo-Iron injection

Characterisation of the microbial community at the field site was performed at the end of the monitoring period, around 600 days after the injection, by 16S rRNA amplicon pyrosequencing. A general overview of the microbial community of Carbo-Iron influenced wells and at the reference well, ordered by the phylogenetic class is shown in Fig. 6A.

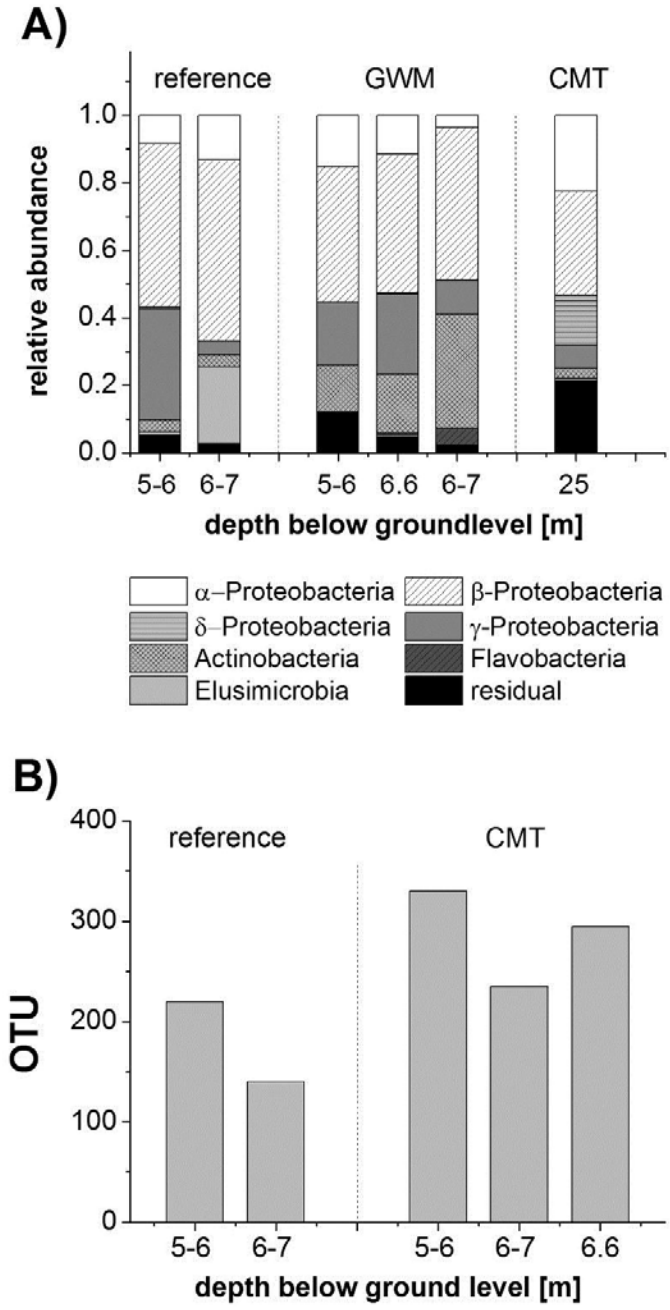

Fig. 6. - A) Relative abundance of bacteria at phylogenetic class level in sediment samples (reference, GWM) and groundwater sample (CMT) around 600 days after the injection of Carbo-Iron. OTUs of bacteria of low abundance are summarised as residual fraction. B) Number of operational taxonomic units (OTUs) of sediment samples at the reference point and Carbo-Iron influenced well GWM.

At all monitoring wells over 70 % of the microorganisms belonged to the phylogenetic classes of β-Proteobacteria, Actinobacteria and α-Proteobacteria. In general, the community composition did not differ strongly between the particle-affected well and the reference. The number of operational taxonomic units (OTUs), as an indicator for microbial diversity, was higher in the Carbo-Iron impacted zone, than at the reference well (see Fig. 6B).

The search for characteristic organisms in the site sediments revealed the presence of those related to *Rhodoferax ferrireducens* in the Carbo-Iron impacted wells. This organism is capable of using Fe(III) as electron acceptor in its respiration (Finneran et al., 2003). The abundance of this species decreased down-gradient at the drilling point near well GWM from 11 % at 5-6 m bgl to 9 % at 6-7m down and then to 1 % at around 8 m bgl. *Rhodoferax ferrireducens* was also found to be present at monitoring well CMT as 1.5 % of the microbial community at a depth of 25 m bgl, while at the reference point this Fe(III)-reducing species was not detected. During the ageing of Carbo-Iron, Fe^{2+} and Fe^{3+} species are generated, which could support the growth and activity of this species.

3.5. Microbial attachment at the Carbo-Iron surface

At the monitoring wells CMT and GWM, which are located downstream of the injection point, a small mobile fraction of Carbo-Iron particles was found several weeks after the injection (Mackenzie et al., 2016). As expected, at the reference site no suspended particles were observed. In order to aid identification of the particles in sediment material and suspended in pore water, temperature-programmed oxidation was applied as described by Mackenzie et al., 2016. Such particles were subjected to CLSM in order to search for attached microorganisms. In Fig. 7 images received by CLSM of the detected particles are shown. Noticeable is the large size of the aggregates (10 – 50 µm), which is far beyond the diameter of the single particles of d_{50} < 1 µm. The particle assemblies chosen for the CLSM analysis were the larger ones, visible by the naked eye. The fraction of particles, which were in the range of a few µm, remained unrecognised here.

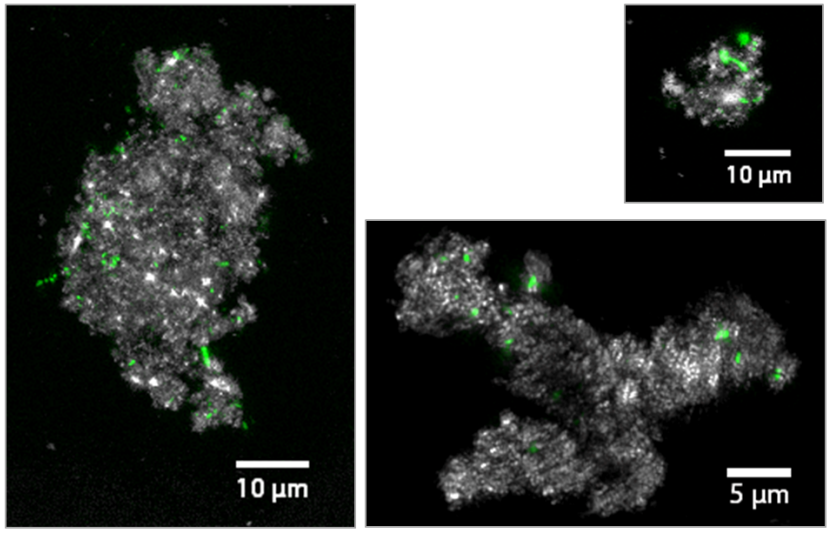

Fig. 7 - Confocal laser scanning microscopy images of Carbo-Iron particles three months after the injection. The grey reflections depict Carbo-Iron itself and the SybrGreen-dyed structures represent at the surface attached microorganisms.

The CLSM images show bacterial attachment at the surface of the particles took place, even for Carbo-Iron collected from the field site during its chemically reactive phase, which still contained metallic iron. In the composite material the majority of the ZVI component is embedded in the pores of the activated carbon, so that microorganisms are less likely to come into direct contact with the reactive metal surface. This is a large advantage over conventional nZVI because the direct attachment of nZVI on cell membranes of microorganisms is considered as a reason for the metal's cytotoxicity (Wang et al., 2016; Xie et al., 2017).

3.6. Possible further interactions of Carbo-Iron with microorganisms

Carbo-Iron offers with its component structure further advantages compared to pure metal particles and therefore additional possibilities to support microbial dechlorination. The attachment of the microorganisms on the particle surface can potentially lead to the formation of a microbial biofilm, which has different properties compared to planktonic suspensions, such as higher tolerance to toxicity, optimised acquisition of nutrients and the resistance to mechanical and environmental stress (Flemming et al., 2016). In addition, Carbo-Iron could have the potential to promote direct interspecies electron transfer, as is known from activated carbon alone (Liu et al., 2012). Furthermore the sorption affinity of the composite activated

carbon towards hydrophobic pollutants drastically reduces the concentration of the contaminants in the freely dissolved state, thus reducing the toxic concentrations of the pollutants. As shown for activated carbon, this reduction in the pollutant concentration below the toxicity level can support general microbial turnover processes (Meynet et al., 2012), from which OHRB could also gain a benefit. Carbo-Iron would also have a large advantage over nZVI such that it can sorb organic toxic intermediates that are formed, preventing their escape from the treatment zone.

4. Conclusion

Data from a field study show that the application of Carbo-Iron in a PCE-contaminated aquifer combines chemical and biological remediation pathways. Carbo-Iron provides chemical reactivity for degradation of PCE to fully dechlorinated products ethene and ethane with negligible by-product formation. In addition it seems also able to support OHRB which can transform PCE to *cis*-DCE over longer time periods. The latter can be supported by ZVI-induced release of hydrogen and/or by the surface and sorption properties of activated carbon. While conventional $nZVI_{NaBH4}$ is characterised by a high reactivity, connected to a high corrosion tendency and a short life-time, the reducing effect of Carbo-Iron is slower, but long-lasting. In contrast to other PCE contaminated field sites with active dechlorinating bacteria, the intermediate *cis*-DCE did not accumulate in the present study. The results of compound-specific isotope analysis in combination with pyrosequencing data let assume the oxidative degradation of *cis*-DCE by an organism related to *Polaromonas* sp. strain JS666. Although the moderate and slow change of environmental conditions by Carbo-Iron allowed support of OHRB, it still offered possibilities for a subsequent oxidative step. In our opinion the coupling of ZVI-induced support of microbial reduction of PCE with subsequent oxidation of *cis*-DCE is a promising strategy and should be preferred in permeable, slightly anoxic aquifers.

Acknowledgements

The authors thank the integrated project “Controlling Chemicals’ Fate” at the Helmholtz Centre for Environmental Research for financial support, Dr. Ronald Krieg for sediment sampling and

Dr. Thomas Neu for performing confocal laser scanning microscopy. Furthermore the authors thank for financial support within the research projects NanoREM (Project Nr.: 309517, EU 7th FP, NMP.2012.1.2) and Fe-Nanosit (Project Nr.: BMBF 03X0082A).

References

Abe Y, Aravena R, Zopfi J, Shouakar-Stash O, Cox E, Roberts JD et al. Carbon and chlorine isotope fractionation during aerobic oxidation and reductive dechlorination of vinyl chloride and cis-1,2-dichloroethene. Environmental Science & Technology 2009;43(1):101–7.

Adrian L, Löffler FE, editors. Organohalide-respiring bacteria: Springer Berlin Heidelberg; 2016.

Bassil NM, Bryan N, Lloyd JR. Microbial degradation of isosaccharinic acid at high pH. The ISME journal 2015;9(2):310–20.

Bleyl S, Kopinke F, Georgi A, Mackenzie K. Carbo-Iron - ein massgeschneidertes Reagenz zur *In-situ*-Grundwassersanierung. Chemie Ingenieur Technik 2013;85(8):1302–11.

Bleyl S, Kopinke F, Mackenzie K. Carbo-Iron® - synthesis and stabilization of Fe(0)-doped colloidal activated carbon for in situ groundwater treatment. Chemical Engineering Journal 2012;191:588–95.

Bombach P, Richnow HH, Kästner M, Fischer A. Current approaches for the assessment of in situ biodegradation. Applied Microbiology and Biotechnology 2010;86(3):839–52.

Bradley PM. History and ecology of chloroethene biodegradation: A Review. Bioremediation Journal 2003;7(2):81–109.

Bradley PM, Chapelle FH. Biodegradation of chlorinated ethenes. In: Stroo HF, Ward CH, editors. In situ remediation of chlorinated solvent plumes. New York, NY: Springer New York; 2010. p. 39–67.

Braeckevelt M, Fischer A, Kästner M. Field applicability of compound-specific isotope analysis (CSIA) for characterization and quantification of in situ contaminant degradation in aquifers. Applied Microbiology and Biotechnology 2012;94(6):1401–21.

Chen J, Xiu Z, Lowry GV, Alvarez PJJ. Effect of natural organic matter on toxicity and reactivity of nano-scale zero-valent iron. Water Research 2011;45(5):1995–2001.

Coplen TB. Guidelines and recommended terms for expression of stable-isotope-ratio and gas-ratio measurement results. Rapid Communications in Mass Spectrometry 2011;25(17):2538–60.

Diao M, Yao M. Use of zero-valent iron nanoparticles in inactivating microbes. Water Research 2009;43(20):5243–51.

Fajardo C, Gil-Díaz M, Costa G, Alonso J, Guerrero AM, Nande M et al. Residual impact of aged nZVI on heavy metal-polluted soils. Science of the Total Environment 2015;535:79–84.

Fajardo C, Ortíz LT, Rodríguez-Membibre ML, Nande M, Lobo MC, Martin M. Assessing the impact of zero-valent iron (ZVI) nanotechnology on soil microbial structure and functionality: a molecular approach. Chemosphere 2012;86(8):802–8.

Fajardo C, Sacca ML, Martinez-Gomariz M, Costa G, Nande M, Martin M. Transcriptional and proteomic stress responses of a soil bacterium Bacillus cereus to nanosized zero-valent iron (nZVI) particles. Chemosphere 2013;93(6):1077–83.

Fan D, O'Brien Johnson G, Tratnyek PG, Johnson RL. Sulfidation of nano zerovalent iron (nZVI) for improved selectivity during *in-situ* chemical reduction (ISCR). Environmental Science & Technology 2016;50(17):9558–65.

Fennell DE, Gossett JM, Zinder SH. Comparison of butyric acid, ethanol, lactic acid, and propionic acid as hydrogen donors for the reductive dechlorination of tetrachloroethene. Environmental Science & Technology 1997;31(3):918–26.

Finneran KT, Johnsen CV, Lovley DR. Rhodoferax ferrireducens sp. nov., a psychrotolerant, facultatively anaerobic bacterium that oxidizes acetate with the reduction of Fe(III). International Journal of Systematic and Evolutionary Microbiology 2003;53(Pt 3):669–73.

Flemming H, Wingender J, Szewzyk U, Steinberg P, Rice SA, Kjelleberg S. Biofilms: an emergent form of bacterial life. Nature reviews. Microbiology 2016;14(9):563–75.

Fu F, Dionysiou DD, Liu H. The use of zero-valent iron for groundwater remediation and wastewater treatment: a review. Journal of Hazardous Materials 2014;267:194–205.

Giddings CGS, Liu F, Gossett JM. Microcosm assessment of Polaromonas sp. JS666 as a bioaugmentation agent for degradation of cis-1,2-dichloroethene in aerobic, subsurface environments. Ground Water Monitoring & Remediation 2010;30(2):106–13.

Grieger KD, Fjordboge A, Hartmann NB, Eriksson E, Bjerg PL, Baun A. Environmental benefits and risks of zero-valent iron nanoparticles (nZVI) for in situ remediation: risk mitigation or trade-off? Journal of Contaminant Hydrology 2010;118(3-4):165–83.

He F, Zhao D, Paul C. Field assessment of carboxymethyl cellulose stabilized iron nanoparticles for in situ destruction of chlorinated solvents in source zones. Water Research 2010;44(7):2360–70.

Herrero-Martin S, Nijenhuis I, Richnow HH, Gehre M. Coupling of a headspace autosampler with a programmed temperature vaporizer for stable carbon and hydrogen isotope analysis of volatile organic compounds at microgram per liter concentrations. Analytical Chemistry 2015;87(2):951–9.

Jennings LK, Chartrand MMG, Lacrampe-Couloume G, Lollar BS, Spain JC, Gossett JM. Proteomic and transcriptomic analyses reveal genes upregulated by cis-dichloroethene in Polaromonas sp. strain JS666. Applied and Environmental Microbiology 2009;75(11):3733–44.

Kirschling TL, Gregory KB, Minkley EG, Lowry GV, Tilton RD. Impact of nanoscale zero valent iron on geochemistry and microbial populations in trichloroethylene contaminated aquifer materials. Environmental Science & Technology 2010;44(9):3474–80.

Kocur CMD, Lomheim L, Boparai HK, Chowdhury AIA, Weber KP, Austrins LM et al. Contributions of abiotic and biotic dechlorination following carboxymethyl cellulose stabilized nanoscale zero valent iron injection. Environmental Science & Technology 2015;49(14):8648–56.

Kocur CMD, Lomheim L, Molenda O, Weber KP, Austrins LM, Sleep BE et al. Long-term field study of microbial community and dechlorinating activity following carboxymethyl cellulose-stabilized nanoscale zero-valent iron injection. Environmental Science & Technology 2016;50(14):7658–70.

Kumar N, Omoregie EO, Rose J, Masion A, Lloyd JR, Diels L et al. Inhibition of sulfate reducing bacteria in aquifer sediment by iron nanoparticles. Water Research 2014;51:64–72.

Li Z, Greden K, Alvarez PJJ, Gregory KB, Lowry GV. Adsorbed polymer and NOM limits adhesion and toxicity of nano scale zerovalent iron to E. coli. Environmental Science & Technology 2010;44(9):3462–7.

Liu F, Rotaru A, Shrestha PM, Malvankar NS, Nevin KP, Lovley DR. Promoting direct interspecies electron transfer with activated carbon. Energy & Environmental Science 2012;5(10):8982.

Liu Y, Majetich SA, Tilton RD, Sholl DS, Lowry GV. TCE Dechlorination rates, pathways, and efficiency of nanoscale iron particles with different properties. Environmental Science & Technology 2005;39(5):1338–45.

Ma Y, Metch JW, Vejerano EP, Miller IJ, Leon EC, Marr LC et al. Microbial community response of nitrifying sequencing batch reactors to silver, zero-valent iron, titanium dioxide and cerium dioxide nanomaterials. Water Research 2015;68:87–97.

Mackenzie K, Bleyl S, Georgi A, Kopinke F. Carbo-Iron - An Fe/AC composite - As alternative to nano-iron for groundwater treatment. Water Research 2012;46(12):3817–26.

Mackenzie K, Bleyl S, Kopinke F, Doose H, Bruns J. Carbo-Iron as improvement of the nanoiron technology: From laboratory design to the field test. Science of the Total Environment 2016;563-564:641–8.

Mattes TE, Alexander AK, Richardson PM, Munk AC, Han CS, Stothard P et al. The genome of Polaromonas sp. strain JS666: insights into the evolution of a hydrocarbon- and xenobiotic-degrading bacterium, and features of relevance to biotechnology. Applied and Environmental Microbiology 2008;74(20):6405–16.

Meynet P, Hale SE, Davenport RJ, Cornelissen G, Breedveld GD, Werner D. Effect of activated carbon amendment on bacterial community structure and functions in a PAH impacted urban soil. Environmental Science & Technology 2012;46(9):5057–66.

Nijenhuis I, Andert J, Beck K, Kastner M, Diekert G, Richnow HH. Stable isotope fractionation of tetrachloroethene during reductive dechlorination by Sulfurospirillum multivorans and Desulfitobacterium sp. strain PCE-S and abiotic reactions with cyanocobalamin. Applied and Environmental Microbiology 2005;71(7):3413–9.

Nijenhuis I, Schmidt M, Pellegatti E, Paramatti E, Richnow HH, Gargini A. A stable isotope approach for source apportionment of chlorinated ethene plumes at a complex multi-contamination events urban site. Journal of Contaminant Hydrology 2013;153:92–105.

Pawlett M, Ritz K, Dorey RA, Rocks S, Ramsden J, Harris JA. The impact of zero-valent iron nanoparticles upon soil microbial communities is context dependent. Environmental Science and Pollution Research International 2013;20(2):1041–9.

Sacca ML, Fajardo C, Costa G, Lobo C, Nande M, Martin M. Integrating classical and molecular approaches to evaluate the impact of nanosized zero-valent iron (nZVI) on soil organisms. Chemosphere 2014;104:184–9.

Sunkara B, Su Y, Zhan J, He J, McPherson GL, John VT. Iron-carbon composite microspheres prepared through a facile aerosol-based process for the simultaneous adsorption and reduction of chlorinated hydrocarbons. Frontiers of Environmental Science & Engineering 2015;9(5):939–47.

Tilston EL, Collins CD, Mitchell GR, Principalle J, Shaw LJ. Nanoscale zerovalent iron alters soil bacterial community structure and inhibits chloroaromatic biodegradation potential in Aroclor 1242-contaminated soil. Environmental Pollution 2013;173:38–46.

van Warmerdam EM, Frape SK, Aravena R, Drimmie RJ, Flatt H, Cherry JA. Stable chlorine and carbon isotope measurements of selected chlorinated organic solvents. Applied Geochemistry 1995;10(5):547–52.

Vogel M, Georgi A, Kopinke F, Mackenzie K. Sulphidation of C/Fe composites leads to highly corrosion-resistant nanoremediation particles with extended life-time. in preparation 2018.

Wang S, Chen S, Wang Y, Low A, Lu Q, Qiu R. Integration of organohalide-respiring bacteria and nanoscale zero-valent iron (Bio-nZVI-RD): A perfect marriage for the remediation of organohalide pollutants? Biotechnology Advances 2016;34(8):1384–95.

Wu D, Shen Y, Ding A, Mahmood Q, Liu S, Tu Q. Effects of nanoscale zero-valent iron particles on biological nitrogen and phosphorus removal and microorganisms in activated sludge. Journal of Hazardous Materials 2013;262:649–55.

Xie Y, Dong H, Zeng G, Tang L, Jiang Z, Zhang C et al. The interactions between nanoscale zero-valent iron and microbes in the subsurface environment: A review. Journal of Hazardous Materials 2017;321:390–407.

Xiu Z, Gregory KB, Lowry GV, Alvarez PJJ. Effect of bare and coated nanoscale zerovalent iron on tceA and vcrA gene expression in *Dehalococcoides* spp. Environmental Science & Technology 2010a;44(19):7647–51.

Xiu Z, Jin Z, Li T, Mahendra S, Lowry GV, Alvarez PJJ. Effects of nano-scale zero-valent iron particles on a mixed culture dechlorinating trichloroethylene. Bioresource Technology 2010b;101(4):1141–6.

Yan W, Lien H, Koel BE, Zhang W. Iron nanoparticles for environmental clean-up: Recent developments and future outlook. Environmental Science: Processes & Impacts 2013;15(1):63–77.

Zhou L, Le Thanh T, Gong J, Kim J, Kim E, Chang Y. Carboxymethyl cellulose coating decreases toxicity and oxidizing capacity of nanoscale zerovalent iron. Chemosphere 2014;104:155–61.

Zwank L, Elsner M, Aeberhard A, Schwarzenbach RP, Haderlein SB. Carbon isotope fractionation in the reductive dehalogenation of carbon tetrachloride at iron (hydr)oxide and iron sulfide minerals. Environmental Science & Technology 2005;39(15):5634–41.

Supporting Information for "Combined chemical and microbiological degradation of PCE during the application of Carbo-Iron at a contaminated field site"

Maria Vogel[a], Ivonne Nijenhuis[b], Jonathan Lloyd[c], Christopher Boothman[c], Marlén Pöritz[b], Katrin Mackenzie[a]

[a] *Helmholtz Centre for Environmental Research – UFZ, Department of Environmental Engineering, D-04318 Leipzig, Germany*

[b] *Helmholtz Centre for Environmental Research – UFZ, Department of Isotope Biogeochemistry, D-04318 Leipzig, Germany*

[c] *School of Earth and Environmental Sciences, University of Manchester, Manchester* M13 9PL*, United Kingdom*

[*] Corresponding author e-mail: katrin.mackenzie@ufz.de

Content:

Table SI 1 Analysis of groundwater parameter

Table SI 2 Applied primers for PCR analysis

Calculation of annealing temperature

Table SI 3 Groundwater analysis before the injection of Carbo-Iron

Figure SI 1 pH of groundwater from the Carbo-Iron-influenced monitoring wells GWM and CMT and at the reference well at different sampling depths before (-1 d) and maximal 504 days after the first injection of Carbo-Iron

Table SI 1 - Analysis of groundwater parameter.

Parameter	Method
chlorinated hydrocarbons (PCE, TCE, DCEs, VC)	DIN EN ISO 10301-3
chloride	DIN EN ISO 10304 (1/2)
nitrate	DIN EN ISO 10304 (1/2)
nitrite	DIN EN 26777
phosphate	DIN EN ISO 6878-4 D11
sulphate	DIN EN ISO 10304 (1/2)
sulphide (easily released)	DIN 38405 D27
iron	DIN EN ISO 11885
total organic carbon (TOC)	DIN EN 1484
pH-Wert	Golder standard operation procedure
electrical conductivity	Golder standard operation procedure
oxidation reduction potential (Ag/AgCl)	Golder standard operation procedure
oxygen	Golder standard operation procedure

Table SI 2 - Applied primers for PCR analysis.

Name	Sequence (5' → 3')	Targeted gene	Reference
Organism-specific primer			
27F	AGAGTTTGATCMTGGCTCAG	16S rRNA-gene-fragment bacteria	(Schumann, 1991)
1378R	GGGCGGWGTGTACAAGGC		(Heuer et al., 1997)
DHC1f	GATGAACGCTAGCGGCG	16S rRNA-Gen-fragment *Dehalococcoides mccartyi* spp.	(Hendrickson et al., 2002)
DHC1377r	GGTTGGCACATCGACTTCAA		
DHC774f	GGGAGTATCGACCCTCTC		
DHC1212r	GGATTAGCTCCAGTTCACACTG		
DET730f	GCGGTTTTCTAGGTTGTC		(Bunge et al., 2003)
DET1350r	CACCTTGCTGATATGCGG		
CBDB1350r	CACCATGCTGATATGCGG		
Dre441f	GTTAGGGAAGAACGGCATCTGT	16S rRNA gene fragment *Dehalobacter* sp.	(Smits et al., 2004)
Dre645r	CCTCTCCTGTCCTCAAGCCATA		
Dre1013r	CGAAGCACTCCCATATCT		
Geo196f	GAATATGCTCCTGATTC	16S rRNA gene fragment *Geobacter* sp.	(Ding and He, 2012)
Geo535r	TAAATCCGAACAACGCTT		
Geo999r	ACCCTCTACTTTCATAG		
Sulfuro114f	GCTAACCTGCCCTTTAGTGG	16S rRNA gene fragment *Sulfurospirillum multivorans*	(Duhamel and Edwards, 2006)
Sulfuro421r	GTTTACACACCGAAATGCGT		
Dsb406F	GTACGACGAAGGCCTTCGGGT	16S rRNA gene fragment *Desul-fitobacterium* spp.	(Smits et al., 2004)
Dsb619R	CCCAGGGTTGAGCCCTAGGT		
Dsb1027r	CTCATAGCTCCCCGAAGG		

Name	Sequence (5' → 3')	Targeted gene	Reference
Organism-specific primer			
BB1f/Dsf 205f	AACCTTCGGGTCCTACTGTC	16S rRNA gene fragment *Desul-furomonas* spp	(Loffler et al., 2000)
BB1r/Dsf1020r	GCCGAACTGACCCCTATGTT		
Dehalogenase gene specific primer			
bvcAf	TGCCTCAAGTACAGGTGGT	Orthologous genes of *bvcA*	(Krajmalnik-Brown et al., 2004)
bvcAr	ATTGTGGAGGACCTACCT		
cbdbA1588f	CTGAAAGGAATAGGTCTGG	Orthologous genes of cbdbA1588 (*pceA*)	(Wagner et al., 2009)
cbdbA1588r	GTAGACTGGGATCCATGC		
vcrAf	TGCTGGTGGCGTTGGTGCTCT	Orthologous genes of *vcrA*	(Muller et al., 2004)
vcrAr	TGCCCGTCAAAAGTGGTAAAG		
vcrA642f	GAAAGCTCAGCCGATGACTC		(Perez-de-Mora et al., 2014)
vcrA846r	TGGTTGAGGTAGGGTGAAGG		
tceA797f	ACGCCAAAGTGCGAAAAGC	Orthologous genes of *tceA*	(Johnson et al., 2005)
tceA2490r	TAATCTATTCCATCCTTTCTC		

Calculation of annealing temperature

Equation (SI 1): $T_{Annealing}$ [°C] = (4°C x $n_{\underline{G}uanine + \underline{C}ytosine}$) + (2°C x $n_{\underline{A}denine + \underline{T}hymine}$) – 2°C

Table SI - 3 Groundwater analysis before the injection of Carbo-Iron.

Groundwater analysis at 12 - 14 m bgl	
temperature	10.5 °C
electric conductivity	390 µS/cm
pH	6.47
dissolved oxygen	< 0.5 mg L^{-1}
dissolved organic carbon (DOC)	1.1 mg L^{-1}
bicarbonate HCO_3^-	110 mg L^{-1}
iron	9 mg L^{-1}
nitrate	< 0.05 mg L^{-1}
nitrite	< 0.005 mg L^{-1}
chloride	23 mg L^{-1}
sulphate	69 mg L^{-1}

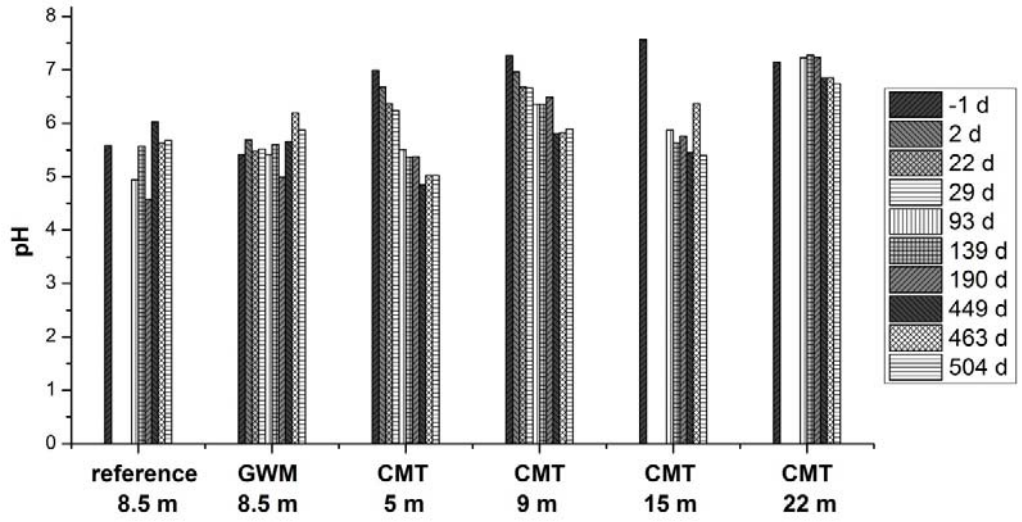

Figure SI 1 - pH of groundwater from the Carbo-Iron-influenced wells GWM and CMT and at the reference well at different sampling depths before (-1 d) and maximal 504 days after the first injection of Carbo-Iron.

References

Bunge M, Adrian L, Kraus A, Opel M, Lorenz WG, Andreesen JR et al. Reductive dehalogenation of chlorinated dioxins by an anaerobic bacterium. Nature 2003;421(6921):357–60.

Ding C, He J. Molecular techniques in the biotechnological fight against halogenated compounds in anoxic environments. Microbial biotechnology 2012;5(3):347–67.

Duhamel M, Edwards EA. Microbial composition of chlorinated ethene-degrading cultures dominated by *Dehalococcoides*. FEMS microbiology ecology 2006;58(3):538–49.

Hendrickson ER, Payne JA, Young RM, Starr MG, Perry MP, Fahnestock S et al. Molecular analysis of *Dehalococcoides* 16S Ribosomal DNA from chloroethene-contaminated sites throughout North America and Europe. Applied and Environmental Microbiology 2002;68(2):485–95.

Heuer H, Krsek M, Baker P, Smalla K, Wellington EM. Analysis of actinomycete communities by specific amplification of genes encoding 16S rRNA and gel-electrophoretic separation in denaturing gradients. Applied and Environmental Microbiology 1997;63(8):3233–41.

Johnson DR, Lee PKH, Holmes VF, Fortin AC, Alvarez-Cohen L. Transcriptional expression of the tceA gene in a *Dehalococcoides*-containing microbial enrichment. Applied and Environmental Microbiology 2005;71(11):7145–51.

Krajmalnik-Brown R, Holscher T, Thomson IN, Saunders FM, Ritalahti KM, Loffler FE. Genetic identification of a putative vinyl chloride reductase in *Dehalococcoides* sp. strain BAV1. Applied and Environmental Microbiology 2004;70(10):6347–51.

Loffler FE, Sun Q, Li J, Tiedje JM. 16S rRNA gene-based detection of tetrachloroethene-dechlorinating Desulfuromonas and *Dehalococcoides* Species. Applied and Environmental Microbiology 2000;66(4):1369–74.

Muller JA, Rosner BM, Abendroth G von, Meshulam-Simon G, McCarty PL, Spormann AM. Molecular identification of the catabolic vinyl chloride reductase from *Dehalococcoides* sp. strain VS and its environmental distribution. Applied and Environmental Microbiology 2004;70(8):4880–8.

Perez-de-Mora A, Zila A, McMaster ML, Edwards EA. Bioremediation of chlorinated ethenes in fractured bedrock and associated changes in dechlorinating and nondechlorinating microbial populations. Environmental Science & Technology 2014;48(10):5770–9.

Schumann P. E. Stackebrandt and M. Goodfellow (Editors), Nucleic acid techniques in bacterial systematics (Modern microbiological methods). XXIX + 329 S., 46 Abb., 28 Tab. Chichester — New York — Brisbane — Toronto — Singapore 1991. John Wiley & Sons. $ 55.00. ISBN: 0–471–92906–9. Journal of Basic Microbiology 1991;31(6):479–80.

Smits THM, Devenoges C, Szynalski K, Maillard J, Holliger C. Development of a real-time PCR method for quantification of the three genera *Dehalobacter*, *Dehalococcoides*, and *Desulfitobacterium* in microbial communities. Journal of Microbiological Methods 2004;57(3):369–78.

Wagner A, Adrian L, Kleinsteuber S, Andreesen JR, Lechner U. Transcription analysis of genes encoding homologues of reductive dehalogenases in "*Dehalococcoides*" sp. strain CBDB1 by using terminal restriction fragment length polymorphism and quantitative PCR. Applied and Environmental Microbiology 2009;75(7):1876–84.

4. Zusammenfassung

Gegenstand der vorliegenden Dissertation ist die Untersuchung von Eisen-Aktivkohle-Systemen für den *In-situ*-Abbau chlorierter Ethene in Grundwasserleitern, wobei ein Schwerpunkt auf das Kompositmaterial Carbo-Iron gelegt wurde. Nachdem die prinzipielle Eignung des Komposits bereits in früheren Labor- und Feldstudien gezeigt werden konnte, sind Ziele dieser Dissertation, das mechanistische Zusammenspiel von Eisen und Aktivkohle bei der Dechlorierung besser zu verstehen, die Auswirkungen von Carbo-Iron auf den mikrobiologischen Schadstoffabbau zu untersuchen sowie die Partikel hinsichtlich ihrer Selektivität und Lebensdauer zu optimieren.
Die Ergebnisse zu diesen Fragestellungen liegen in Form von drei Publikationen vor, die bei der in der Zeitschrift „Science of the Total Environment“ erschienen sind. Die Zusammenfassung der Ergebnisse erfolgt zur besseren Übersicht themenspezifisch.

I. Einfluss textiler Aktivkohle auf die eisenbasierte Reduktion chlorierter Ethene

Der Einfluss von Aktivkohle auf die Kinetik und Selektivität der eisenbasierten Reduktion chlorierter Ethene wurde am Beispiel eines Modellsystems untersucht, bei dem mikroskalige Eisenpartikel in Kontakt mit verschiedenen textilen Aktivkohlesorten gebracht wurden. Der direkte Kontakt zwischen den adsorbierten Schadstoffen (PCE, TCE) an der Aktivkohle und den reaktiven Eisenpartikeln war dabei verhindert.
Die Ergebnisse der Untersuchungen zeigen, dass die Dechlorierungsgeschwindigkeit im Eisen-Aktivkohle-System im Vergleich zur rein eisenbasierten Reduktion zum Teil drastisch gesteigert werden kann. In Gegenwart des filzartigen Aktivkohlevlieses FC 10 (Actitex, Frankreich) beträgt die formale, auf die Eisenoberfläche normierte Geschwindigkeitskonstante für den Abbau von TCE $k_{SA,TCE,Fe\text{-}AK} = 2.6 \cdot 10^{-3}$ bis $2.0 \cdot 10^{-2}$ l m^{-2} h^{-1} und ist damit mehrere Größenordnungen höher als an reinem Mikroeisen in Abwesenheit von Aktivkohle ($k_{SA,TCE,Fe} = 3.4 \cdot 10^{-6}$ l m^{-2} h^{-1}).
Die untersuchten textilen Aktivkohlesorten unterscheiden sich stark hinsichtlich ihrer Fähigkeit, die Dechlorierung von chlorierten Ethenen in Gegenwart von Mikroeisen zu beschleunigen. Dabei konnte ein Zusammenhang mit dem Gehalt und der Art sauerstoffhaltiger funktioneller Gruppen an der Aktivkohle beobachtet werden. Tendenziell werden bei den Aktivkohlearten mit hohem Sauerstoffanteil (14–16 Ma.-%) höhere Dechlorierungsraten beobachtet als bei Proben

in der Messreihe mit geringen Sauerstoffanteilen (2,5 bis 5 Ma.-%). Daneben spielt die Art der funktionellen Gruppen eine wesentliche Rolle. Die Untersuchung der textilen Aktivkohleproben durch temperaturprogrammierte Desorption/Pyrolyse (TPD-Analyse) ergab, dass die Dechlorierungsreaktion vor allem durch die Beteiligung redoxaktiver Chinon/Hydrochinon-Gruppen beschleunigt werden kann, wobei die Beteiligung anderer funktioneller Gruppen, wie Pyrone oder Chromene nicht ausgeschlossen werden kann. Die involvierten Chinon/Hydrochinon-Gruppen auf der Aktivkohleoberfläche können die Dechlorierung von TCE katalysieren. Demnach werden sie während des Schadstoffabbaus nicht verbraucht, sondern durch reaktive Spezies vom Reduktionsmittel Eisen regeneriert.

Der Kontakt von Eisenpartikeln mit textiler Aktivkohle bei der Dechlorierung von TCE führt im Vergleich zum rein eisenbasierten Abbau zu einer signifikanten Veränderung des Produktspektrums hin zu weniger hydrierten Produkten, wobei als Hauptprodukt Ethin entsteht. Partiell chlorierte Intermediate, wie Dichlorethene und Vinylchlorid treten während der Reaktion ebenfalls auf, können aber im Reaktionsverlauf weiter abgebaut werden und zählen daher nicht zu den Endprodukten der Reaktion. Als Ursache für den Reaktionsverlauf und das daraus resultierende Produktspektrum werden ein Mangel an reaktiven Wasserstoffspezies sowie die unterschiedliche Sorption der chlorierten Ethene an Aktivkohle im Vergleich zur Eisenoberfläche diskutiert.

Die Geschwindigkeitskonstante pseudo-erster Ordnung für die anaerobe Korrosion von mikroskaligem Eisen ist in Gegenwart von textiler Aktivkohle leicht erhöht gegenüber dem reinen Eisensystem ($k_{Fe} = 3.2 \cdot 10^{-6}\ h^{-1}$ und $k_{Fe\text{-}AK} = 4.4 \cdot 10^{-6}\ h^{-1}$). Es ist davon auszugehen, dass Eisen und Aktivkohle als Lokalelement fungieren können, wie es im stärkeren Ausmaß von Eisen-Graphit-Systemen bekannt ist. Generell ist die Dechlorierungseffizienz in dem untersuchten Eisen-Aktivkohle-System im Vergleich zum reinen Eisensystem durch die erhöhte Dechlorierungsgeschwindigkeit bei etwa konstanter Korrosionsrate deutlich erhöht.

Die Kombination von Mikroeisen und Aktivkohle mit redoxaktiven Oberflächengruppen ermöglicht einen schnellen und effizienten Abbau chlorierter Ethene, sodass selbst mit reaktionsträgen Eisenpartikeln Reaktionsgeschwindigkeiten im Bereich von Nanoeisen erreicht werden können. Das Prinzip überzeugt durch seine Einfachheit und hat ein hohes Potenzial in der Praxis Anwendung zu finden. Durch die Verwendung geeigneter Aktivkohlen kann die Größe

von Reaktoren deutlich reduziert werden, was für die Gestaltung von reaktiven Barrieren, aber auch für Festbettreaktoren von großer Bedeutung ist. So könnte beispielsweise ein Reaktor mit Eisenpartikeln (Länge = 1 m, Durchmesser = 0,3 m, 140 kg Eisenfüllung) in Gegenwart des filzartigen Aktivkohlevlieses FC 10 theoretisch auf eine Länge von wenigen Zentimetern verkleinert und die Eisenmenge auf etwa 1 % minimiert werden, selbst wenn lediglich 10 % der im Labor beobachteten Dechlorierungsaktivität angenommen wird. Weiterführende Untersuchungen hinsichtlich des Langzeitverhaltens sowie des Reaktionsverhaltens in kontinuierlich durchflossenen Säulensystemen sollten zukünftig durchgeführt werden, um die vielversprechenden Erkenntnisse dieser Arbeit für praktische Anwendungen nutzbar zu machen.

II. Auswirkung reduzierter Schwefelspezies auf die chemische Reaktivität von Carbo-Iron

Wie alle eisenbasierten Reagenzien weist Carbo-Iron neben einer hohen Reaktivität gegenüber ausgewählten Schadstoffen auch eine starke Neigung zur anaeroben Korrosion auf, wodurch die Lebensdauer der Partikel begrenzt wird. Inwiefern sich die chemische Reaktivität des Materials durch Sulfidierung beeinflussen lässt, wurde in diesem Teil der Dissertation näher untersucht.

Die Ergebnisse der Röntgenbeugungsanalyse zeigen, dass bei einer Sulfidierung der Partikel durch Vorbehandlung mit gasförmigem H_2S kristallines FeS (Mackinawit) gebildet wird, welches als eine Ursache für die veränderten Partikeleigenschaften diskutiert wird.

Die Anwesenheit reduzierter Schwefelspezies im Reaktionsmedium führt zu einer drastischen Inhibierung der anaeroben Korrosion des in Carbo-Iron enthaltenen Eisens. Bereits bei einem Zusatz von Natriumsulfid zur Partikelsuspension (molares Verhältnis S/Fe = 0.004) vor dem Schadstoffabbau kann die Korrosionsrate im Vergleich zum unbehandelten Material um den Faktor 65 gesenkt werden. Auch die Anwesenheit anderer reduzierter Schwefelspezies, wie Sulfit, Thiosulfat, Dithionit oder L-Cystein führt zu vergleichbaren Effekten.

Im Gegensatz zu Nanoeisen, welches durch Reduktion mit Natriumborhydrid synthetisiert wurde, bewirkt eine Sulfidierung bei Carbo-Iron eine wesentlich stärkere Korrosionshemmung. Als Ursachen für das unterschiedliche Verhalten werden unter anderem die hohe Kristallinität des Eisens im Kompositmaterial sowie eine mögliche Beteiligung der Aktivkohle am Sulfidierungsprozess diskutiert. In einem Langzeitversuch über 160 Tage konnten unter stark korrosionsfördernden Bedingungen (50 mM $NaHCO_3$-Lösung) der korrosionsinhibierende Effekt

verschiedener Sulfidbehandlungen sowie der Erhalt der Reaktivität gegenüber Schadstoffen gezeigt werden. Während die unbehandelten Carbo-Iron-Partikel bereits innerhalb von 15 Tagen 70 % ihres ursprünglichen reduktiven Potenzials durch die Reaktion mit Wasser verloren, wurden bei sulfidiertem Carbo-Iron lediglich 25 % des Eisens innerhalb von 160 Tagen verbraucht. Am Ende dieses Beobachtungszeitraumes stand bei den behandelten Partikeln über 50 % der ursprünglichen Reduktionskraft des Eisens für die Dehalogenierung von 1,2-Dibromethan, eines schnell abbaubaren Schadstoffes, zu Verfügung. Berücksichtigt man lediglich die anaerobe Korrosion als einzige Parallelreaktion zum Schadstoffabbau, kann unter natürlichen, weniger korrosionsfördernden Bedingungen (< 5 mM $NaHCO_3$) eine theoretische Halbwertszeit des enthaltenen Eisens von etwa zwei Jahren angenommen werden. Diese liegt weit über den bisher beschriebenen Standzeiten von reinen Nanoeisenpartikeln, welche in der Praxis eingesetzt werden [15–18,38,41].

Die Geschwindigkeitskonstante für die Dechlorierung von PCE mit Carbo-Iron kann durch die Behandlung mit reduzierten Schwefelverbindungen (S/Fe = 0.004–0.11) um etwa den Faktor drei erhöht werden. Mit der veränderten Kinetik der Reaktion geht auch eine Veränderung der gebildeten C_2-Kohlenwasserstoffe hin zu weniger hydrierten Produkten einher. Während beim Abbau von PCE durch unbehandeltes Carbo-Iron vor allem Ethen- und Ethanbildung beobachtet wurde, dominierte bei der Reaktion mit sulfidierten Partikeln zunächst die Bildung von Ethin, welches schrittweise hydriert wurde. Als Ursache für die beschleunigte Dechlorierung wird die verbesserte elektrische Leitfähigkeit von FeS im Vergleich zu oberflächengebundenen Eisen(III)-oxiden gesehen, wobei aber auch eine Beteiligung der schwefelmodifizierten Aktivkohle am beschleunigten Schadstoffabbau möglich erscheint.

Die Dechlorierungseffizienz (definiert als die für die Dechlorierung verbrauchte Eisenmenge im Verhältnis zum Gesamteisenverbrauch zu Beginn der Reaktion) kann unter den herrschenden Reaktionsbedingungen von etwa 30 % auf 98 % erhöht werden (für $c_{\text{Carbo-Iron}} = 4\ \text{g l}^{-1}$). Das heißt, dass nahezu das gesamte reduktive Potenzial des Eisens für den Schadstoffabbau genutzt werden kann, wodurch eine effiziente und wirtschaftliche Sanierung ermöglicht wird.

Sulfidiertes Carbo-Iron stellt insgesamt eine elegante Kombination von Eisen, Kohlenstoff und Schwefel dar und weist im Gegensatz zu herkömmlichem Nanoeisen ein deutlich größeres Potenzial für die Anwendung als *In-situ*-Reagenz auf.

III. Einfluss von Carbo-Iron auf den mikrobiologischen Schadstoffabbau im Aquifer

Im abschließenden Teil der Arbeit wurden die mikrobiologischen Prozesse während bzw. nach einer chemischen Sanierungsmaßnahme mit Carbo-Iron am Feldstandort Lohheide durch Anwendung chemischer und molekularbiologischer Techniken näher untersucht. Bei dem Feldstandort handelt es sich um einen mit PCE kontaminierten Aquifer, bei dem der Eintrag der Kontaminanten mehr als 20 Jahre zurücklag.

Das Fehlen von Abbauprodukten, wie *cis*-DCE und Vinylchlorid, sowie die Ergebnisse der $^{13}C/^{12}C$-Isotopenanalyse des Schadstoffes PCE weisen darauf hin, dass vor der Injektion von Carbo-Iron der biologische Schadstoffabbau bis in Tiefen von etwa 15 m keine wesentliche Rolle spielte. Eine Ursache dafür stellt das starke Einströmen von sauerstoffhaltigem Oberflächenwasser in den Aquifer dar, wodurch Wachstum und Aktivität von organohalid-respirierenden Bakterien gehemmt wurden. Der Hauptteil der Kontamination ist jedoch in etwa 6 m Tiefe zu finden, sodass eine rein natürliche Sanierung des Standortes nicht möglich war.

Mit der Injektion von Carbo-Iron kam es zu einer langsamen, aber stetigen Senkung des Redoxpotenzials des Grundwassers, sodass zum Teil sulfatreduzierende Bedingungen erreicht werden, welche den mikrobiologischen Abbau von PCE begünstigen. Carbo-Iron weist gegenüber reinem Nanoeisen den Vorteil auf, dass es durch seine deutlich höhere Mobilität im Aquifer einen größeren Einflussradius besitzt und damit auch mehr Möglichkeiten hat, mit den am Standort vorkommenden dehalogenierenden Mikroorganismen in Wechselwirkung zu treten. Ein weiterer Vorteil besteht in der Langlebigkeit des Eisen-Aktivkohle-Kompositmaterials. Im Gegensatz zu herkömmlichem Nanoeisen, das bereits nach wenigen Tagen bis Wochen seine Aktivität verliert, konnte bei Carbo-Iron noch nach über sechs Monaten ein reduzierender Effekt nachgewiesen werden. Die Bildung von Ethen und Ethan nach über 1,5 Jahren weist zudem auf eine chemische Langzeitaktivität des *In-situ*-Reagenzes hin. Als Ursachen werden dabei die hohe Kristallinität der Eisenpartikel sowie eine *In-situ*-Sulfidierung des Kompositmaterials diskutiert.

Die Bildung von *cis*-DCE etwa ein Jahr nach der Injektion von Carbo-Iron in Aquiferbereichen mit günstigen Redoxbedingungen lässt auf eine Unterstützung des mikrobiologischen Schadstoffabbaus schließen und wird mit den am Standort detektierten Spezies *Sulfurospirillum multivorans* spp., *Desulfitobacterium* spp. und *Dehalococcoides mccartyi* in Verbindung gebracht. Die Bildung von Vinylchlorid konnte dagegen nicht beobachtet werden.

Die Unterstützung der Mikroorganismen kann möglicherweise auf die eisenbedingte Verbesserung der Aquiferbedingungen zurückgeführt werden, wie z.B. die Senkung des Redoxpotenzials des Grundwassers oder die Freisetzung von molekularem Wasserstoff. Darüber hinaus könnten Eisen-Aktivkohle-Systeme gegenüber reinem Eisen weitere Vorteile haben: So ist etwa das reaktive Metall in die Aktivkohlestruktur eingebettet und kommt somit nicht direkt in Kontakt mit Mikroorganismen, was eine Ursache für die zytotoxische Wirkung darstellt.
Am Standort konnte mit Hilfe der $^{13}C/^{12}C$-Isotopenfraktionierungsanalyse gezeigt werden, dass *cis*-DCE abgebaut wird. Dieser Vorgang wird auf die am Standort detektierte Spezies *Polaromonas* sp. zurückgeführt, welche in der Lage ist, das Intermediat metabolisch zu CO_2 zu oxidieren. Es kann angenommen werden, dass die langsame und moderate Absenkung des Redoxpotenzials durch die chemische Aktivität von Carbo-Iron einerseits unterstützend auf organohalid-respirierende Bakterien wirkt und andererseits einen anschließenden oxidativen Schritt ermöglicht. Die Verbindung von chemischem Schadstoffabbau durch Carbo-Iron und der unterstützten mikrobiologischen Reduktion des Schadstoffes sowie einer anschließenden Oxidation von *cis*-DCE ist ein vielversprechender Ansatz für eine ganzheitliche Sanierung kontaminierter Aquifere.

Fazit

Insgesamt liefert die vorliegende Dissertation einen substanziellen Beitrag zur Entwicklung und Anwendung von Eisen-Aktivkohle-Systemen für die *In-situ*-Sanierung von kontaminierten Aquiferen. Die Effizienz der Systeme kann einerseits durch die deutlich verbesserten Korrosions- und Dechlorierungseigenschaften des eingebetteten Eisens optimiert werden, andererseits aber auch durch die Anwendung von Aktivkohle als Redoxmediator. Korrosionsstabile, dechlorierungseffiziente und langlebige Eisen-Aktivkohle-Systeme stellen eine vielversprechende Alternative zu herkömmlich eingesetzten Nanoeisensuspensionen und granulären Eisenbarrieren dar. Die in der Dissertation vorgestellten Erkenntnisse besitzen dank ihrer Einfachheit und Wirtschaftlichkeit ein hohes Potenzial, in die Praxis umgesetzt zu werden.

5. Literaturverzeichnis

[1] Umweltbundesamt, Bundesweite Übersicht zur Altlastenstatistik, 2017, https://www.umweltbundesamt.de/sites/default/files/medien/384/bilder/dateien/2_tab_altlastenstatistik_2017-09-29.pdf, accessed 22 December 2017.

[2] Agency for Toxic Substances and Disease Registry, Toxicological profile for tetrachloroethylene, 2014.

[3] Agency for Toxic Substances and Disease Registry, Toxicological profile for trichloroethylene, 2014.

[4] G. Teutsch, P. Gratwohl, T. Schiedik, Literaturstudie zum natürlichen Rückhalt / Abbau von Schadstoffen im Grundwasser, 1997.

[5] H.D. Stupp, A. Bakenhus, M. Gass, D. Lorenz, I. Schwaar, MNA als Strategie zur Bearbeitung von CKW-Grundwasserschäden - Grundlagen und Kriterien zur Anwendung, Altlastenspektrum (2007) 1–12.

[6] W. Yan, H.-L. Lien, B.E. Koel, W.-X. Zhang, Iron nanoparticles for environmental clean-up: recent developments and future outlook, Environ. Sci. Process. Impact 15 (2013) 63–77.

[7] D.R. Burris, T.J. Campbell, V.S. Manoranjan, Sorption of trichloroethylene and tetrachloroethylene in a batch reactive metallic iron-water system, Environ. Sci. Technol. 29 (1995) 2850–2855.

[8] W.X. Zhang, Nanoscale iron particles for environmental remediation: an overview, Journal of Nanoparticle Research 5 (2003) 323–332.

[9] S. Bleyl, F.-D. Kopinke, A. Georgi, K. Mackenzie, Carbo-Iron - ein maßgeschneidertes Reagenz zur In-situ-Grundwassersanierung, Chem.-Ing.-Tech. 85 (2013) 1302–1311.

[10] K. Mackenzie, S. Bleyl, A. Georgi, F.-D. Kopinke, Carbo-Iron - an Fe/AC composite - as alternative to nano-iron for groundwater treatment, Water Res. 46 (2012) 3817–3826.

[11] K. Mackenzie, S. Bleyl, F.-D. Kopinke, H. Doose, J. Bruns, Carbo-Iron as improvement of the nanoiron technology: From laboratory design to the field test, Sci. Total Environ. 563-564 (2016) 641–648.

[12] S. Bleyl, F.-D. Kopinke, K. Mackenzie, Carbo-Iron®—Synthesis and stabilization of Fe(0)-doped colloidal activated carbon for in situ groundwater treatment, Chemical Engineering Journal 191 (2012) 588–595.

[13] F.-D. Kopinke, G. Speichert, K. Mackenzie, E. Hey-Hawkins, Reductive dechlorination in water: Interplay of sorption and reactivity, Appl. Catal., B 181 (2016) 747–753.

[14] H. Tang, D. Zhu, T. Li, H. Kong, W. Chen, Reductive dechlorination of activated carbon-adsorbed trichloroethylene by zero-valent iron: carbon as electron shuttle, J. Environ. Qual. 40 (2011) 1878–1885.

[15] M. Velimirovic, L. Carniato, Q. Simons, G. Schoups, P. Seuntjens, L. Bastiaens, Corrosion rate estimations of microscale zerovalent iron particles via direct hydrogen production measurements, J. Hazard. Mater. 270 (2014) 18–26.

[16] P. Schöftner, G. Waldner, W. Lottermoser, M. Stöger-Pollach, P. Freitag, T.G. Reichenauer, Electron efficiency of nZVI does not change with variation of environmental parameters, Sci. Total Environ. 535 (2015) 69–78.

[17] Y. Liu, S.A. Majetich, R.D. Tilton, D.S. Sholl, G.V. Lowry, TCE dechlorination rates, pathways, and efficiency of nanoscale iron particles with different properties, Environ. Sci. Technol. 39 (2005) 1338–1345.

[18] M.M. Eglal, A.S. Ramamurthy, Nanofer ZVI, J. Nanomater. 2014 (2014) 1–11.

[19] D. Fan, Y. Lan, P.G. Tratnyek, R.L. Johnson, J. Filip, D.M. O'Carroll, A. Nunez Garcia, A. Agrawal, Sulfidation of iron-based Materials: a review of processes and implications for water treatment and remediation, Environ. Sci. Technol. (2017) 13070–13085.

[20] J. Li, X. Zhang, Y. Sun, L. Liang, B. Pan, W. Zhang, X. Guan, Advances in sulfidation of zerovalent iron for water decontamination, Environ. Sci. Technol. (2017) 13070–13085.

[21] S. Wang, S. Chen, Y. Wang, A. Low, Q. Lu, R. Qiu, Integration of organohalide-respiring bacteria and nanoscale zero-valent iron (Bio-nZVI-RD): A perfect marriage for the remediation of organohalide pollutants?, Biotechnol. Adv. 34 (2016) 1384–1395.

[22] Y. Xie, H. Dong, G. Zeng, L. Tang, Z. Jiang, C. Zhang, J. Deng, L. Zhang, Y. Zhang, The interactions between nanoscale zero-valent iron and microbes in the subsurface environment: a review, J. Hazard. Mater. 321 (2017) 390–407.

[23] R.A. Ritter, P. Werner, HKW-Abbau im Boden: Abbau und Biotransformation von leichtflüchtigen Halogenkohlenwasserstoffen im Untergrund, 1st ed., Ecomed, Landsberg/Lech, 1991.

[24] D.M. Cwiertny, M.M. Scherer, Chlorinated solvent chemistry: structures, nomenclature and properties, in: H.F. Stroo, C.H. Ward (Eds.), In situ remediation of chlorinated solvent plumes, Springer New York, New York, 2010, pp. 29–37.

[25] H.F. Stroo, C.H. Ward (Eds.), In situ remediation of chlorinated solvent plumes, Springer New York, New York, 2010.

[26] V. Franzius (Ed.), Handbuch Altlastensanierung und Flächenmanagement, 3rd ed., Rehm; Müller, Heidelberg, Heidelberg, 2003.

[27] R.W. Gillham, S.F. O'Hannesin, Enhanced degradation of halogenated aliphatics by zero-valent iron, Ground Water 32 (1994) 958–967.

[28] R. Crane, Nanoscale zero-valent iron: a new technology for groundwater remediation?, 2013, https://slideplayer.com/slide/2414041/, accessed 18 October 2018.

[29] J.T. Nurmi, P.G. Tratnyek, V. Sarathy, D.R. Baer, J.E. Amonette, K. Pecher, C. Wang, J.C. Linehan, D.W. Matson, R.L. Penn, M.D. Driessen, Characterization and properties of metallic iron nanoparticles, Environ. Sci. Technol. 39 (2005) 1221–1230.

[30] P.D. Mackenzie, D.P. Horney, T.M. Sivavec, Mineral precipitation and porosity losses in granular iron columns, J. Hazard. Mater. 68 (1999) 1–17.

[31] A.K. Ibrahem, T. Abdel Moghny, Y.M. Mustafa, N.E. Maysour, Mohamed Saad El Din El Dars, Farida, R. Farouk Hassan, Degradation of trichloroethylene contaminated soil by zero-valent iron nanoparticles, ISRN Soil Science 2012 (2012) 1–9.

[32] W.A. Arnold, A.L. Roberts, Pathways and kinetics of chlorinated ethylene and chlorinated acetylene reaction with Fe(0) particles, Environ. Sci. Technol. 34 (2000) 1794–1805.

[33] J. Wang, J. Farrell, Investigating the role of atomic hydrogen on chloroethene reactions with iron using Tafel analysis and electrochemical impedance spectroscopy, Environ. Sci. Technol. 37 (2003) 3891–3896.

[34] S. Bleyl, Eisen-Aktivkohle-Komposite zur Grundwassersanierung. Dissertation, 2014.

[35] T.L. Johnson, M.M. Scherer, P.G. Tratnyek, Kinetics of halogenated organic compound degradation by iron metal, Environ. Sci. Technol. 30 (1996) 2634–2640.

[36] Y. Sun, J. Li, T. Huang, X. Guan, The influences of iron characteristics, operating conditions and solution chemistry on contaminants removal by zero-valent iron: A review, Water Res. 100 (2016) 277–295.

[37] S.-W. Jeen, R.T. Amos, D.W. Blowes, Modeling gas formation and mineral precipitation in a granular iron column, Environ. Sci. Technol. 46 (2012) 6742–6749.

[38] Y. Liu, H. Choi, D. Dionysiou, G.V. Lowry, Trichloroethene hydrodechlorination in water by highly disordered monometallic nanoiron, Chem. Mater. 17 (2005) 5315–5322.

[39] Y. Liu, T. Phenrat, G.V. Lowry, Effect of TCE concentration and dissolved groundwater solutes on nZVI-promoted TCE dechlorination and H2 evolution, Environ. Sci. Technol. 41 (2007) 7881–7887.

[40] D. Fan, G. O'Brien Johnson, P.G. Tratnyek, R.L. Johnson, Sulfidation of nano zerovalent iron (nZVI) for improved selectivity during in-situ chemical reduction (ISCR), Environ. Sci. Technol. 50 (2016) 9558–9565.

[41] A. Agrawal, W.J. Ferguson, B.O. Gardner, J.A. Christ, J.Z. Bandstra, P.G. Tratnyek, Effects of carbonate species on the kinetics of dechlorination of 1,1,1-trichloroethane by zero-valent iron, Environ. Sci. Technol. 36 (2002) 4326–4333.

[42] B.I. Kharisov, H.V. Rasika Dias, O.V. Kharissova, V. Manuel Jiménez-Pérez, B. Olvera Pérez, B. Muñoz Flores, Iron-containing nanomaterials, RSC Adv. 2 (2012) 9325–9358.

[43] S.M. Hassan, Reduction of halogenated hydrocarbons in aqueous media, Chemosphere 40 (2000) 1357–1363.

[44] E.C. Butler, K.F. Hayes, Factors influencing rates and products in the transformation of trichloroethylene by iron sulfide and iron metal, Environ. Sci. Technol. 35 (2001) 3884–3891.

[45] Y. Liu, G.V. Lowry, Effect of particle age (Fe 0 Content) and solution pH on nZVI reactivity, Environ. Sci. Technol. 40 (2006) 6085–6090.

[46] M. Uegami, J. Kawano, T. Okita, Y. Fujii, K. Okinaka, K. Kakuya, S. Yatagai, Iron particles for purifying contaminated soil or ground water, US 7022256 B2 (2006).

[47] S.R.C. Rajajayavel, S. Ghoshal, Enhanced reductive dechlorination of trichloroethylene by sulfidated nanoscale zerovalent iron, Water Res. 78 (2015) 144–153.

[48] E.-J. Kim, J.-H. Kim, A.-M. Azad, Y.-S. Chang, Facile synthesis and characterization of Fe/FeS nanoparticles for environmental applications, ACS Appl. Mater. Interfaces 3 (2011) 1457–1462.

[49] Y. Han, W. Yan, Reductive dechlorination of trichloroethene by zero-valent iron nanoparticles: reactivity enhancement through sulfidation treatment, Environ. Sci. Technol. 50 (2016) 12992–13001.

[50] R.M. Cornell, U. Schwertmann, The iron oxides: Structure, properties, reactions, occurences and uses, 2nd ed., Wiley-VCH, Weinheim, 2003.

[51] D. Li, Z. Mao, Y. Zhong, W. Huang, Y. Wu, P. Peng, Reductive transformation of tetrabromobisphenol A by sulfidated nano zerovalent iron, Water Res. 103 (2016) 1–9.

[52] S.-W. Park, S.-K. Kim, J.-B. Kim, S.-W. Choi, H.I. Inyang, S. Tokunaga, Particle surface hydrophobicity and the dechlorination of chloro-compounds by iron sulfides, Water Air Soil Pollut. 6 (2006) 97–110.

[53] J. Oudar, Sulfur adsorption and poisoning of metallic catalysts, Cat. Rev. - Sci. Eng. 22 (1980) 171–195.

[54] D. Turcio-Ortega, D. Fan, P.G. Tratnyek, E.-J. Kim, Y.-S. Chang, Reactivity of Fe/FeS nanoparticles: electrolyte composition effects on corrosion electrochemistry, Environ. Sci. Technol. 46 (2012) 12484–12492.

[55] E.B. Hansson, M.S. Odziemkowski, R.W. Gillham, Influence of Na2S on the degradation kinetics of CCl4 in the presence of very pure iron, J. Contam. Hydrol. 98 (2008) 128–134.

[56] D. Enning, J. Garrelfs, Corrosion of iron by sulfate-reducing bacteria: new views of an old problem, Appl. Environ. Microbiol. 80 (2014) 1226–1236.

[57] D.R. Burris, R.M. Allen-King, V.S. Manoranjan, T.J. Campbell, G.A. Loraine, B. Deng, Chlorinated ethene reduction by cast iron, J. Environ. Eng. 124 (1998) 1012–1019.

[58] R.M. Allen-King, R.M. Halket, D.R. Burris, Reductive transformation and sorption of cis - and trans -1,2-dichloroethene in a metallic iron-water system, Environ. Toxicol. Chem. 16 (1997) 424–429.

[59] M. Lawrinenko, Z. Wang, R. Horton, D. Mendivelso-Perez, E.A. Smith, T.E. Webster, D.A. Laird, J.H. van Leeuwen, Macroporous carbon supported zerovalent iron for remediation of trichloroethylene, ACS Sustain. Chem. Eng. 5 (2017) 1586–1593.

[60] Y.F. Su, Y.L. Cheng, Y.H. Shih, Removal of trichloroethylene by zerovalent iron/activated carbon derived from agricultural wastes, J. Environ. Manage. 129 (2013) 361–366.

[61] Z. Liu, F. Zhang, S.K. Hoekman, T. Liu, C. Gai, N. Peng, Homogeneously dispersed zerovalent iron nanoparticles supported on hydrochar-derived porous carbon, ACS Sustain. Chem. Eng. 4 (2016) 3261–3267.

[62] H.-H. Tseng, J.-G. Su, C. Liang, Synthesis of granular activated carbon/zero valent iron composites for simultaneous adsorption/dechlorination of trichloroethylene, J. Hazard. Mater. 192 (2011) 500–506.

[63] Y. Zhou, B. Gao, A.R. Zimmerman, H. Chen, M. Zhang, X. Cao, Biochar-supported zerovalent iron for removal of various contaminants from aqueous solutions, Bioresour. Technol. 152 (2014) 538–542.

[64] X. Peng, X. Liu, Y. Zhou, B. Peng, L. Tang, L. Luo, B. Yao, Y. Deng, J. Tang, G. Zeng, New insights into the activity of a biochar supported nanoscale zerovalent iron composite and nanoscale zero valent iron under anaerobic or aerobic conditions, RSC Adv. 7 (2017) 8755–8761.

[65] L. Han, S. Xue, S. Zhao, J. Yan, L. Qian, M. Chen, Biochar supported nanoscale iron particles for the efficient removal of methyl orange dye in aqueous solutions, PloS one 10 (2015) e0132067.

[66] W.F. Chen, L. Pan, L.F. Chen, Q. Wang, C.C. Yan, Dechlorination of hexachlorobenzene by nano zero-valent iron/activated carbon composite, RSC Adv. 4 (2014) 46689–46696.

[67] J. Gao, W. Wang, A.J. Rondinone, F. He, L. Liang, Degradation of trichloroethene with a novel ball milled Fe-C nanocomposite, J. Hazard. Mater. 300 (2015) 443–450.

[68] K. Mackenzie, J. Battke, R. Koehler, F.-D. Kopinke, Catalytic effects of activated carbon on hydrolysis reactions of chlorinated organic compounds. Part 2. 1,1,2,2-Tetrachloroethane, Appl. Catal., B 59 (2005) 171–179.

[69] W. Chen, Y. Li, D. Zhu, S. Zheng, W. Chen, Dehydrochlorination of activated carbon-bound 1,1,2,2-tetrachloroethane, Carbon 78 (2014) 578–588.

[70] H. Fu, D. Zhu, Graphene oxide-facilitated reduction of nitrobenzene in sulfide-containing aqueous solutions, Environ. Sci. Technol. 47 (2013) 4204–4210.

[71] W. Xu, K.E. Dana, W.A. Mitch, Black carbon-mediated destruction of nitroglycerin and RDX by hydrogen sulfide, Environ. Sci. Technol. 44 (2010) 6409–6415.

[72] W. Xu, J.J. Pignatello, W.A. Mitch, Reduction of nitroaromatics sorbed to black carbon by direct reaction with sorbed sulfides, Environ. Sci. Technol. 49 (2015) 3419–3426.

[73] H.J. Amezquita-Garcia, E. Razo-Flores, F.J. Cervantes, J.R. Rangel-Mendez, Activated carbon fibers as redox mediators for the increased reduction of nitroaromatics, Carbon 55 (2013) 276–284.

[74] F. Rodríguez-Reinoso, The role of carbon materials in heterogeneous catalysis, Carbon 36 (1998) 159–175.

[75] R.A. Pereira, M.F.R. Pereira, M.M. Alves, L. Pereira, Carbon based materials as novel redox mediators for dye wastewater biodegradation, Appl. Catal., B 144 (2014) 713–720.

[76] F.P. Van der Zee, I.A.E. Bisschops, G. Lettinga, J.A. Field, Activated carbon as an electron acceptor and redox mediator during the anaerobic biotransformation of azo dyes, Environ. Sci. Technol. 37 (2003) 402–408.

[77] S.-Y. Oh, D.K. Cha, P.C. Chiu, Graphite-mediated reduction of 2,4-Dinitrotoluene with elemental iron, Environ. Sci. Technol. 36 (2002) 2178–2184.

[78] P.M. Bradley, History and ecology of chloroethene biodegradation, Bioremediat J. 7 (2003) 81–109.

[79] A. Tiehm, K.R. Schmidt, Sequential anaerobic/aerobic biodegradation of chloroethenes--aspects of field application, Curr. Opin. Biotechnol. 22 (2011) 415–421.

[80] T. Schubert, L. Adrian, G. Diekert, Organohalid-Atmung bei Mikroorganismen, Biospektrum 22 (2016) 462–464.

[81] D. Leys, L. Adrian, H. Smidt, Organohalide respiration, Philos. Trans. R. Soc. Lond., B, Biol. Sci. 368 (2013) 20120316.

[82] F.E. Löffler, J. Yan, K.M. Ritalahti, L. Adrian, E.A. Edwards, K.T. Konstantinidis, J.A. Müller, H. Fullerton, S.H. Zinder, A.M. Spormann, Dehalococcoides mccartyi gen. nov., sp. nov.,

obligately organohalide-respiring anaerobic bacteria relevant to halogen cycling and bioremediation, belong to a novel bacterial class, Dehalococcoidia classis nov., order Dehalococcoidales ord. nov. and family Dehalococcoidaceae fam. nov., within the phylum Chloroflexi, Int. J. Syst. Evol. Microbiol. 63 (2013) 625–635.

[83] P.M. Bradley, F.H. Chapelle, Biodegradation of chlorinated ethenes, in: H.F. Stroo, C.H. Ward (Eds.), In situ remediation of chlorinated solvent plumes, Springer New York, New York, 2010, pp. 39–67.

[84] T.A. Bruton, B.F.G. Pycke, R.U. Halden, Effect of nanoscale zero-valent iron treatment on biological reductive dechlorination, Crit. Rev. Environ. Sci. Technol. 45 (2014) 1148–1175.

[85] C. Fajardo, M.L. Saccà, M. Martinez-Gomariz, G. Costa, M. Nande, M. Martin, Transcriptional and proteomic stress responses of a soil bacterium Bacillus cereus to nanosized zero-valent iron (nZVI) particles, Chemosphere 93 (2013) 1077–1083.

[86] M. Diao, M. Yao, Use of zero-valent iron nanoparticles in inactivating microbes, Water Res. 43 (2009) 5243–5251.

[87] Z. Li, K. Greden, P.J.J. Alvarez, K.B. Gregory, G.V. Lowry, Adsorbed polymer and NOM limits adhesion and toxicity of nano scale zerovalent iron to E. coli, Environ. Sci. Technol. 44 (2010) 3462–3467.

[88] C. Lee, J.Y. Kim, W.I. Lee, K.L. Nelson, J. Yoon, D.L. Sedlak, Bactericidal effect of zero-valent iron nanoparticles on Escherichia coli, Environ. Sci. Technol. 42 (2008) 4927–4933.

[89] J.Y. Kim, H.-J. Park, C. Lee, K.L. Nelson, D.L. Sedlak, J. Yoon, Inactivation of Escherichia coli by nanoparticulate zerovalent iron and ferrous ion, Appl. Environ. Microbiol. 76 (2010) 7668–7670.

[90] J. Chen, Z. Xiu, G.V. Lowry, P.J.J. Alvarez, Effect of natural organic matter on toxicity and reactivity of nano-scale zero-valent iron, Water Res. 45 (2011) 1995–2001.

[91] Z.-M. Xiu, K.B. Gregory, G.V. Lowry, P.J.J. Alvarez, Effect of bare and coated nanoscale zerovalent iron on tceA and vcrA gene expression in Dehalococcoides spp, Environ. Sci. Technol. 44 (2010) 7647–7651.

[92] L. Zhou, T. Le Thanh, J. Gong, J.-H. Kim, E.-J. Kim, Y.-S. Chang, Carboxymethyl cellulose coating decreases toxicity and oxidizing capacity of nanoscale zerovalent iron, Chemosphere 104 (2014) 155–161.

[93] H. Dong, Y. Xie, G. Zeng, L. Tang, J. Liang, Q. He, F. Zhao, Y. Zeng, Y. Wu, The dual effects of carboxymethyl cellulose on the colloidal stability and toxicity of nanoscale zero-valent iron, Chemosphere 144 (2016) 1682–1689.

[94] H. Rosenthal, L. Adrian, M. Steiof, Dechlorination of PCE in the presence of Fe0 enhanced by a mixed culture containing two Dehalococcoides strains, Chemosphere 55 (2004) 661–669.

[95] C.M.D. Kocur, L. Lomheim, O. Molenda, K.P. Weber, L.M. Austrins, B.E. Sleep, H.K. Boparai, E.A. Edwards, D.M. O'Carroll, Long-term field study of microbial community and dechlorinating activity following carboxymethyl cellulose-stabilized nanoscale zero-valent iron injection, Environ. Sci. Technol. 50 (2016) 7658–7670.

[96] F. He, D. Zhao, C. Paul, Field assessment of carboxymethyl cellulose stabilized iron nanoparticles for in situ destruction of chlorinated solvents in source zones, Water Res. 44 (2010) 2360–2370.

[97] B.K. Amos, K.M. Ritalahti, C. Cruz-Garcia, E. Padilla-Crespo, F.E. Löffler, Oxygen effect on Dehalococcoides viability and biomarker quantification, Environ. Sci. Technol. 42 (2008) 5718–5726.

[98] F. Aulenta, M. Majone, V. Tandoi, Enhanced anaerobic bioremediation of chlorinated solvents: environmental factors influencing microbial activity and their relevance under field conditions, J. Chem. Technol. Biotechnol. 81 (2006) 1463–1474.

[99] B.S. Ballapragada, H.D. Stensel, J.A. Puhakka, J.F. Ferguson, Effect of hydrogen on reductive dechlorination of chlorinated ethenes, Environ. Sci. Technol. 31 (1997) 1728–1734.

[100] D.E. Fennell, J.M. Gossett, S.H. Zinder, Comparison of butyric acid, ethanol, lactic acid, and propionic acid as hydrogen donors for the reductive dechlorination of tetrachloroethene, Environ. Sci. Technol. 31 (1997) 918–926.

[101] Ö. Aktaş, K.R. Schmidt, s. mungenast, C. Stoll, A. Tiehm, Effect of chloroethene concentrations and granular activated carbon on reductive dechlorination rates and growth of Dehalococcoides spp, Bioresour. Technol. 103 (2012) 286–292.

[102] Ö. Aktaş, F. Çeçen, Bioregeneration of activated carbon, Int. Biodeterioration Biodegrad. 59 (2007) 257–272.

Anhang

Abkürzungsverzeichnis

AK	Aktivkohle
ATSDR	Agency for Toxic Substances and Disease Registry
BET	Brunauer-Emmet-Teller
CI	Carbo-Iron
cis-DCE	*cis*-Dichlorethen
CMC	Carboxymethylcellulose
DBA	1,2-Dibromethan
GC-FID	Gaschromatograph gekoppelt mit Flammenionisationsdetektor
GC-MS	Gaschromatograph gekoppelt mit Massenspektrometer
GC-WLD	Gaschromatograph gekoppelt mit Wärmeleitfähigkeitsdetektor
CKW	chlorierte Kohlenwasserstoffe
IC	Ionenchromatographie
mZVI	Mikropartikel aus elementarem Eisen
nZVI	nanoskaliges elementares Eisen
$nZVI_{NaBH4}$	Nanoeisen, hergestellt durch die Reduktion mit Natriumborhydrid
OHRB	organohalid-respirierende Bakterien
PCE	Perchlorethen
PRB	permeable reaktive Barriere
RNIP	reactive nanoscale iron particles
TCE	Trichlorethen
TPD	temperaturprogrammierte Desorption
VC	Vinylchlorid
ZVI	zerovalent iron (elementares Eisen)

Zusätzliche in den Publikationen vorkommende englischsprachige Abkürzungen

AC	activated carbon
bgl	below ground level
CLSM	confocal laser scanning microscopy
CMT	continuous-multi-channel-tubing
CSIA	compound-specific isotope analysis
GWM	groundwater monitoring well
ORP	oxidation reduction potential
OTU	operational taxonomic unit
PCR	polymerase chain reaction
PTFE	polytetrafluoroethylene
PZC	point of zero charge
RDP	Ribosomal Database Project
TCD	thermal conductivity sensor
TON	turnover number
XRD	X-ray diffraction

Symbolverzeichnis

Symbol	Einheit	Deutsch	Englisch
A_{BET}	[m^2 g^{-1}]	spezifische Oberfläche nach Brunauer, Emmet und Teller	specific surface area according to Brunauer, Emmet and Teller
c	[g l^{-1}]	Massenkonzentration	mass concentraton
	[mol l^{-1}]	Stoffmengenkonzentration	molar conentration
$\delta^{13}C$	[‰]	Kohlenstoffisotopenverhältnis in δ-Notation (Standard: Vienna Pee Dee Belemnite)	carbon isotope composition in δ-notation relative to the Vienna Pee Dee Belemnite standard
d_p	[nm, µm]	Partikelgröße	particle size
E^0	[mV]	Standardelektrodenpotenzial	standard electrode potential
k_{obs}	[h^{-1}, µmol h^{-1}]	beobachtete Geschwindigkeitskonstante	observed rate coefficient
k_{SA}	[l h^{-1} m^{-2}]	oberflächennormierte Geschwindigkeitskonstante	surface normalised rate constant
k_m	[µmol l h^{-1} g^{-1}]	massennormierte Geschwindigkeitskonstante	mass-normalized rate constant
m	[g]	Masse	mass
n	[mol]	Stoffmenge	amount of substance
ρ	[g cm^3]	Dichte	density
S_m	[m^2 g_{Fe}^{-1}]	spezifische massebezogene Oberfläche	specific mass-normalized surface
σ	[m^2 l^{-1}]	Oberflächenkonzentration	surface concentration
t	[h, d]	Zeit	time
T	[K, °C]	Temperatur	temperature
x	[wt-%]	Massenanteil	mass fraction

Danksagung

An dieser Stelle möchte ich mich bei all denen bedanken, die mich während der Promotionszeit begleitet und zum Gelingen der Arbeit beigetragen haben.

- An erster Stelle bedanke ich mich bei Herrn Prof. Kopinke für die Bereitstellung des Themas, die gute fachliche Betreuung sowie die damit verbundenen Diskussionen.

- Ein ganz herzlicher Dank geht an Katrin Mackenzie. Die zahlreichen, inspirierenden Gespräche mit ihr, aber auch die sehr gute persönliche Unterstützung sowie ihre schier unendliche Geduld beim Verfassen der Manuskripte haben maßgeblich zum Gelingen der Arbeit beigetragen.

- Ein weiterer Dank geht an Ivonne Nijenhuis für ihre gute fachliche Betreuung und der angenehmen Zusammenarbeit bei der Bearbeitung biologischer Fragestellungen.

- Darüber hinaus möchte ich mich bei allen Kollegen des Departments Technische Umweltchemie für die Hilfsbereitschaft und das angenehme Arbeitsklima bedanken. Ein Dankeschön geht auch an die Kollegen der Isotopenbiogeochemie, die mir mit ihren Ratschlägen in mikrobiologischen Fragestellungen stets beiseite standen.

Meiner Familie, insbesondere Torsten und meiner Schwester Anja sowie meinen Freunden sei an dieser Stelle für die liebevolle Unterstützung, ihre Geduld und die aufmunternden Worte gedankt.

Lebenslauf

Name:	Maria Vogel
Geburtsdatum:	11.04.1987
Geburtsort:	Karl-Marx-Stadt (jetzt Chemnitz)
Familienstand:	ledig
Nationalität	Deutsch

Schulausbildung

08/1993 – 07/1997	Rudolf-Grundschule, Chemnitz
08/1997 – 07/2003	Georgius-Agricola-Gymnasium, Chemnitz
08/2003 – 07/2005	Johann-Wolfgang-von-Goethe-Gymnasium, Chemnitz

Hochschulbildung

10/2005 – 09/2011	Studium der Lebensmittelchemie an der TU Dresden
09/2009 – 07/2010	Auslandsaufenthalt in Córdoba und Granada (Spanien); Studium der Chemie und der Umweltwissenschaften im Rahmen des Erasmus-Förderprogrammes sowie Praktikum an der Universidad de Granada
10/2010 – 09/2011	Diplomarbeit an der Professur für Lebensmittelchemie der Technischen Universität Dresden bei Prof. Henle (Schwerpunkt Methodenentwicklung zur Analytik von Maillard-Reaktionsprodukten in biologischen Matrices mittels HPLC und GC-MS)
12/2011 – 05/2012	Praktikum am University College Cork, Irland
11/2012 – 09/2017	Anfertigung der vorliegenden Dissertation mit dem Thema „Anwendung von Eisen-Aktivkohle-Systemen zur Grundwassersanierung“ unter der Leitung von Dr. Katrin Mackenzie, Dr. Ivonne Nijenhuis und Prof. Frank-Dieter Kopinke am Helmholtz-Zentrum für Umweltforschung GmbH – UFZ

Publikationsliste

Publikationen zum Promotionsthema

M. Vogel, I. Nijenhuis, J. Lloyd, C. Boothman, M. Pöritz, K. Mackenzie, Combined chemical and microbiological degradation of tetrachloroethene during the application of Carbo-Iron at a contaminated field site, Sci. Total Environ. 628-629 (2018) 1027–1036.

M. Vogel, F.-D. Kopinke, K. Mackenzie, Acceleration of microiron-based dechlorination in water by contact with fibrous activated carbon, Sci. Total Environ. 660 (2019) 1274–1282.

M. Vogel, A. Georgi, F.-D. Kopinke, K. Mackenzie, Sulfidation of ZVI/AC composite leads to highly corrosion-resistant nanoremediation particles with extended life-time, Sci. Total Environ. 665 (2019) 235–245.

Weitere Publikationen

Bigall, Nadja C.; Herrmann, Anne-Kristin; Vogel, Maria; Rose, Marcus; Simon, Paul; Carrillo-Cabrera, Wilder et al. (2009): Hydrogels and aerogels from noble metal nanoparticles. In: Angew. Chem. Int. Ed. 48 (51), S. 9731–9734.

Degen, Julia; Vogel, Maria; Richter, Doreen; Hellwig, Michael; Henle, Thomas (2013): Metabolic transit of dietary methylglyoxal. In: J. Agric. Food Chem. 61 (43), S. 10253–10260.

Kurzfassung der wissenschaftlichen Ergebnisse

zur Dissertation

Anwendung von Eisen-Aktivkohle-Systemen zur Grundwassersanierung

Der Fakultät für Chemie und Mineralogie der Universität Leipzig

vorgelegt von

Diplom-Lebensmittelchemikerin Maria Vogel

Angefertigt am Helmholtz-Zentrum für Umweltforschung – UFZ

Einleitung und Motivation

Für die *In-situ*-Reduktion chlorierter Schadstoffe in Aquiferen hat sich in den letzten 20 Jahren die Anwendung von metallischem Eisen als Mittel der Wahl erwiesen. Dennoch bestehen gewisse Limitationen, die eine breite Anwendung der Technologie in der Praxis beschränken: Zu den kritischen Faktoren gehören unter anderem die schwache Sorptionsaffinität der chlorierten Ethene zur Metalloberfläche sowie die geringe Mobilität der Partikel im Aquifer.

Eine Möglichkeit, das Potenzial der Eisenpartikel effektiver zu nutzen, besteht in der Kombination des Reduktionsmittels mit kohlenstoffbasierten, sorptionsaktiven Materialien, wie Bio- oder Aktivkohle. In der vorliegenden Dissertation wird im Speziellen Carbo-Iron, ein Eisen-Aktivkohle-System aus kolloidaler Aktivkohle und darin eingebetteten Nanoeisenstrukturen, näher thematisiert (siehe Abbildung 1). Hierbei kann durch die lokale Anreicherung der hydrophoben Schadstoffe in unmittelbarer Nähe der Eisenzentren sowie die sorptionsbedingte erhöhte Aufenthaltszeit der Substanzen in der *in situ* gebildeten reaktiven Zone vor allem bei niedrigen Schadstoffkonzentrationen eine vorteilhafte Nutzung des Eisens erreicht werden. Als Reduktionsmittel für chlorierte Ethene hat sich das Kompositmaterial seit seiner ersten wissenschaftlichen Darstellung im Jahr 2008 sowohl im Labormaßstab als auch bereits in einem Feldversuch als geeignet erwiesen [1,2].

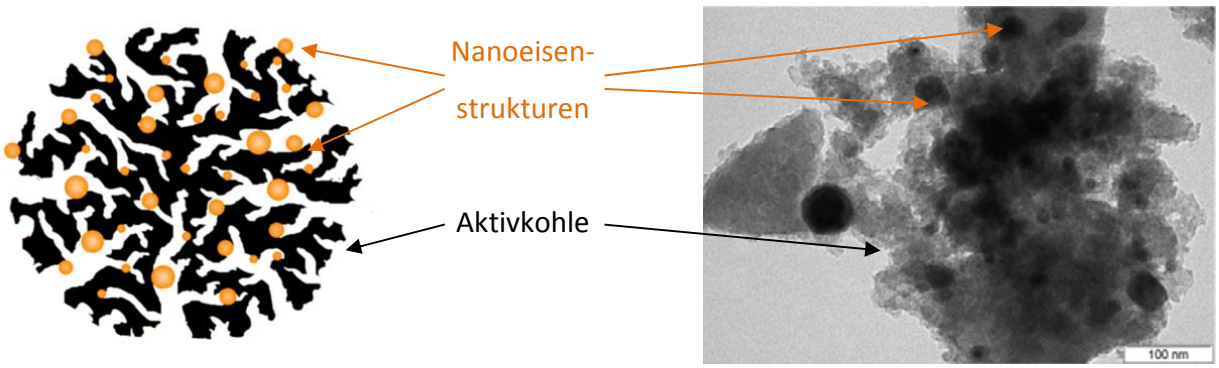

Abbildung 1 - Links: die schematische Darstellung von Carbo-Iron. Rechts: eine TEM-Aufnahme des Kompositmaterials aus Mackenzie et al. [2].

Um das Eisen-Aktivkohle-Kompositmaterial jedoch möglichst wirkungsvoll in der Praxis einsetzen zu können, sind weitere Untersuchungen notwendig. Im Rahmen der Dissertation wurden folgende Schwerpunkte näher thematisiert:

1. Untersuchung des Einflusses von Aktivkohle auf die Kinetik und Selektivität der eisenbasierten Reduktion chlorierter Ethene

   Ziel dieser Untersuchungen ist es, ein besseres Verständnis für das Zusammenspiel der Komponenten zu entwickeln, um möglichst effiziente Eisen-Aktivkohle-Systeme gestalten zu können. Um Informationen über die Einflussmöglichkeiten der Aktivkohle auf den eisenbasierten Schadstoffabbau zu gewinnen, wurde ein Modellsystem aus mikroskaligen Eisenpartikeln und textiler Aktivkohle untersucht. Dabei lagen die beiden Komponenten im Eisen-Aktivkohle-System in direktem Kontakt miteinander vor, sodass ein Transport reaktiver Spezies über Partikelgrenzen hinweg vom Eisen zu den an der Aktivkohle sorbierten Schadstoffen möglich war, der direkte Kontakt von Schadstoff und Eisenpartikel jedoch verhindert war. Der Abbau von TCE und PCE wurde unter Verwendung verschiedener textiler Aktivkohlearten untersucht und in Verbindung zu ihren chemischen Oberflächeneigenschaften gebracht, wobei ein Schwerpunkt auf die sauerstoffhaltigen funktionellen Gruppen gelegt wurde. Die Quantifizierung des Sauerstoffanteils sowie die Charakterisierung der Gruppen erfolgten mittels temperaturprogrammierter Desorption/Pyrolyse. Anhand der experimentell erhaltenen Daten werden mögliche Reaktionsmechanismen diskutiert und Konsequenzen für die Gestaltung von Eisen-Aktivkohle-Systemen gezogen. Dabei wird unter anderem erörtert, inwiefern Aktivkohle geeignet ist, die Effizienz der eisenbasierten Dechlorierung zu steigern.

2. Optimierung des Eisen-Aktivkohle-Kompositmaterials Carbo-Iron hinsichtlich seiner Selektivität und Lebensdauer

   Wie alle eisenbasierten Reagenzien weist Carbo-Iron neben einer hohen Reaktivität gegenüber ausgewählten Schadstoffen auch eine starke Neigung zur anaeroben Korrosion auf, wodurch die Lebensdauer der Partikel begrenzt wird. Inwiefern sich die chemische

Reaktivität des Materials durch Sulfidierung beeinflussen lässt, wurde in diesem Teil der Dissertation näher untersucht.

Die Auswirkungen von Art und Konzentration ausgewählter Schwefelverbindungen auf das Reaktionsverhalten der Partikel wurden in Batchversuchen in Kurz- und Langzeitexperimenten untersucht. Dabei wurden der Abbau von PCE sowie die anaerobe Korrosion des enthaltenen Eisens näher betrachtet. Die Anwendung der Röntgenbeugungsanalyse an schwefelmodifizierten Partikeln unterstützt die Interpretation der experimentellen Daten. Auf Basis der gewonnenen kinetischen Daten wurden Dechlorierungseffizienzen bestimmt, welche die Ausnutzung der Reduktionsäquivalente des Eisens zeigen und somit den Einfluss der Modifikation durch Schwefelspezies verdeutlichen.

3. <u>Auswirkungen von Carbo-Iron auf den mikrobiologischen Schadstoffabbau im Aquifer</u>

   Da der Eintrag des reaktiven *In-situ*-Reagenz in den Aquifer zu einer Veränderung der Grundwasserparameter führt, kann möglicherweise auch der mikrobiologische Schadstoffabbau beeinflusst werden. Um zukünftig abiotische und biotische Vorgänge bestenfalls synergistisch miteinander koppeln zu können, wird in diesem Teil der Arbeit die Interaktion von chemischen und biologischen Abbauvorgängen näher untersucht.

   Am Beispiel des Feldstandortes Lohheide wird dargestellt, inwiefern sich die Aquiferbedingungen nach der Injektion von Carbo-Iron verändern, welche Abbauprodukte innerhalb des Beobachtungszeitraumes von 600 Tagen entstehen und welche schadstoffabbauenden Bakterien damit in Verbindung gebracht werden können. Dabei kamen verschiedene chemisch-analytische Methoden, wie C^{13}/C^{12}-Isotopenanalyse sowie molekularbiologische Techniken, wie z.B. Pyrosequenzierung zur Anwendung. Auf Grundlage der gewonnenen Erkenntnisse werden potenzielle Möglichkeiten des Zusammenspiels von Eisen-Aktivkohle-Kompositen und biotischen Vorgängen diskutiert.

Ergebnisse

1. Einfluss textiler Aktivkohle auf die eisenbasierte Reduktion chlorierter Ethene

- Die Ergebnisse der Untersuchungen zeigen, dass die Dechlorierungsgeschwindigkeit im Eisen-Aktivkohle-System im Vergleich zur rein eisenbasierten Reduktion zum Teil drastisch gesteigert werden kann. In Gegenwart des filzartigen Aktivkohlevlieses FC 10 (Actitex, Frankreich) beträgt die formale, auf die Eisenoberfläche normierte Geschwindigkeitskonstante für den Abbau von TCE $k_{SA,TCE,Fe\text{-}AK} = 2.6 \cdot 10^{-3}$ bis $2.0 \cdot 10^{-2}$ l m^{-2} h^{-1} und ist damit mehrere Größenordnungen höher als an reinem Mikroeisen in Abwesenheit von Aktivkohle ($k_{SA,TCE,Fe} = 3.4 \cdot 10^{-6}$ l m^{-2} h^{-1}).
- Die untersuchten textilen Aktivkohlesorten unterscheiden sich stark hinsichtlich ihrer Fähigkeit, die Dechlorierung von chlorierten Ethenen in Gegenwart von Mikroeisen zu beschleunigen. Dabei konnte ein Zusammenhang mit dem Gehalt und der Art sauerstoffhaltiger funktioneller Gruppen an der Aktivkohle beobachtet werden. Tendenziell werden bei den Aktivkohlearten mit hohem Sauerstoffanteil (14–16 Ma.-%) höhere Dechlorierungsraten beobachtet als bei Proben in der Messreihe mit geringen Sauerstoffanteilen (2,5 bis 5 Ma.-%). Daneben spielt die Art der funktionellen Gruppen eine wesentliche Rolle. Die Untersuchung der textilen Aktivkohleproben durch temperaturprogrammierte Desorption/Pyrolyse (TPD-Analyse) ergab, dass die Dechlorierungsreaktion vor allem durch die Beteiligung redoxaktiver Chinon/Hydrochinon-Gruppen beschleunigt werden kann, wobei die Beteiligung anderer funktioneller Gruppen, wie Pyrone oder Chromene nicht ausgeschlossen werden kann. Die involvierten Chinon/Hydrochinon-Gruppen auf der Aktivkohleoberfläche können die Dechlorierung von TCE katalysieren. Demnach werden sie während des Schadstoffabbaus nicht verbraucht, sondern durch reaktive Spezies vom Reduktionsmittel Eisen regeneriert.
- Der Kontakt von Eisenpartikeln mit textiler Aktivkohle bei der Dechlorierung von TCE führt im Vergleich zum rein eisenbasierten Abbau zu einer signifikanten Veränderung des Produktspektrums hin zu weniger hydrierten Produkten, wobei als Hauptprodukt Ethin entsteht. Partiell chlorierte Intermediate, wie Dichlorethene und Vinylchlorid treten während der Reaktion ebenfalls auf, können aber im Reaktionsverlauf weiter abgebaut

werden und zählen daher nicht zu den Endprodukten der Reaktion. Als Ursache für den Reaktionsverlauf und das daraus resultierende Produktspektrum werden ein Mangel an reaktiven Wasserstoffspezies sowie die unterschiedliche Sorption der chlorierten Ethene an Aktivkohle im Vergleich zur Eisenoberfläche diskutiert.

- Die Geschwindigkeitskonstante pseudo-erster Ordnung für die anaerobe Korrosion von mikroskaligem Eisen ist in Gegenwart von textiler Aktivkohle leicht erhöht gegenüber dem reinen Eisensystem ($k_{Fe} = 3.2 \cdot 10^{-6}\ h^{-1}$ und $k_{Fe\text{-}AK} = 4.4 \cdot 10^{-6}\ h^{-1}$). Es ist davon auszugehen, dass Eisen und Aktivkohle als Lokalelement fungieren können, wie es im stärkeren Ausmaß von Eisen-Graphit-Systemen bekannt ist. Generell ist die Dechlorierungseffizienz in dem untersuchten Eisen-Aktivkohle-System im Vergleich zum reinen Eisensystem durch die erhöhte Dechlorierungsgeschwindigkeit bei etwa konstanter Korrosionsrate deutlich erhöht.

⇨ Die Kombination von Mikroeisen und Aktivkohle mit redoxaktiven Oberflächengruppen ermöglicht einen schnellen und effizienten Abbau chlorierter Ethene, sodass selbst mit reaktionsträgen Eisenpartikeln Reaktionsgeschwindigkeiten im Bereich von Nanoeisen erreicht werden können. Das Prinzip überzeugt durch seine Einfachheit und hat ein hohes Potenzial in der Praxis Anwendung zu finden. Weiterführende Untersuchungen hinsichtlich des Langzeitverhaltens sowie des Reaktionsverhaltens in kontinuierlich durchflossenen Säulensystemen sollten zukünftig durchgeführt werden, um die vielversprechenden Erkenntnisse dieser Arbeit für praktische Anwendungen nutzbar zu machen.

2. Auswirkung reduzierter Schwefelspezies auf die chemische Reaktivität von Carbo-Iron

- Die Ergebnisse der Röntgenbeugungsanalyse zeigen, dass bei einer Sulfidierung der Partikel durch Vorbehandlung mit gasförmigem H_2S kristallines FeS (Mackinawit) gebildet wird, welches als eine Ursache für die veränderten Partikeleigenschaften diskutiert wird.
- Die Anwesenheit reduzierter Schwefelspezies im Reaktionsmedium führt zu einer drastischen Inhibierung der anaeroben Korrosion des in Carbo-Iron enthaltenen Eisens. Bereits bei einem Zusatz von Natriumsulfid zur Partikelsuspension (molares Verhältnis S/Fe = 0.004) vor dem Schadstoffabbau kann die Korrosionsrate im Vergleich zum

unbehandelten Material um den Faktor 65 gesenkt werden. Auch die Anwesenheit anderer reduzierter Schwefelspezies, wie Sulfit, Thiosulfat, Dithionit oder L-Cystein führt zu vergleichbaren Effekten.

- Im Gegensatz zu Nanoeisen, welches durch Reduktion mit Natriumborhydrid synthetisiert wurde, bewirkt eine Sulfidierung bei Carbo-Iron eine wesentlich stärkere Korrosionshemmung. Als Ursachen für das unterschiedliche Verhalten werden unter anderem die hohe Kristallinität des Eisens im Kompositmaterial sowie eine mögliche Beteiligung der Aktivkohle am Sulfidierungsprozess diskutiert.
- In einem Langzeitversuch über 160 Tage konnten unter stark korrosionsfördernden Bedingungen (50 mM $NaHCO_3$-Lösung) der korrosionsinhibierende Effekt verschiedener Sulfidbehandlungen sowie der Erhalt der Reaktivität gegenüber Schadstoffen gezeigt werden. Während die unbehandelten Carbo-Iron-Partikel bereits innerhalb von 15 Tagen 70 % ihres ursprünglichen reduktiven Potenzials durch die Reaktion mit Wasser verloren, wurden bei sulfidiertem Carbo-Iron lediglich 25 % des Eisens innerhalb von 160 Tagen verbraucht. Am Ende dieses Beobachtungszeitraumes standen bei den behandelten Partikeln über 50 % der ursprünglichen Reduktionskraft des Eisens für die Dehalogenierung von 1,2-Dibromethan, eines schnell abbaubaren Schadstoffes, zur Verfügung. Berücksichtigt man lediglich die anaerobe Korrosion als einzige Parallelreaktion zum Schadstoffabbau, kann unter natürlichen, weniger korrosionsfördernden Bedingungen (< 5 mM $NaHCO_3$) eine theoretische Halbwertszeit des enthaltenen Eisens von etwa zwei Jahren angenommen werden. Diese liegt weit über den bisher beschriebenen Standzeiten von reinen Nanoeisen-partikeln, welche in der Praxis eingesetzt werden.
- Die Geschwindigkeitskonstante für die Dechlorierung von PCE mit Carbo-Iron kann durch die Behandlung mit reduzierten Schwefelverbindungen (S/Fe = 0.004–0.11) um etwa den Faktor drei erhöht werden. Mit der veränderten Kinetik der Reaktion geht auch eine Veränderung der gebildeten C_2-Kohlenwasserstoffe hin zu weniger hydrierten Produkten einher. Während beim Abbau von PCE durch unbehandeltes Carbo-Iron vor allem Ethen- und Ethanbildung beobachtet wurde, dominierte bei der Reaktion mit sulfidierten Partikeln zunächst die Bildung von Ethin, welches schrittweise hydriert wurde. Als Ursache für die beschleunigte

Dechlorierung wird die verbesserte elektrische Leitfähigkeit von FeS im Vergleich zu oberflächengebundenen Eisen(III)-oxiden gesehen, wobei aber auch eine Beteiligung der schwefelmodifizierten Aktivkohle am beschleunigten Schadstoffabbau möglich erscheint.

- Die Dechlorierungseffizienz (definiert als die für die Dechlorierung verbrauchte Eisenmenge im Verhältnis zum Gesamteisenverbrauch zu Beginn der Reaktion) kann unter den herrschenden Reaktionsbedingungen von etwa 30 % auf 98 % erhöht werden (für $c_{\text{Carbo-Iron}}$ = 4 g l^{-1}). Das heißt, dass nahezu das gesamte reduktive Potenzial des Eisens für den Schadstoffabbau genutzt werden kann, wodurch eine effiziente und wirtschaftliche Sanierung ermöglicht wird.

⇨ Sulfidiertes Carbo-Iron stellt insgesamt eine elegante Kombination von Eisen, Kohlenstoff und Schwefel dar und weist im Gegensatz zu herkömmlichem Nanoeisen ein deutlich größeres Potenzial für die Anwendung als *In-situ*-Reagenz auf.

3. Einfluss von Carbo-Iron auf den mikrobiologischen Schadstoffabbau im Aquifer

- Das Fehlen von Abbauprodukten, wie *cis*-DCE und Vinylchlorid, sowie die Ergebnisse der $^{13}C/^{12}C$-Isotopenanalyse des Schadstoffes PCE weisen darauf hin, dass vor der Injektion von Carbo-Iron der biologische Schadstoffabbau bis in Tiefen von etwa 15 m keine wesentliche Rolle spielte. Eine Ursache dafür stellt das starke Einströmen von sauerstoffhaltigem Oberflächenwasser in den Aquifer dar, wodurch Wachstum und Aktivität von organohalid-respirierenden Bakterien gehemmt werden. Der Hauptteil der Kontamination ist jedoch in etwa 6 m Tiefe zu finden, sodass eine rein natürliche Sanierung des Standortes nicht möglich war.
- Mit der Injektion von Carbo-Iron kam es zu einer langsamen, aber stetigen Senkung des Redoxpotenzials des Grundwassers, sodass zum Teil sulfatreduzierende Bedingungen erreicht werden, welche den mikrobiologischen Abbau von PCE begünstigen.
- Carbo-Iron weist gegenüber reinem Nanoeisen den Vorteil auf, dass es durch seine deutlich höhere Mobilität im Aquifer einen größeren Einflussradius besitzt und damit auch mehr Möglichkeiten hat, mit den am Standort vorkommenden dehalogenierenden

Mikroorganismen in Wechselwirkung zu treten. Ein weiterer Vorteil besteht in der Langlebigkeit des Eisen-Aktivkohle-Kompositmaterials. Im Gegensatz zu herkömmlichem Nanoeisen, das bereits nach wenigen Tagen bis Wochen seine Aktivität verliert, konnte bei Carbo-Iron noch nach über sechs Monaten ein reduzierender Effekt nachgewiesen werden. Die Bildung von Ethen und Ethan nach über 1,5 Jahren weist zudem auf eine chemische Langzeitaktivität des *In-situ*-Reagenzes hin. Als Ursachen werden dabei die hohe Kristallinität der Eisenpartikel sowie eine *In-situ*-Sulfidierung des Kompositmaterials diskutiert.

- Die Bildung von *cis*-DCE etwa ein Jahr nach der Injektion von Carbo-Iron in Aquiferbereichen mit günstigen Redoxbedingungen lässt auf eine Unterstützung des mikrobiologischen Schadstoffabbaus schließen und wird mit den am Standort detektierten Spezies *Sulfurospirillum multivorans* spp., *Desulfitobacterium* spp. und *Dehalococcoides mccartyi* in Verbindung gebracht. Die Bildung von Vinylchlorid konnte dagegen nicht beobachtet werden.
- Die Unterstützung der Mikroorganismen kann möglicherweise auf die eisenbedingte Verbesserung der Aquiferbedingungen zurückgeführt werden, wie z.B. die Senkung des Redoxpotenzials des Grundwassers oder die Freisetzung von molekularem Wasserstoff. Darüber hinaus könnten Eisen-Aktivkohle-Systeme gegenüber reinem Eisen weitere Vorteile haben: So ist etwa das reaktive Metall in die Aktivkohlestruktur eingebettet und kommt somit nicht direkt in Kontakt mit Mikroorganismen, was eine Ursache für die zytotoxische Wirkung darstellt.
- Am Standort konnte mit Hilfe der $^{13}C/^{12}C$-Isotopenfraktionierungsanalyse gezeigt werden, dass *cis*-DCE abgebaut wird. Dieser Vorgang wird auf die am Standort detektierte Spezies *Polaromonas* sp. zurückgeführt, welche in der Lage ist, das Intermediat metabolisch zu CO_2 zu oxidieren. Es kann angenommen werden, dass die langsame und moderate Absenkung des Redoxpotenzials durch die chemische Aktivität von Carbo-Iron einerseits unterstützend auf organohalid-respirierende Bakterien wirkt und andererseits einen anschließenden oxidativen Schritt ermöglicht.

⇨ Die Verbindung von chemischem Schadstoffabbau durch Carbo-Iron und der unterstützten mikrobiologischen Reduktion des Schadstoffes sowie einer

anschließenden Oxidation von *cis*-DCE ist ein vielversprechender Ansatz für eine ganzheitliche Sanierung kontaminierter Aquifere.

Fazit

Insgesamt liefert die vorliegende Dissertation einen substanziellen Beitrag zur Entwicklung und Anwendung von Eisen-Aktivkohle-Systemen für die *In-situ*-Sanierung von kontaminierten Aquiferen. Die Effizienz der Systeme kann einerseits durch die deutlich verbesserten Korrosions- und Dechlorierungseigenschaften des eingebetteten Eisens durch Sulfidierung erzielt werden, aber auch durch die Anwendung von Aktivkohle als Redoxmediator. Korrosionsstabile, dechlorierungseffiziente und langlebige Eisen-Aktivkohle-Systeme stellen eine vielversprechende Alternative zu herkömmlich eingesetzten Nanoeisensuspensionen und granulären Eisenbarrieren dar. Die in der Dissertation vorgestellten Erkenntnisse besitzen dank ihrer Einfachheit und Wirtschaftlichkeit ein hohes Potenzial, in die Praxis umgesetzt zu werden.

Referenzliste

[1] K. Mackenzie, S. Bleyl, A. Georgi, F.-D. Kopinke, Carbo-Iron - an Fe/AC composite - as alternative to nano-iron for groundwater treatment, Water Res. 46 (2012) 3817–3826.

[2] K. Mackenzie, S. Bleyl, F.-D. Kopinke, H. Doose, J. Bruns, Carbo-Iron as improvement of the nanoiron technology: From laboratory design to the field test, Sci. Total Environ. 563-564 (2016) 641–648.

Publikationen zum Promotionsthema

M. Vogel, I. Nijenhuis, J. Lloyd, C. Boothman, M. Pöritz, K. Mackenzie, Combined chemical and microbiological degradation of tetrachloroethene during the application of Carbo-Iron at a contaminated field site, Sci. Total Environ. 628-629 (2018) 1027–1036.

M. Vogel, F.-D. Kopinke, K. Mackenzie, Acceleration of microiron-based dechlorination in water by contact with fibrous activated carbon, Sci. Total Environ. 660 (2019) 1274–1282.

M. Vogel, A. Georgi, F.-D. Kopinke, K. Mackenzie, Sulfidation of ZVI/AC composite leads to highly corrosion-resistant nanoremediation particles with extended life-time, Sci. Total Environ. 665 (2019) 235–245.